NASA CONTRACTOR REPORT 166614

Study of Alternate Optical and Fine Guidance Sensor Designs for the Space Infrared Telescope Facility (SIRTF)

(NASA-CR-166614) STUDY OF ALTERNATE OPTICAL AND FINE GUIDANCE SENSOR DESIGNS FOR THE SPACE INFRARED TELESCOPE FACILITY (SIRTF) (Perkin-Elmer Corp., Danbury, Conn.) 152 p HC A08/MF A01 CSCL 03A G3/18

N85-15794

Unclas 13245

A. Wissinger
M. Steir
M. McFarlane
A. Fuschetto

CONTRACT NAS2- 11551

November 1984

NASA

NASA CONTRACTOR REPORT 166614

Study of Alternate Optical and Fine Guidance Sensor Designs for the Space Infrared Telescope Facility (SIRTF)

A. Wissinger
M. Steir
M. McFarlane
A. Fuschetto
Perkin-Elmer Corporation
Optical Group
Danbury, Connecticut

Prepared for
Ames Research Center
under Contract NAS2-11551

National Aeronautics and
Space Administration

Ames Research Center
Moffett Field, California 94035

CONTENTS

SECTION 1

EXECUTIVE SUMMARY

1.1 OBJECTIVE OF TIS FOLLOW-ON STUDY

This final report is the result of a follow-on effort to the SIRTF Technology Integrated System (TIS) Study (CR 166489) completed by Perkin-Elmer in July 1983. NASA, in the "SIRTF Free Flyer, Phase A System Concept Description" (Document No. PD-1006, May 3, 1984), showed that there will be considerable benefit to the science effectiveness of infra-red astronomy by changing from the attached Shuttle concept operating in the sortie mode to a long duration free flyer configuration. Thus, the acronym "SIRTF" has changed from "Shuttle Infra-Red Telescope Facility" to "Space Infra-Red Telescope Facility". In this context, Perkin-Elmer and NASA/Ames agreed to examine a few telescope technology areas that are important in the free flyer configuration.

Many of the constraints of the Shuttle bay (namely the constraint that the length of the facility must be less than two pallets) are eliminated in the free flyer mode, opening the door to possible improvements in the optical form (such as a longer telescope). A lingering problem has been the very small field of view that is diffraction-limited when the telescope is symmetrically chopped by rotating the secondary mirror about the minimum-inertia point (the c.g., or the nominal mirror vertex). Our objective has been to determine possible improvements in the optical form for a chopped telescope given the relaxed constraints of a free flyer configuration.

The long duration (one year lifetime on orbit, two year goal) mission places a premium on achieving the absolute minimum heat load imposed on the cryogenic cooling system. Here our objective has been to study the possibility of reducing or eliminating the heat load of the fine guidance sensor (FGS) from the multiple instrument chamber (MIC) by removing it entirely and optically linking the boresight of the telescope and FGS, or by optically coupling the heat-producing FGS components to the focal plane through a non-heat conducting means such as fiber optics. A third possibility that was studied is a configuration with a slow, internal FGS that views a portion of the same star field as an external, fast FGS. Comparison of the relative positions of the same star image gives the boresight error between the two sensors and alleviates the problem of inadequate frequency response of the internal FGS.

1.2 SUMMARY OF RESULTS

Optical Forms

We have determined the design prescription for a telescope that is compensated for the coma that is introduced when the secondary mirror is symmetrically tilted for the purpose of space-chopping the field of view. As shown in the next section, the selection of this design is contingent upon a number of factors, some of which are still to be determined by the science considerations. The coma compensated telescope design should not be thought of as a panacea, however, because as is often the case, optimizing for one factor requires a reduction in some other factor. In this case, decreasing the coma at the center of the field with the secondary mirror tilted reduces the total area of the field that is diffraction-limited. These results are presented in detail in paragraph 2.1 and 2.2 of this report.

Design prescriptions for three-mirror telescopes were found having very good performance and offering the possibility of chopping with a very small mirror behind the primary mirror. However, as shown in paragraph 2.3 these concepts suffer from packaging problems in the MIC region, and have the additional drawback that the beam moves on both the primary and secondary mirrors.

Paragraph 2.4 describes an optical design for an internal fine guidance sensor based on an inverted (backward) Cassegrain reflective optical relay system that has several advantages over the refractive relay design we studied in the previous TIS study. The design offers simplicity, convenient packaging; and, if the coma-compensated telescope design is selected, an opportunity to compensate for telescope aberrations in the FGS optical relay. The design also has several merits that could helpful in designing the SIs.

Secondary Mirror Chopper Mechanism

The design of a secondary mirror chopper that meets the SIRTF requirements, including the derived requirement that no forces or torques are reacted on the spider of the secondary mirror is described in Section 3. An important part of the study is the design of a beryllium secondary mirror that offers a minimum mass moment of inertia that is consistent with optical finishing and the chopping-induced stresses. The mirror is mounted so that the heat-producing components are isolated and buffered by a full diameter cooling manifold. We are confident that the concept will meet the very stringent thermal requirements for the secondary mirror.

Fine Guidance Studies

Concepts for both internal and external FGSs were studied. The external FGS has the attraction of permitting a much wider field of view than an FGS operating through the main telescope. The wider field of view increases the probability of finding brighter stars for offset guiding. Brighter stars reduce the need for a large collecting area in the FGS lens. Several parametric curves showing the interrelationship of these factors are included in paragraphs 4.3 and 4.4.

Several currently unknown factors tend to weigh against the external FGS. Typical of these is the question of the stability of the intervening structure between the SI's and the external FGS. Our approach to formulating the decision of external vs. internal FGS is given in the next section.

A significant part of the problem of both internal and external FGS is the number of CCDs needed to cover the field of view, which is set by the effective focal length required to satisfy pointing error budgets. A mechanism similar to the star selectors in the FGS of Space Telescope is a potential way out of this problem, and for that reason, the Space Telescope FGS is described in paragraph 4.9. A derivative of the star selectors would certainly be needed for the image-dividing fiber optic device that was examined and is reported in paragraph 4.8.

1.3 RECOMMENDATIONS AND CONCLUSIONS

Before definite recommendations can be made concerning the best optical form for SIRTF and the best FGS configuration, other parts of the facility must be defined through further design work. However, we are in a good position to define the design data that should be developed in order that a clear decision can be made.

A formal decision process can be organized in the form of an upside-down tree, representing a number of "if/then" statements. The motivation for organizing the decision process in the form of a tree is to avoid the labor of developing all the facts before the decision (at the root of the tree) is, or can be, reached. Parts of the tree can be "pruned" when the logic of the argument shows that connected factors rule out certain solutions or subsolutions. The technique is being popularized by workers in artificial intelligence. (For readers interested in delving deeper, see "Artificial Intelligence," Patrick Henry Winston, Addison-Wesley Publishing Company, pg. 102.) The connectives in the statements can be either "and" or "or". If all of the "ands" are satisfied, then the decision can proceed to the next higher level, while only one "or" need be satisfied at a decision point before proceeding to the next higher decision level. In cases where a number of "ands" lead to a decision point and one of the factors is deemed to be unlikely by analysis or assessment, then none of the other connected factors need to be investigated. This formalized decision technique is illustrated by the figures and text below. Our recommendations (the need to perform additional design work) and their rationale then become obvious from their place in the decision tree.

We expect the decision tree to change as the SIRTF program continues to mature. This approach documents the reasons for program decisions and allows for review and reconsideration of discarded options should unforeseen developments force a change in design.

Optical Forms

The factors involved in the decision on the best optical form for SIRTF may be formulated as follows

If

- chopping is the "normal" operation

and

- diffraction-limited imagery at a wavelength of 2 μm is critical to science

and

- SIs and FGS have re-imaging optics

and

- an approximately ∿3 arcmin (diffraction-limited at 2 μm) field of view is acceptable to the science instruments

Then coma-compensated telescope design is the design of choice.

The three mirror designs are not recommended because of potential packaging problems.

OPTICS DECISION TREE

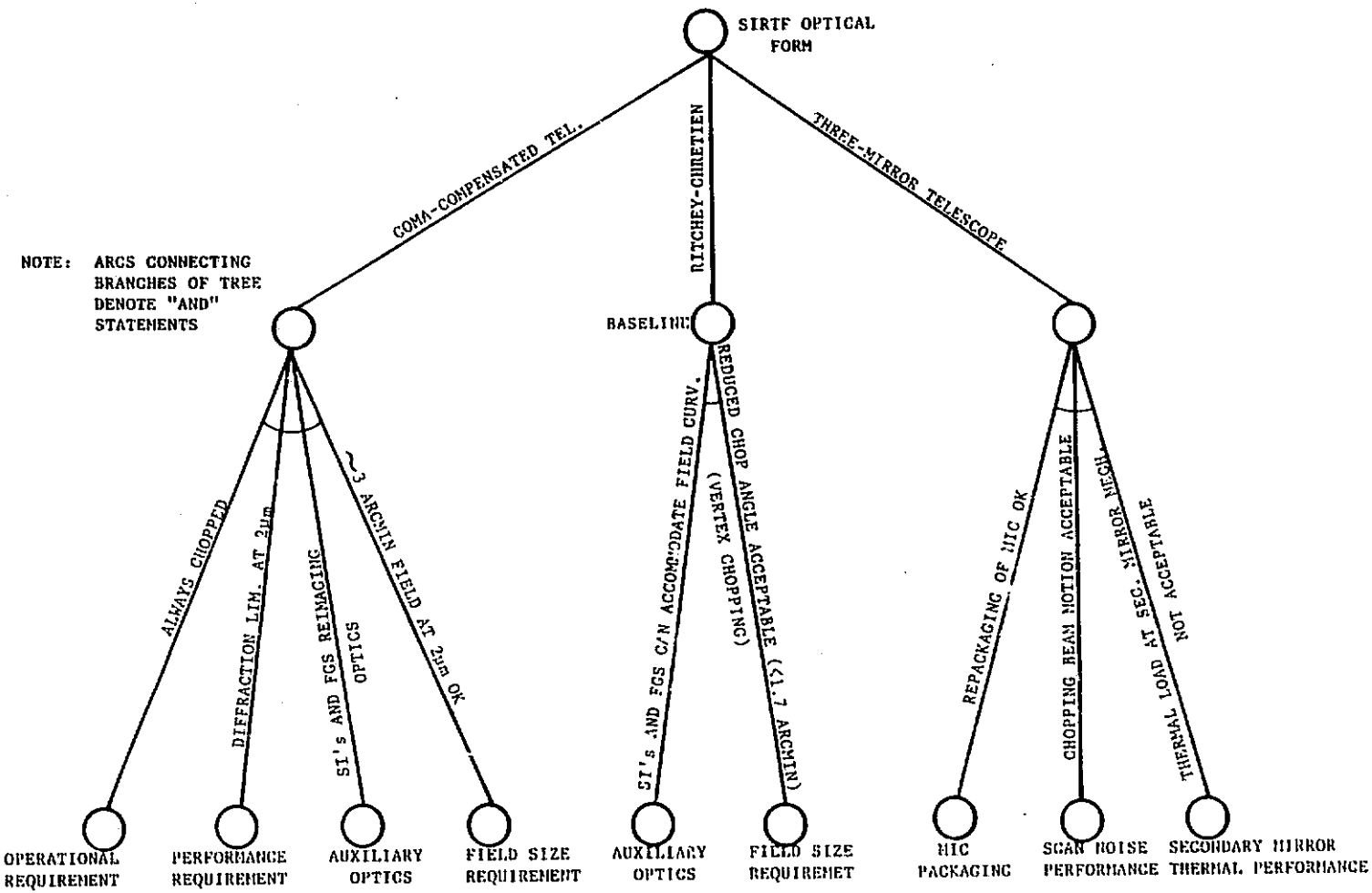

Internal Versus External FGS

A similar formalism helps clarify the issues surrounding the selection of the FGS concept. Again, we can state the decision problem in the form of an "if/ then" statement.

If

- The SIRTF envelope with an external FGS will fit in the shuttle bay

and

- a wide FGS bandpass is needed (e.g. control bandwidth must be high because solar panels or other appendages oscillate at low frequencies) requiring short (<0.5 sec) integration times

and

- on-orbit replacement of FGS is essential

and

- structure connecting FGS to SIs is sufficiently stable to meet error budget

or

- a boresight FGS alignment mirror in the main telescope aperture does not interfere with the natural background limit objective or disrupt the aperture symmetry

and

- closely coupled, wide-bandwidth roll stabilization is needed (implying 2 guide stars)

then

- external FGS is the design of choice.

A similar statement concerning the internal FGS has been formulated. Both statements are illustrated in the decision tree.

SIRTF FGS CONFIGURATION DECISION TREE

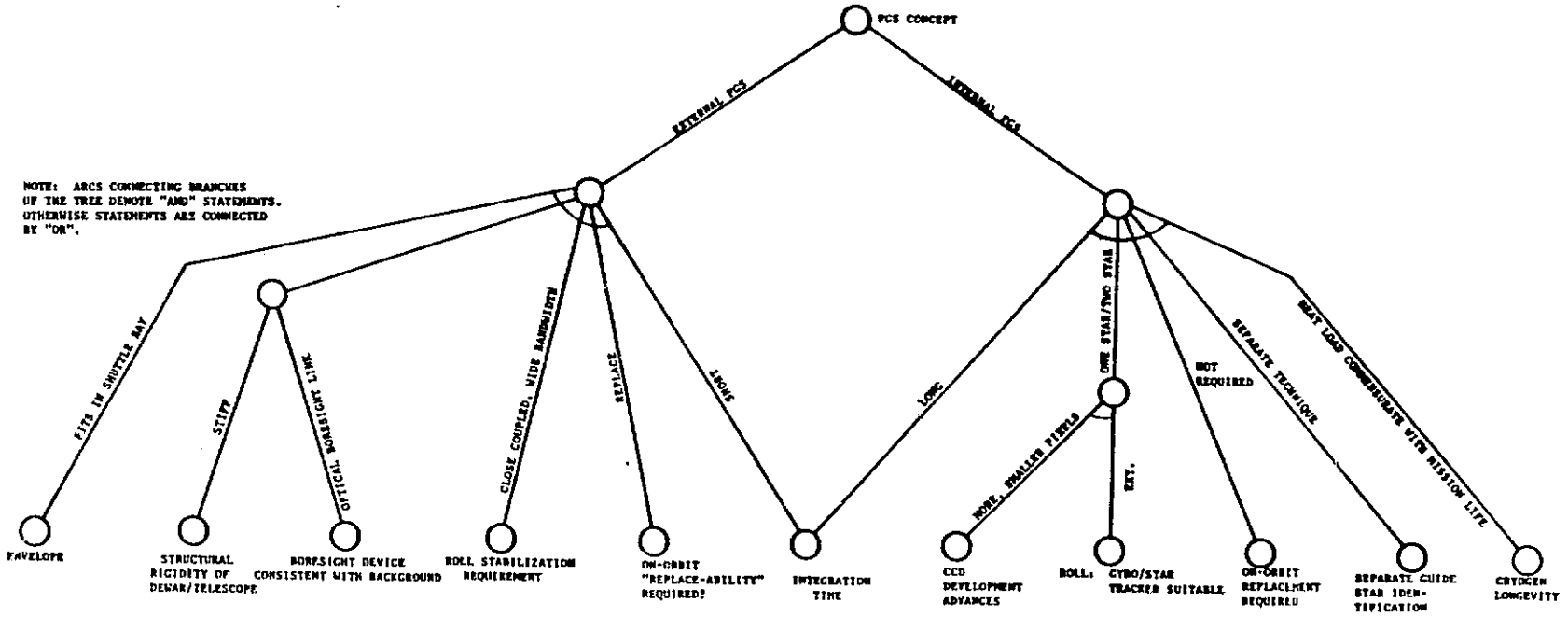

SECTION 2

OPTICAL DESIGN

2.1 COMA-COMPENSATED TELESCOPE

SIRTF's goal of diffraction-limited performance at 2 μm is accomplished using the baseline of f/24 Ritchey-Chretien design. However, the need for spatial chopping introduces coma since the secondary mirror is rotated to perform the chopping. One approach to reducing the coma caused by chopping would be to rotate the secondary mirror about the coma-free or neutral point of the telescope. Because this point is located between the secondary mirror and the focal point of the primary mirror and is a considerable distance behind the secondary mirror, the large effective moment of inertia of the secondary mirror motion makes this approach undesirable. In effect, it is necessary both to rotate the mirror and translate it laterally in order to effect the proper motion. The amplitude of this motion is several millimeters for a 3.5 arcmin chop amplitude, imposing severe mechanical requirements on the chopping mechanics. Thus,

- Rotation about R-C neutral point allows chopping without coma
- Amplitude of secondary mirror motion is very large (several mm)
- Nature of motion is combination tilt and rotation, difficult to mechanize

An alternate approach involves an optical design that compensates the field-dependent coma by balancing the field-independent coma caused by tilting the secondary mirror about its vertex. The drawback of this approach is that without reimaging optics, diffraction-limited images can be obtained only for less than half of the 7 arcmin field. The coma-compensation approach is described in more detail in this section.

COMA-COMPENSATED TELESCOPE

REQUIREMENTS

- DIFFRACTION-LIMITED PERFORMANCE AT 2 μ M (GOAL), AND
- SPATIAL CHOPPING

METHODS OF SOLUTION

- APLANATIC TELESCOPE (I.E. RITCHEY-CHRETIEN) CHOPPED BY ROTATION OF SECONDARY NEUTRAL POINT
- "COMPENSATED" TELESCOPE WHOSE FIELD DEPENDENT COMA JUST BALANCES THE FIELD INDEPENDENT COMA CAUSED BY TILTING THE SECONDARY

When the secondary mirror of a telescope is tilted, a detector on the mechanical axis of the primary mirror is effectively looking at some field angle linearly related to the tilt angle of the secondary. This is commonly known as boresight error. Most telescope configurations (except the Ritchey-Chretien) will have some coma whose value depends on the shape of the secondary and on the boresight error. The coma introduced by tilting the secondary is independent of the secondary mirror's shape. Therefore, adjusting the shape of the secondary to balance the field dependent coma at the boresight angle against the tilt coma of the secondary mirror will completely eliminate coma on the mechanical axis of the telescope. The shape of the primary can then be chosen to eliminate spherical aberration, providing an image on the mechanical axis that is excellent over a very wide range of chopping angles. This is the design principle of the coma-compensated telescope.

COMA-COMPENSATED TELESCOPE: DESIGN PRINCIPLES

- WHEN CHOPPING THE SECONDARY, THE FIELD ANGLE CHANGES LINEARLY WITH CHOP ANGLE.
- WHEN CHOPPING THE SECONDARY, THE TILT COMA CHANGES LINEARLY WITH CHOP ANGLE.
- THE SECONDARY MIRROR CAN BE SHAPED SO THAT FIELD-DEPENDENT COMA AND TILT COMA ARE CANCELLED ON-AXIS FOR ALL TILT ANGLES.
- THE SHAPE OF THE PRIMARY CAN THEN BE CHOSEN TO CANCEL SPHERICAL ABERRATION.

The shapes of the mirrors for the coma-compensated telescope depart from spherical by more than either an equivalent Cassegrain or Ritchey-Chretien telescope. However, the mirrors are both nyperboloids and no particular problems would be expected in testing and fabricating these mirrors.

By a fortunate circumstance, the astigmatism of this configuration is such that the image surface of minimum OPD is less curved than the Petzval surface. Thus the field is flatter than in the other telescope types and little or no refocusing would be required when changing chop amplitude.

As will be discussed later, it is possible to design a high-performance, wide-field focal reducer/corrector for this type of telescope which allows guiding in the visible.

At other points than the axial detector, the field coma of this telescope is large. If M is the magnification of the secondary mirror (about 10.4 for SIRTF), then the coma of this telescope has a magnitude of $M^2/2$ times that of an equivalent Cassegrain telescope. Thus, significant image degradation occurs even a few millimeters off the mechanical axis.

COMA-COMPENSATED TELESCOPE

- Mirror Shapes
  - Primary - Hyperboloid, deeper than parabola
  - Secondary - Hyperboloid, deeper than classical Cassegrain secondary
- Intrinsic coma is $M^2/2$ times that of a Cassegrain
- The astigmatism is such that the surface of least confusion is less curved than the Petzval surface. This field flattening helps during chopping.
- Wide field imaging for offset guiding is possible.

The performance of three proposed configurations for the SIRTF telescope has been evaluated with regard to the maximum chop angle that can be achieved taking worst case conditions. The three configurations are the coma-compensated (cc) telescope, a Ritchey-Chretien telescope chopped about its vertex (rc) and a Ritchey-Chretien telescope chopped by rotating the secondary about its neutral point (np). To be as fair as possible, all three systems were focused for minimum rms wavefront at a field angle of ± 3 arcmin (± 0.05 degree). This focal position was then held constant for all angles at which calculations were made. The data for chop semi-angles of up to ± 0.2 degree (12-arcmin) are shown in the figure. Changing the focus will have a small effect on the curves because the IR depth of field at f/24 is large.

rms WAVEFRONT VS. CHOP ANGLE IN OBJECT SPACE

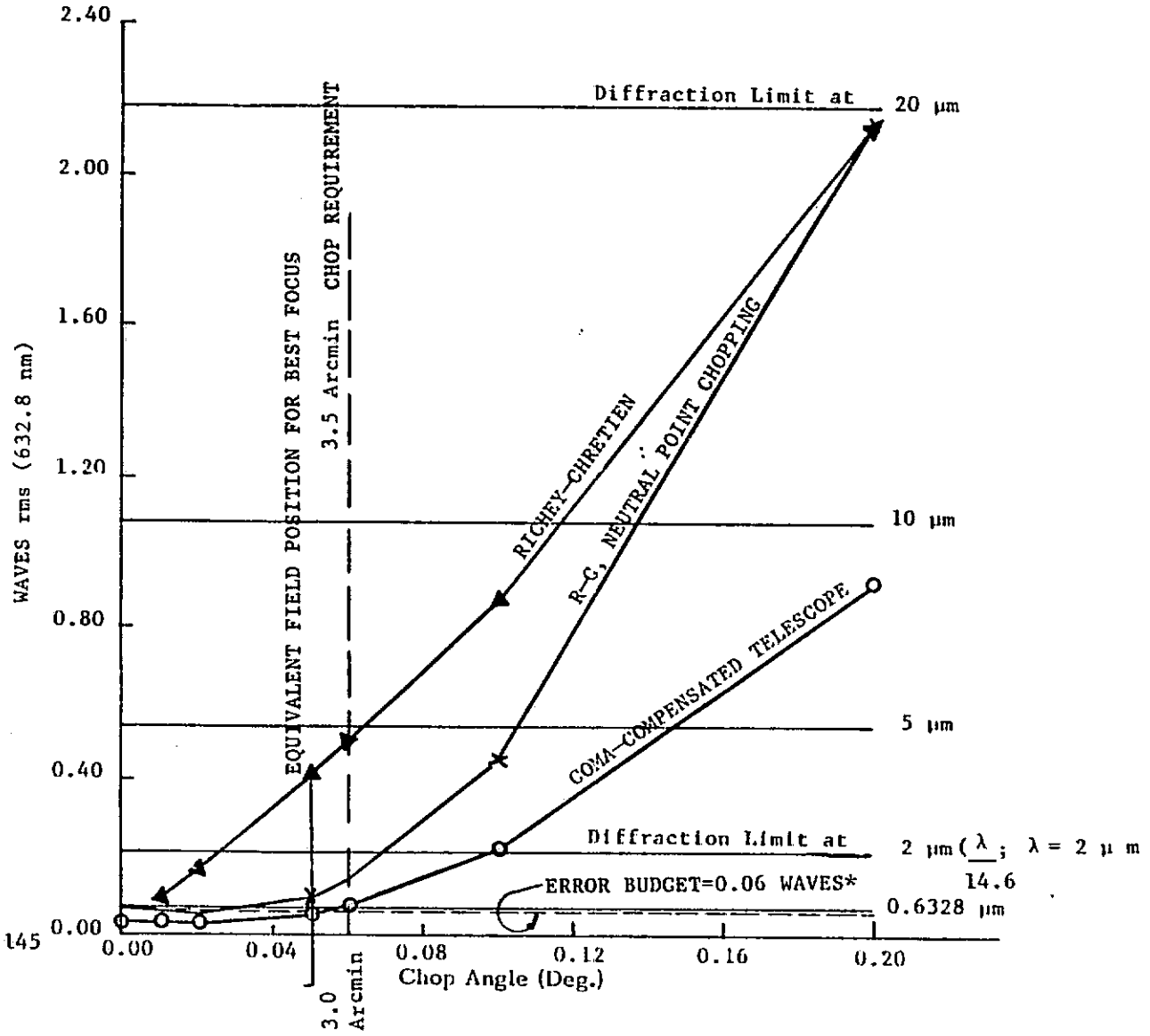

*REF. CR 166489, PG. 145

2.2 ERROR-BUDGETED FIELD COVERAGE VS. CHOPPING ANGLE

These spot diagrams represent the coma compensated telescope in its unchopped position with the secondary mirror normal to the optical axis of the primary. The bottom spot diagram is on-axis, the middle is for 2.5 arc-minutes off-axis and the top is for a point 3.5 arc-minutes off-axis. Each of the spot diagrams is for a different optimized focal position near the paraxial focus. The presence of a 37% linear obstruction of the beam is included although it is not obvious. The diameter of the outer circles is 500 micrometers or about 5 arcsec and the inner circle diameter is equal to the first dark ring of the airy diffraction pattern (λ = 2 μm). Note that the angular coma of this telescope at 3.5 arc-minutes off-axis is about 1/60 of the angular field. The coma also is of opposite sign to that of a normal Cassegrain telescope; that is, the coma figure points away from the optical axis.

THE COMA-COMPENSATED TELESCOPE IN ITS UNCHOPPED POSITION

DETECTOR AT 3.5 ARCMIN

DETECTOR AT 2.5 ARCMIN

DETECTOR CENTERED ON MECH. AXIS

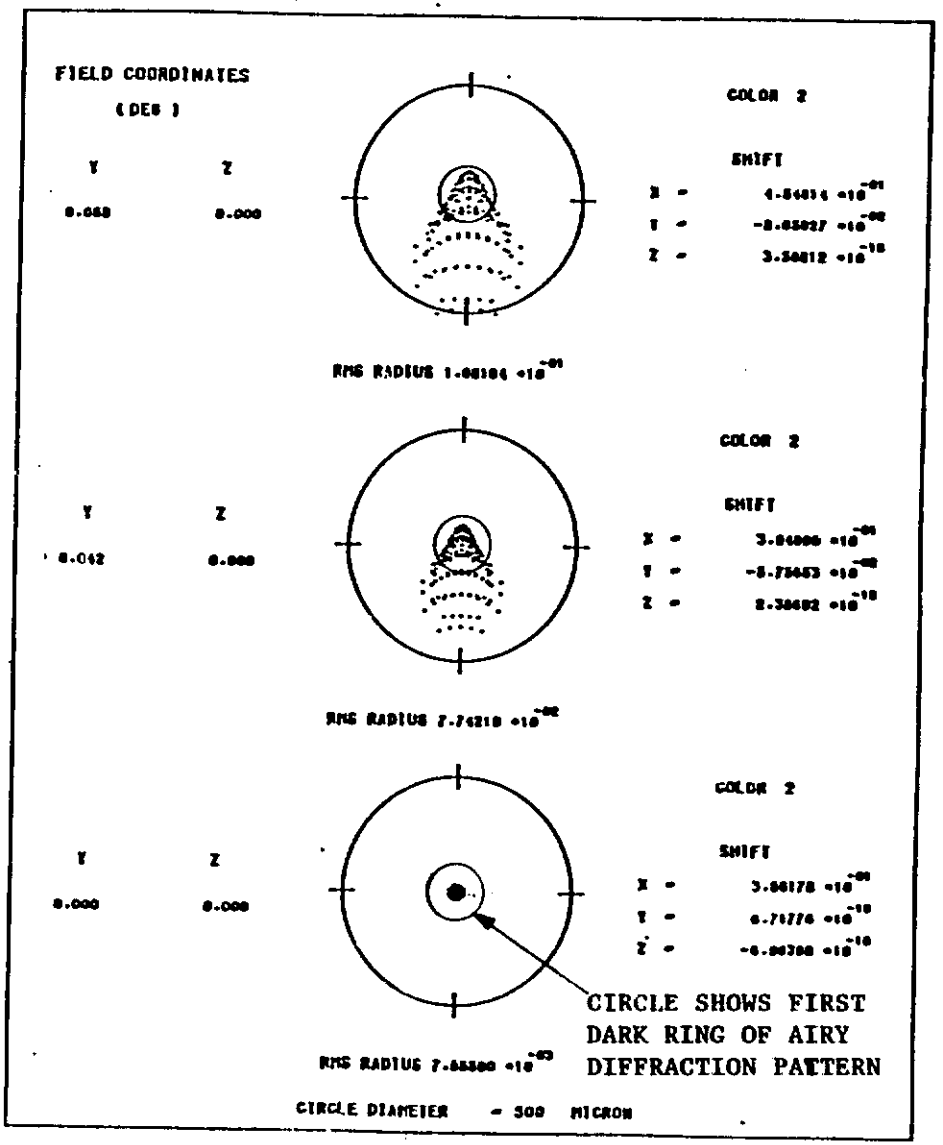

These modulation transfer functions correspond to the spot diagrams on the previous page although they are diffraction transfer functions, not geometrical. On-axis, the telescope is diffraction-limited, but it degrades very rapidly with field size. However, the MTFs do not change with chop angle as those for the Ritchey-Chretien do. Thus, if the reimaging optics of the SIs and FGS are designed to compensate for the residual coma, the field can be widened and will be independent of effects such as Image Motion Compensation (IMC) and field scanning with the secondary mirror.

MODULATION TRANSFER FUNCTION (UNCHOPPED)

COMA-COMPENSATED SIRTF TELESCOPE

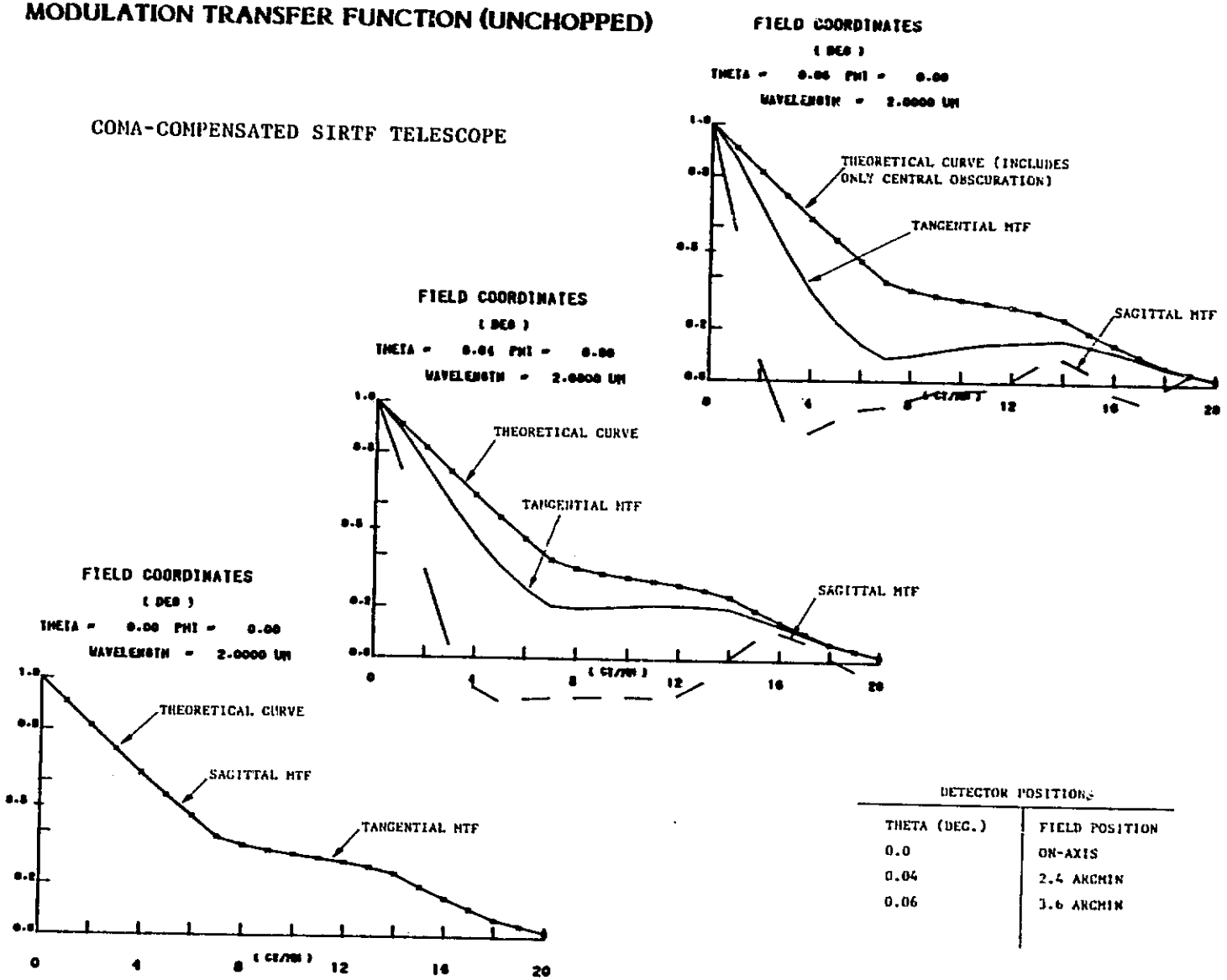

DETECTOR POSITIONS

THETA (DEG.)	FIELD POSITION
0.0	ON-AXIS
0.04	2.4 ARCMIN
0.06	3.6 ARCMIN

These spot diagrams are for the coma-compensation telescope with the secondary mirror tilted to produce a chop angle of 3.5 arcmin. The bottom spot diagram is on the tilted axis of the chopped configuration. That is, the field point is now imaged on the mechanical axis of the telescope. The other two field points also correspond exactly to the previous spot diagram. These are virtually identical to the previous diagrams, showing that, indeed, the axial coma in the tilted configuration is almost perfectly cancelled.

THE COMA-COMPENSATED TELESCOPE WITH A 3.5 ARCMIN CHOP ANGLE

DETECTOR AT 3.5 ARCMIN

DETECTOR AT 2.5 ARCMIN

DETECTOR CENTERED ON MECH. AXIS

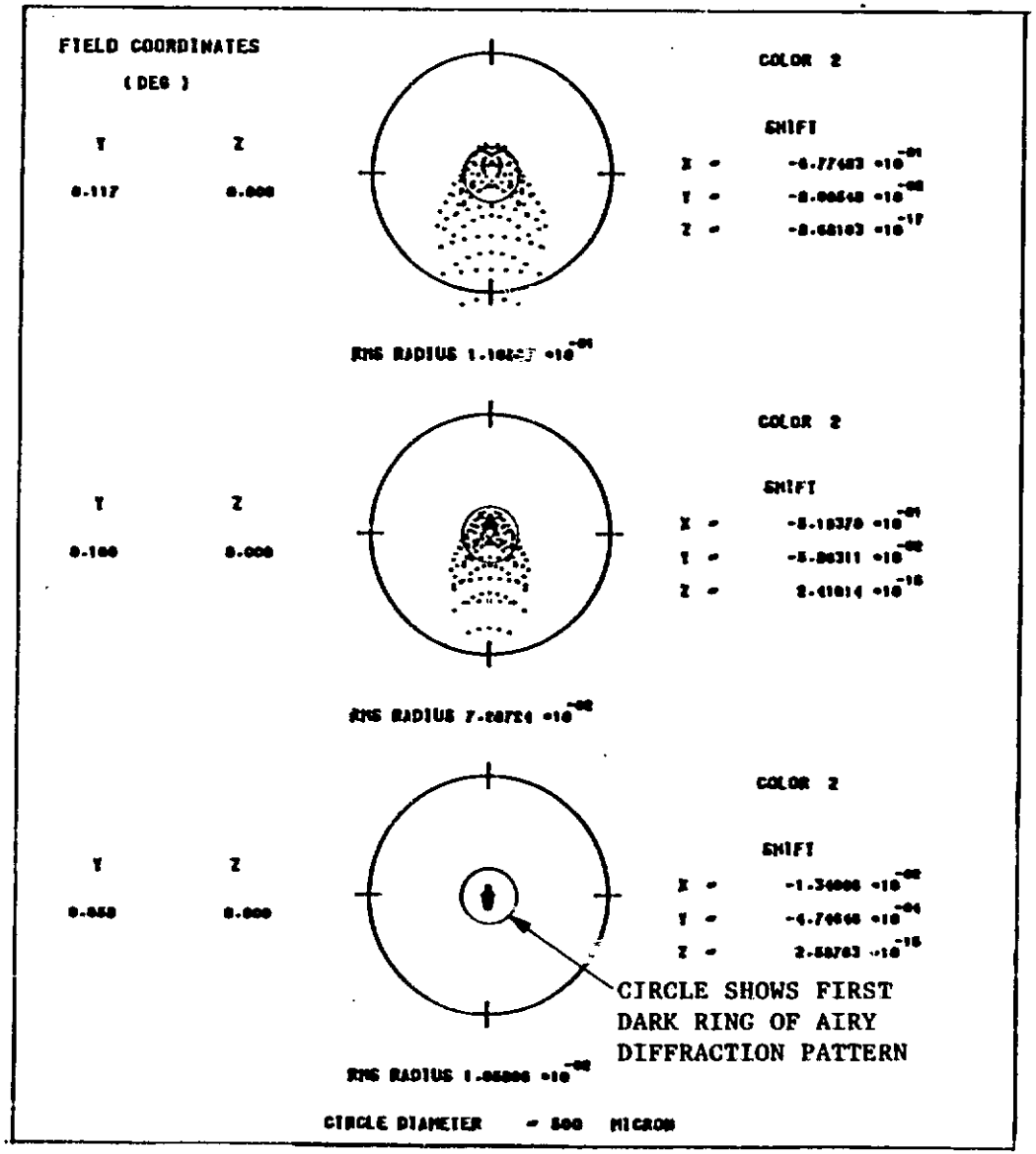

Modulation transfer functions corresponding to the spot diagrams on the previous page are again almost indistinguishable from the unchopped version of the telescope. Thus the images in the field near the mechanical axis of the telescope are not affected by secondary mirror tilt. The tilt alignment requirement for this coma-compensated telescope is easily met.

MODULATION TRANSFER FUNCTION (3.5 ARCMIN CHOP ANGLE)

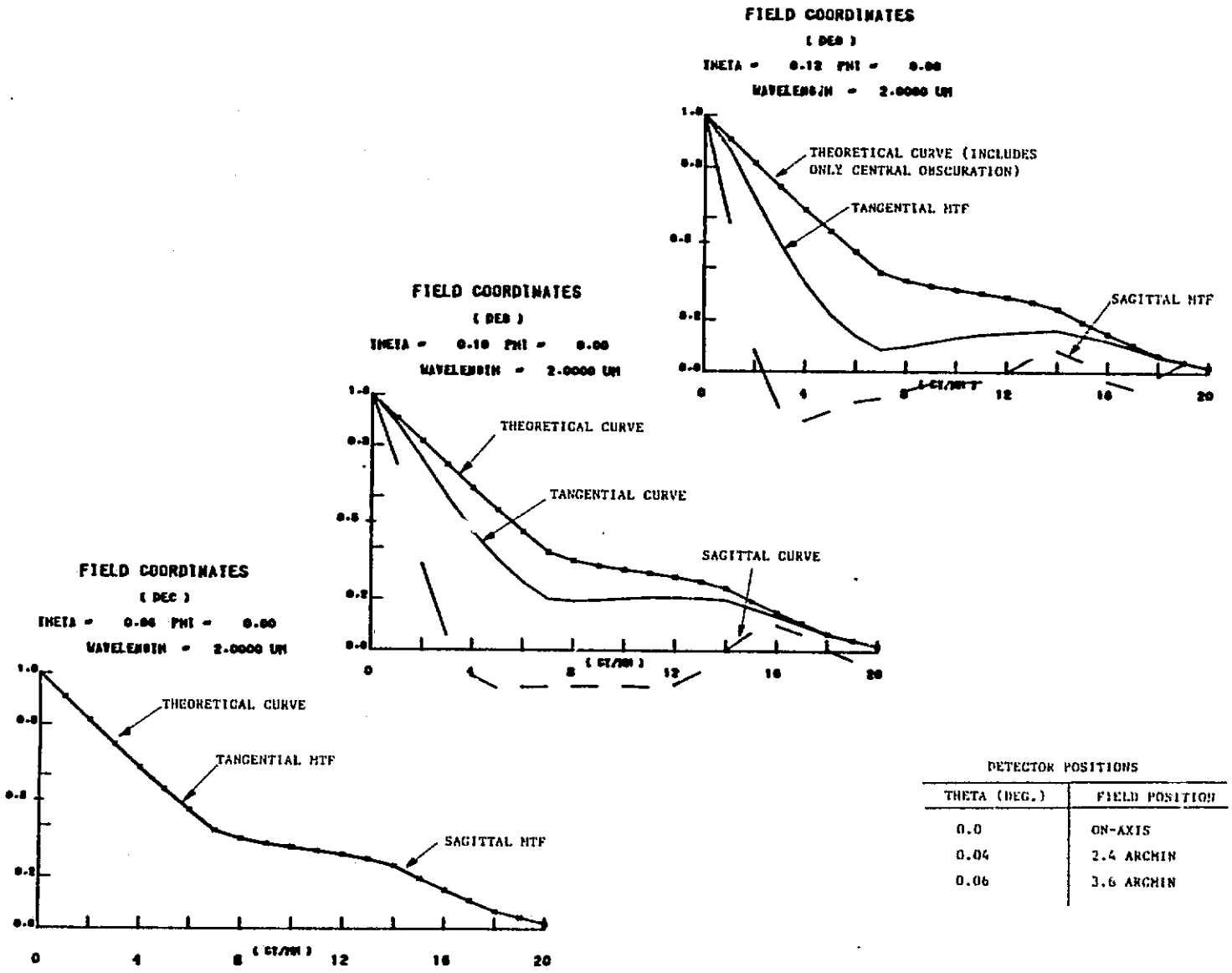

DETECTOR POSITIONS

THETA (DEG.)	FIELD POSITION
0.0	ON-AXIS
0.04	2.4 ARCMIN
0.06	3.6 ARCMIN

To determine the reason for the chopped image degradation, we performed a Zernike decomposition on each wavefront. The coefficients of primary coma and primary astigmatism are presented in these tables. The relatively poor performance of the neutral point configuration is due to the fact that the secondary mirror must be rotated by a much larger angle than in the other configurations to give the same amount of chop in image space, causing large amounts of astigmatism. This comparison is made only for a detector on the mechanical axis of the telescope.

The situation will be considerably worse for asymmetric chopping of the Ritchey-Chretien telescope, even if the chopping is about the neutral point, because there is appreciable field curvature in this design. Thus, each instrument would require a refocusing motion in synchronism with the chopping in order to achieve diffraction-limited performance at the maximum chopping amplitude.

ZERNIKE COMA Z_{31} (WAVES @ 632.8 nm) vs. CHOP ANGLE IN OBJECT SPACE

l (Deg.)	CC	RC	NP
.00	0	0	0
.01	.0010	-.0797	.0003
.02	.0018	-.1595	-.0004
.05	.0042	-.3986	-.0009
.06	.0050	-.4782	-.0011
.10	.0084	-.7968	-.0016
.20	.0183	-1.5904	-.0036

ZERNIKE ASTIGMATISM Z_{22} (WAVES @ 632.8 nm) vs. CHOP ANGLE IN OBJECT SPACE

l Deg.)	CC	RC	NP
.00	0	0	0
.01	.0019	.0027	.0033
.02	.0079	.0110	.0137
.05	.0494	.0685	.0918
.06	.0712	.0986	.1344
.10	.1978	.2738	.3931
.20	.7908	1.0947	1.7616

This figure plots the diameter of the field for a flat detector (over which the image quality is diffraction-limited for $\lambda = 2$ μm and for $\lambda = 4$ μm) as a function of chop angle on the sky. The focus position was varied, however, for each chop angle. With field-flattening relay optics, this focal shifting could be eliminated. The neutral point chopped Ritchy-Chretien has a very large field that is independent of chop angle. The vertex-chopped Ritchey-Chretien, however, has a large field for a centered secondary mirror, but the field decreases rapidly when the secondary mirror is tilted. The coma compensated telescope, while not having as large a field of view even for a centered secondary, has only a very weak field dependence on chop angle. Note that for chop angles greater than about 1.65 arcmin the coma-compensated telescope's field exceeds that of a vertex-chopped Ritchey-Chretien at $\lambda = 2$ μm. Increasing the wavelength at which the diffraction-limited performance is defined will shift these curves up and to the right as shown for the example of diffraction-limited performance at $\lambda = 4$ μm. These curves allow comparison of the performance of three concepts. However, since error budgets are <u>not</u> taken into account in these plots, they should not be used to predict actual performance.

FIELD DIAMETER VS. CHOP ANGLE

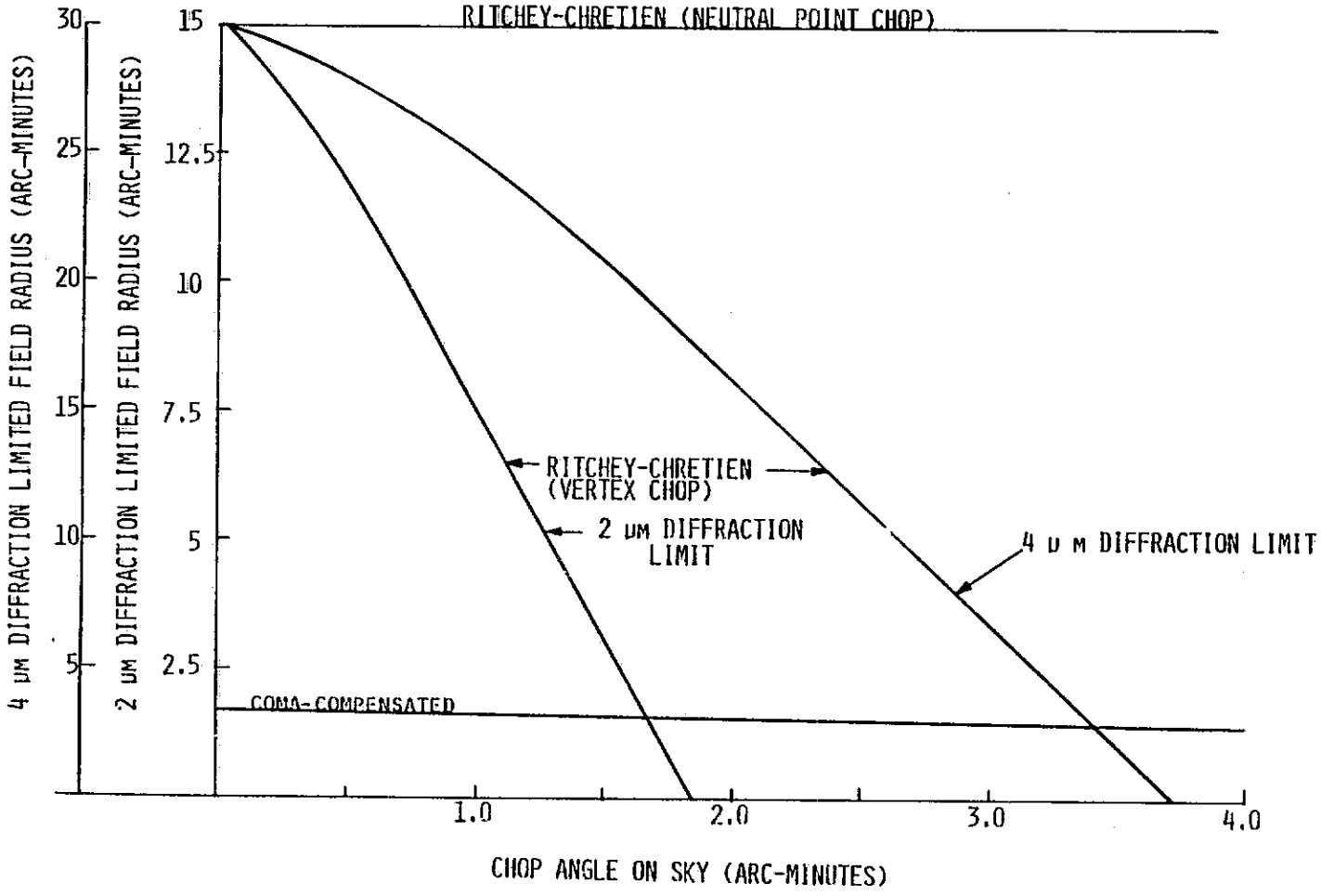

2.3 RE-IMAGING TELESCOPE

An optical form featuring three mirrors presents an interesting option for chopping. Using a Toric Mirror as a field mirror, the optical configuration re-images the stop onto a small fourth mirror, which can be used as the chopping element.

In the infrared, element reflectivities can be extremely high and the light loss due to two extra mirrors is negligible. The presence of two extra mirrors does, however, complicate the geometry of the instrument package somewhat. This complication could be accommodated for in the preliminary mechanical design.

The presence of a Toric mirror as the field element poses no particular fabrication problem other than the problems encountered in cryo-figuring other mirrors.

The problem of detector microphonics should perhaps be studied further but it is not believed to be serious.

REIMAGING SYSTEMS FOR CHOPPING

ADVANTAGES

CHOPPING MIRRORS CAN BE SMALL

THEY CAN BE CONVENIENTLY LOCATED

POWER DISSIPATION IS VERY SMALL

SECONDARY ASSEMBLY CAN BE SIMPLIFIED

ENTRANCE PUPIL CAN BE AT PRIMARY MIRROR

OFFSET GUIDING CAN BE SIMPLER AND MORE ACCURATE

DISADVANTAGES

MORE OPTICAL ELEMENTS

TORIC OPTICAL ELEMENTS

DETECTOR MICROPHONICS??

Re-imaging

Light from the secondary mirror (M2) is bounced off of the large 45° dichroic filter (D). At the telescope focus is a 45° toric mirror (M3) which reimages the stop (now located at the primary) onto the small chopping mirror (M4). This mirror reimages the light to a final focus (F). This is the location of one of the science instruments.

SIRTF TELESCOPE WITH RE-IMAGING SCANNING MIRROR

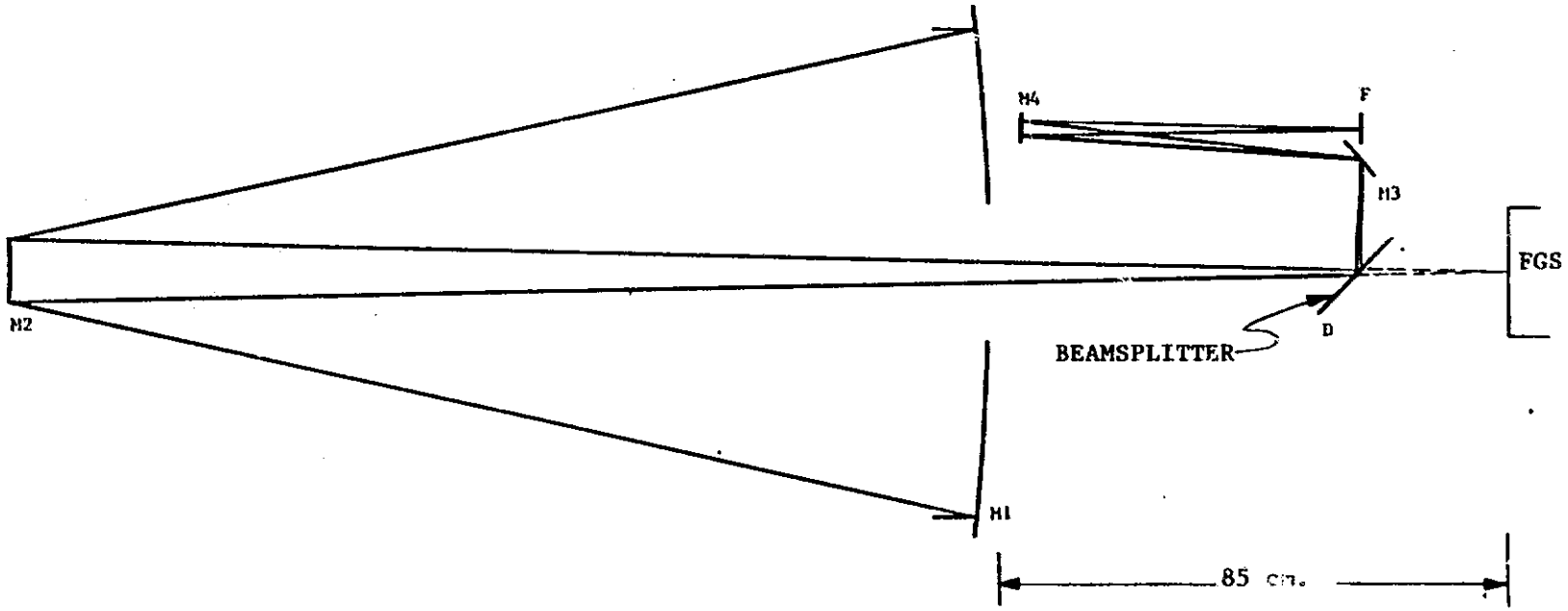

Re-imaging Scanning Mirror

This enlargement shows the extreme rays for a $\pm$ 3.5 arcmin chop. The mirror (M4) is a unit magnification mirror but this is not necessary. The reimaging can be done over a wide range of magnifications. In chopping, the detector sees different parts of the mirror M3, but it also sees different parts of the dichroic D. Because the mirrors are at a temperature of a few degrees Kelvin, this does not appear to be fatal to the scheme.

RE-IMAGING SCANNING MIRROR

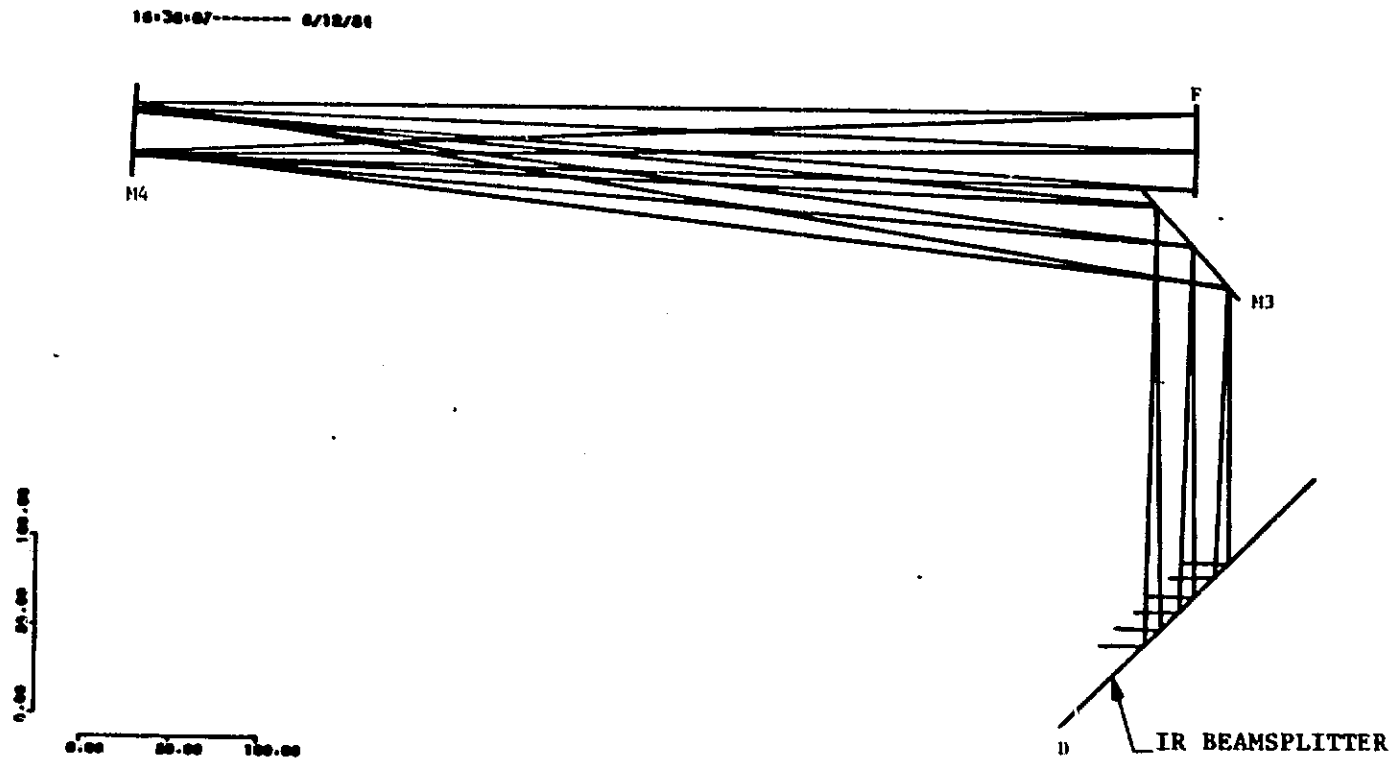

Chop Angle and Wavefront

The plot of rms wavefront error vs. chop angle is somewhat asymmetrical since the mirror, M4, is tilted for all chop angles. For the configuration on the previous page the telescope is diffraction-limited at 0.6328 μm for a total 7 arcmin chop. The diffraction-limited range will be increased by increasing the M3-M4 spacing and increasing the mirrors' radii in proportion. Since the limiting aberration is astigmatism, the range of diffraction-limited chop angle will increase as the square-root of the mirror space M3-M4.

CHOP ANGLE VS. rms WAVEFRONT

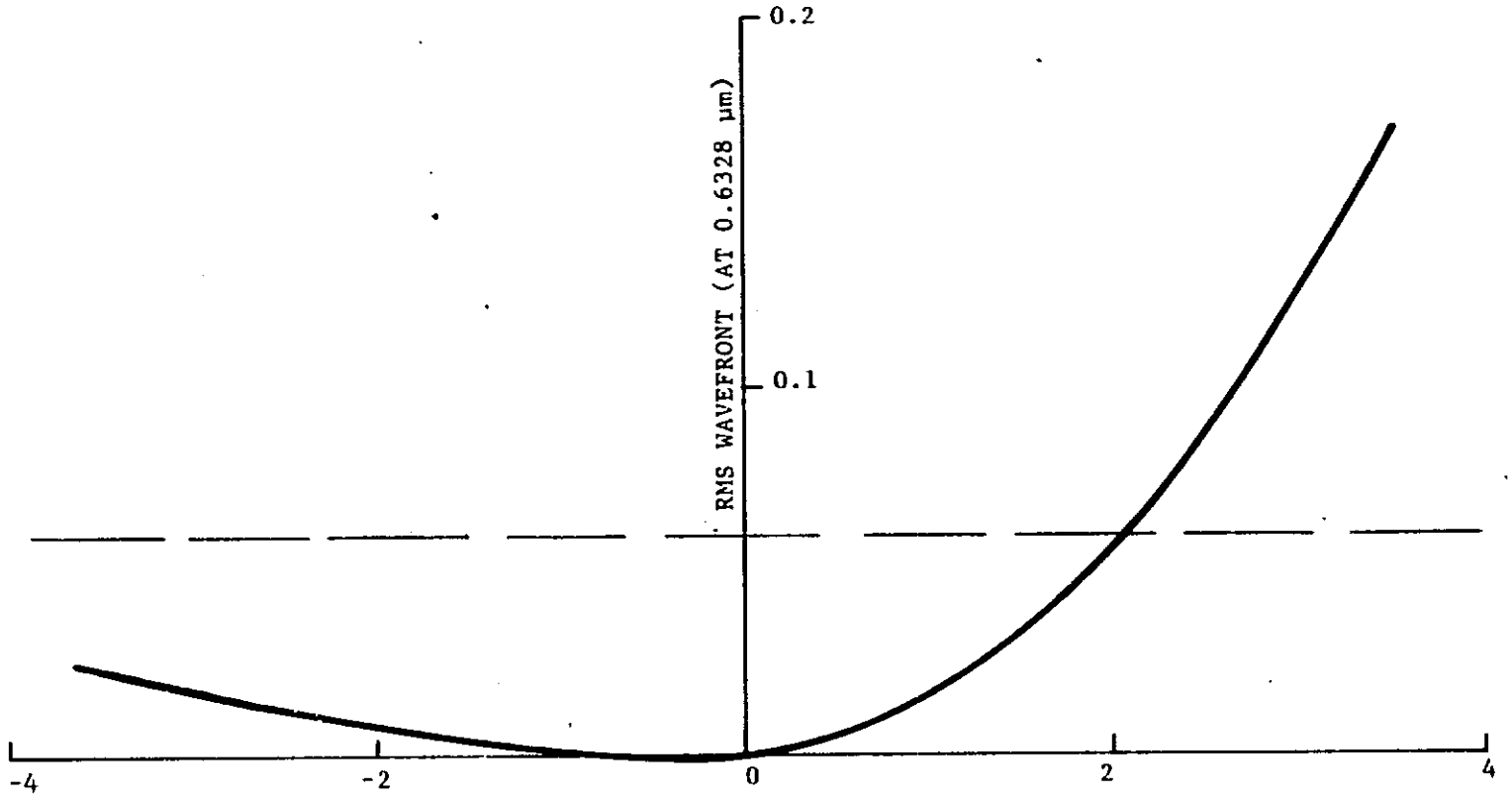

Experience with ground-based infrared telescopes has consistently shown that modulation of the IR beam by wobbling the secondary mirror gives superior performance to other types of choppers. The difficulty with the alternate approaches has been that they often exhibit a large "DC offset" (a large AC signal when observing two nominally identical locations on the sky). But this experience is based on room temperature telescopes. Because all SIRTF mirrors will be cold, there should be no measurable DC offset resulting from mirror emission at the shorter wavelengths and, at most, a small contribution at the longest wavelengths. We also note that the re-imaging chopper design would not chop the optical-wavelength image needed by SIRTF's FGS.

CONCLUSIONS

- RE-IMAGING MIRRORS OFFER PROMISE AS SCANNING DEVICES.
- ASTIGMATISM FORCES MIRRORS TO HAVE A 75-100 CM OPTICAL SEPARATION AND 4 CM DIAMETER.
- HIGH PERFORMANCE REQUIRES MILDLY TORIC MIRRORS

2.4 INVERTED CASSEGRAIN FOR AN INTERNAL FGS

The baseline SIRTF FGS optical design has several refracting elements; because of uncertainties in the index of refraction of glasses at cryogenic temperatures, reducing the number of elements would be advantageous. The inverse Cassegrain design described in this section uses only one refracting element--a field lens--and achieves diffraction-limited performance.

FINE GUIDANCE RELAY

- REQUIRE A DIFFRACTION-LIMITED, HIGH-APERTURE RELAY FOR GUIDANCE
- FIELD OF VIEW IS TO BE AT LEAST 15 ARCMIN
- SYSTEM SHOULD BE OPTICALLY SIMPLE SINCE LARGE TEMPERATURE CHANGES COULD CAUSE DN/DT PROBLEMS

Perkin-Elmer decided to employ a reflecting relay system because of its conceptual simplicity. Since all of the power in this system comes from mirrors, the only effect of cooling the relay to near absolute zero would be to introduce a defocus which can be corrected mechanically. An all-refracting relay would rely on a delicate distribution of refractive indices among the various elements for aberration correction. When these elements are cooled the refractive indices and powers as well as the sizes and spacings of these elements would change. The change in all of these parameters would be nonlinear over a temperature range of 200 K. Thus the simplicity of the reflecting relay combined with its achromatism and its ability to correct the telescope's aberrations make it an interesting candidate for use in a fine-guidance sensor.

Two-mirror systems working in an inverse Cassegrain configuration acting as an image relay offer an attractive possibility for a wide-field fine guidance sensor. This system offers a number of degrees of freedom for controlling aberrations, a wide range of magnification, and a minimum of transmitting elements. For the Ritchey-Chretien telescope, two concentric spherical mirrors and a simple fused silica field lens are the only optical elements necessary. For the coma-compensated telescope, the mirrors must be general conic sections and a small aspheric Schmidt plate must be inserted in the beam to achieve the required correction. Both of these systems are nearly diffraction-limited in the visible over a 15-20 arc-minute field.

INVERSE CASSEGRAIN SOLUTION

DIFFRACTION-LIMITED IMAGERY IS PROVIDED ON CURVED FOCAL SURFACE, (FIBER OPTIC FACEPLATE FOR CCD POTENTIAL SOLUTION)

THE DESIGN IS OPTICALL SIMPLE; THE ONLY REFRACTING ELEMENT IS A FIELD LENS

FOR A RITCHEY-CHRETIEN TELESCOPE, RELAY MIRRORS ARE ASPHERICAL

WITH ASPHERIC MIRRORS AND A SCHMIDT PLATE, THE COMA-COMPENSATED TELESCOPE PROVIDES DIFFRACTION-LIMITED IMAGERY

THE CONCEPT CAN BE USED OVER A WIDE RANGE OF MAGNIFICATIONS AND FOR RANGE OF MIRROR SHAPES

An optical schematic of the Ritchey-Chretien telescope with its focal reducer shows how compact and simple this concept can be. The entire focal reducer could fit in a tube about 200 mm in diameter and 750 mm long. Several design options are available in this configuration, and the overall length can be either shorter or longer.

FOCAL REDUCER FOR RITCHEY-CHRETIEN TELESCOPE

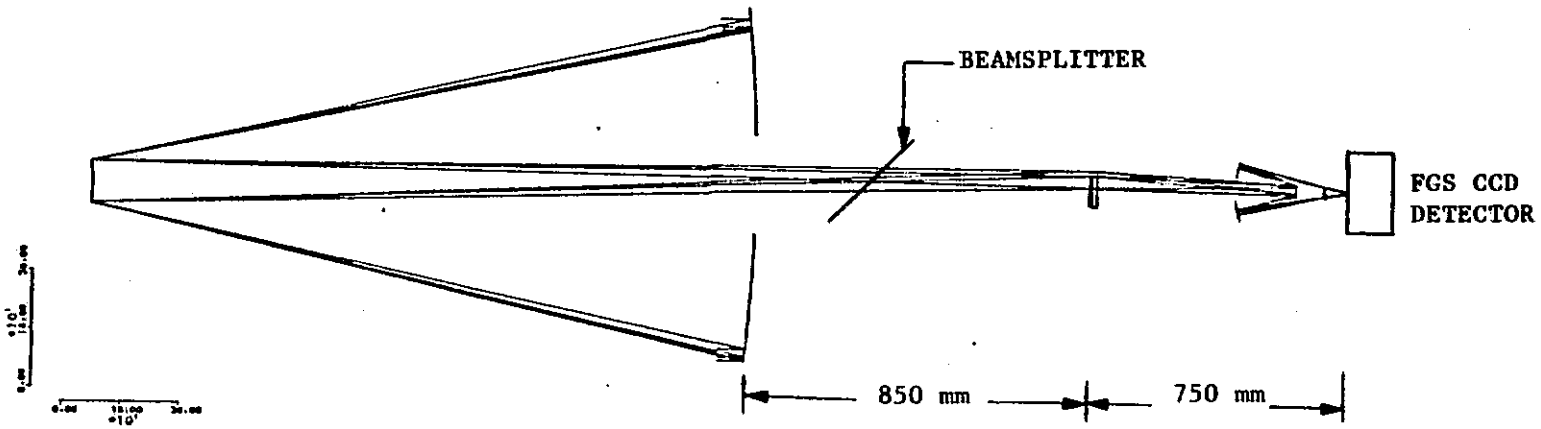

A detailed view of the focal reducer reveals its extreme simplicity. At the focus of the SIRTF telescope is a plano-convex field lens that reimages the stop (secondary mirror) on the principal plane of the focal reducer. Light from the field lens is intercepted by a small convex spherical mirror and reflected to a large (150 mm diameter) concave mirror. Both mirrors are concentric with their common center at the principal plane of the system. The final focus can be made outside the optical path so no obscuration problems arise.

A DETAILED VIEW SHOWS THE PLANO-CONVEX FIELD LENS

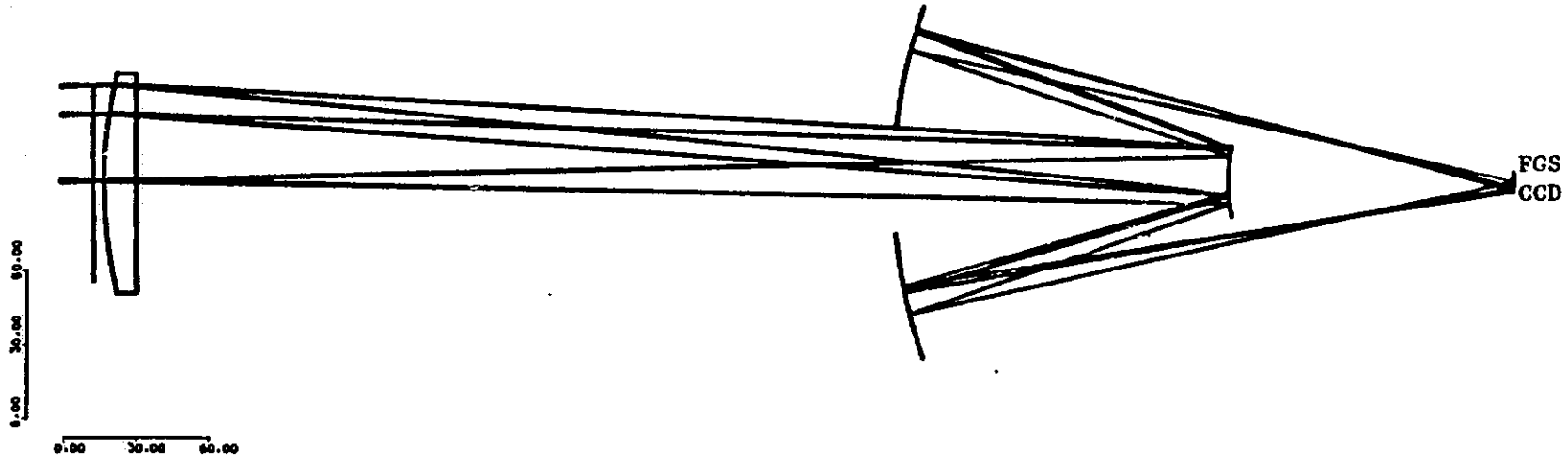

The focal reducer for the coma-compensated telescope looks superficially very similar to the previous design. The only visible difference is the addition of a small, zero-power aspheric plate.

THE COMA-COMPENSATED DESIGN WITH A SMALL, ZERO-POWER ASPHERIC PLATE

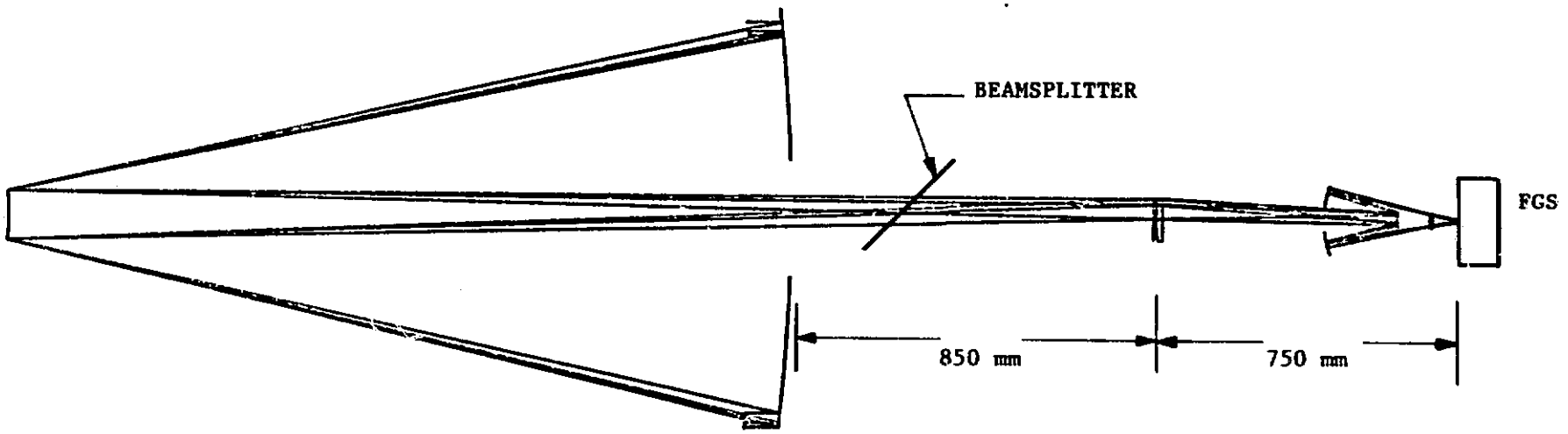

The aspheric plate is located between the large concave mirror and the final focus. As shown, it is at the common center of the two concentric mirrors and the focal surface, which is also concentric. With some additional computer optimization, this plate will move a small distance from the common center.

Analysis of the performance of this FGS relay design shows that it is fully capable of supplying the images required by a CCD FGS: uniform spot size over the FGS field with the spots matched to a 3 x 3 pixel array. There will be almost no variation in the images as the secondary mirror is chopped.

DETAILED VIEW WITH ASPHERIC PLATE

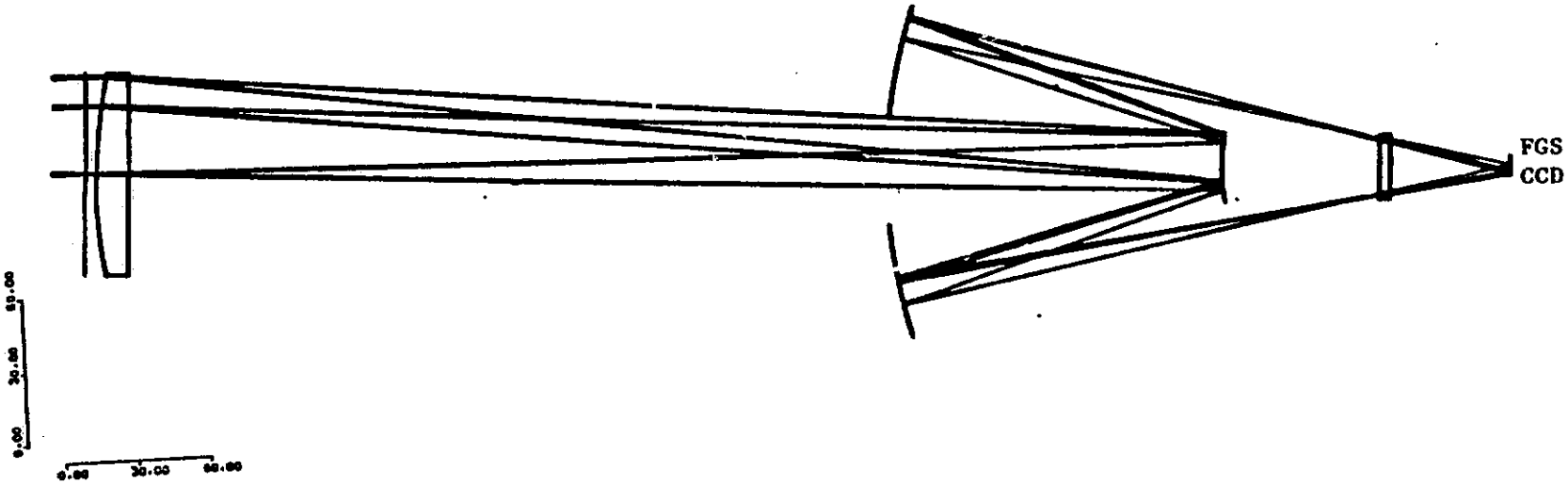

SECTION 3

SECONDARY MIRROR CHOPPER DESIGN INVESTIGATION

The secondary mirror and its mechanism must satisfy several requirements. It must operate at low temperature (5-6K) and the temperature must be very stable (millikelvins per second) in order to meet the natural background performance limit for SIRTF. The mirror's angular accelerations must be extremely high to perform the chopping and image motion compensation functions. The mirror itself must therefore be designed to have the lowest possible mass moment of inertia so that the kinetic energy imparted to the mirror is minimized. The mechanism that drives the mirror must have high efficiency so that the energy dissipated as heat is minimal. Finally, the mirror mechanism must be nearly reactionless; that is, no periodic torques or forces can be reacted through the secondary mirror spider.

The facing chart shows a tabulation of the quantitative requirements for the secondary mirror and its mechanism.

SECONDARY MIRROR DESIGN GOALS

• Secondary mirror diameter	106 mm
• Surface figure	0.06 λ at 0.6328 μm
• Chopping motion (two axis)	
- Total angular throw	30 arcmin
- Half angular throw	15 arcmin
- Maximum chopping rate	20 Hz
- Duty cycle	80%
• Reactionless system	
• Desirable power dissipation at secondary mirror	0
• Secondary mirror operating temperature	6K
• Thermal drift in secondary mirror	1mK/sec
• Position sensor	
- Bandwidth	1 kHz
- Noise equivalent position error	20 nm
• Mirror motion profile	See following illustration

Required Mirror Motion

The chart shows the nominal chopping profile used in the design study. We assumed that the acceleration and deceleration parts of the cycle would simulate a sine wave, thereby smoothing all derivatives of the motion and maintaining all the disturbance frequencies within a narrow band. At the 20 Hz chop rate, the angular frequency is 630 rad/sec (100 Hz) for the 80% duty cycle case. All the values shown are for the maxima in each parameter. The design permits commanded variations over the full dynamic range.

The average power, given by the equation at the right of the figure, is proportional to the driven inertia. Reductions in the inertia pay off rapidly in easing the performance required of the mechanism and in reducing the heat load on the cryogen.

REQUIRED MIRROR MOTION

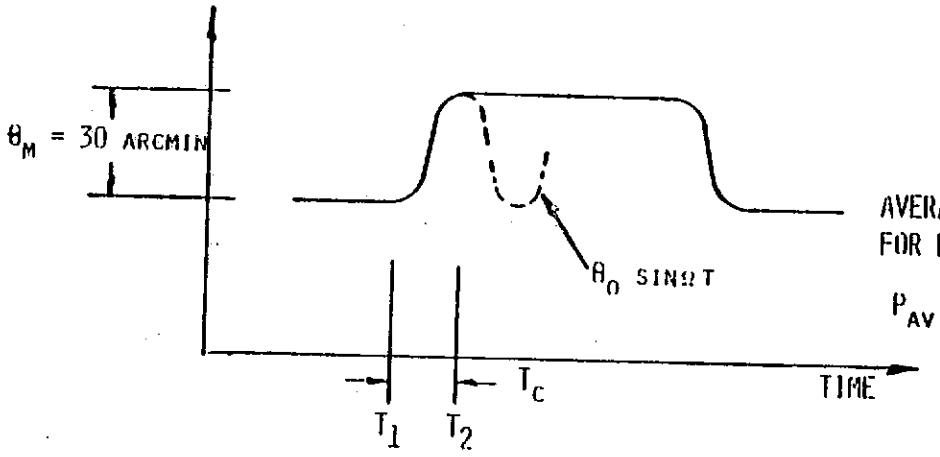

AVERAGE POWER P_{AV}
FOR FULL CHOP CYCLE

$$P_{AV} = KIF^3\left(\frac{\theta_M}{1-D}\right)^2$$

D IS DUTY CYCLE
I IS INERTIA
F IS FREQUENCY
K IS CONSTANT

FOR SINUSOIDAL MOTION:

$\theta = \theta_0$ SINΩT

θ = 15 ARCMIN (0.00436 RAD)

AT A 20 Hz CHOPPING RATE AND 80% DUTY CYCLE:

$T_1 - T_2$ = 5.0 MSEC

$\Omega = 0.63 \times 10^3$ RAD/SEC

MAX ANGULAR VELOCITY = 2.75 RAD/SEC
MAX ANGULAR ACCELERATION = 1.73×10^3 RAD/SEC^2

Chopper Pointing Accuracy Rationale

A critical performance requirement for the secondary mirror mechanism is the positional accuracy that must be achieved during its various functions. The facing chart traces the chopping accuracy requirements from the generic requirement, through the error budget and the angular magnification of mirror motion relative to the object space line-of-sight motion and, finally (in the last line), gives the displacement measurement accuracy that is required at the edge of the mirror, since this is where a position sensor for the servo loop would be located.

CHOPPER POINTING ACCURACY RATIONALE

• λ	2 μM
• IR BEAM SIZE	1.2 ARCSEC
• ROT. OF SEC. FOR 1 BEAM THROW ON SKY	4.7 ARCSEC
• STABILITY OF LOS	0.12 ARCSEC
• IMC POSITION SENSOR ERROR BUDGET ON SKY	0.018 ARCSEC
• IMC POSITION SENSOR ERROR BUDGET ON MIRROR	0.071 ARCSEC
• DISPLACEMENT AT EDGE OF MIRROR FOR TOTAL ERROR BUDGET	20 NM

Reticulated Mirror Blank

The drawing shows the secondary mirror blank designed for minimum mass moment of inertia while meeting the deflection, manufacturability, and mounting integrity requirements of the SIRTF mission. The material is beryllium fabricated by the patented hot isostatic pressed (HIP) process devised jointly by Perkin-Elmer and Battelle Laboratories. The process permits extremely high structural efficiency, hence low weight and low inertia.

The weight of the blank as shown in the drawing is 0.151 lb (0.0685 kg) and the moment of inertia about the c.g. is 5.92 x 10^{-5} kg-m*2. The weight of the moving mass is the sum of the blank weight, actuator coils and actuator pad, given in a subsequent chart.

Perkin-Elmer has had sufficient experience with HIP beryllium mirror blanks and their optical finishing to be confident that this design can be produced with a minimum of difficulty.

RETICULATED MIRROR BLANK

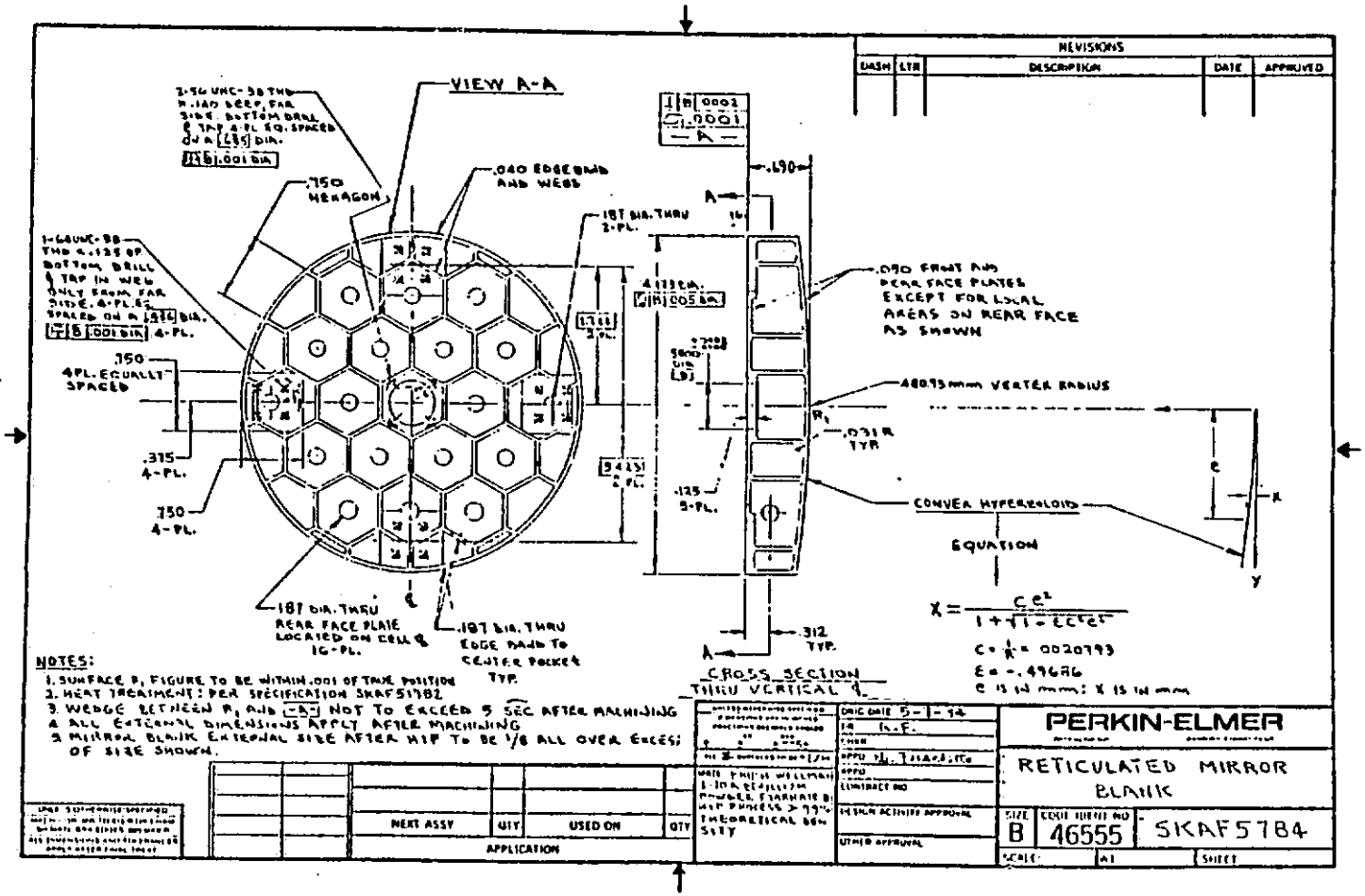

SIRTF Secondary Mirror Assembly Concept

The SIRTF secondary mirror is supported on a novel two degrees of freedom flexure bearing developed by Perkin-Elmer some time ago. Mirror angular position is sensed by the inductive differential sensor pair mounted at the edge of the mirror. The electromagnetic voice-coil actuators use superconducting magnets for maximum efficiency. The forces developed by the actuators are reacted by the reaction plate, which is mounted to the cooling manifold and main support. This kinematically correct arrangement causes no reaction torques or reaction forces (which have been drawbacks of previous concepts).

Minimum heating of the mirror is ensured by the placement of the cooling manifold between the mirror and the main heat-producing components of the assembly. The largest source of heat will most likely be eddy currents in the magnetic circuit structure, and for this reason, the magnet assembly is mounted on the reaction plate. The voice coil itself will have negligible power dissipation because of the use of wire that is superconducting below 9K. A subsequent chart lists the power dissipators and their distribution.

Thermal energy is conducted out of the mirror by four small copper bands connecting the mirror to the cooling manifold. Ample margin is available because the thermal conductivity of copper is extremely high at cryogenic temperatures.

The components that extend beyond the periphery of the mirror will be shielded from the focal plane by a fixed aperture stop in front of the secondary mirror and the conical baffle mounted at the secondary mirror position.

SECONDARY MIRROR ASSEMBLY

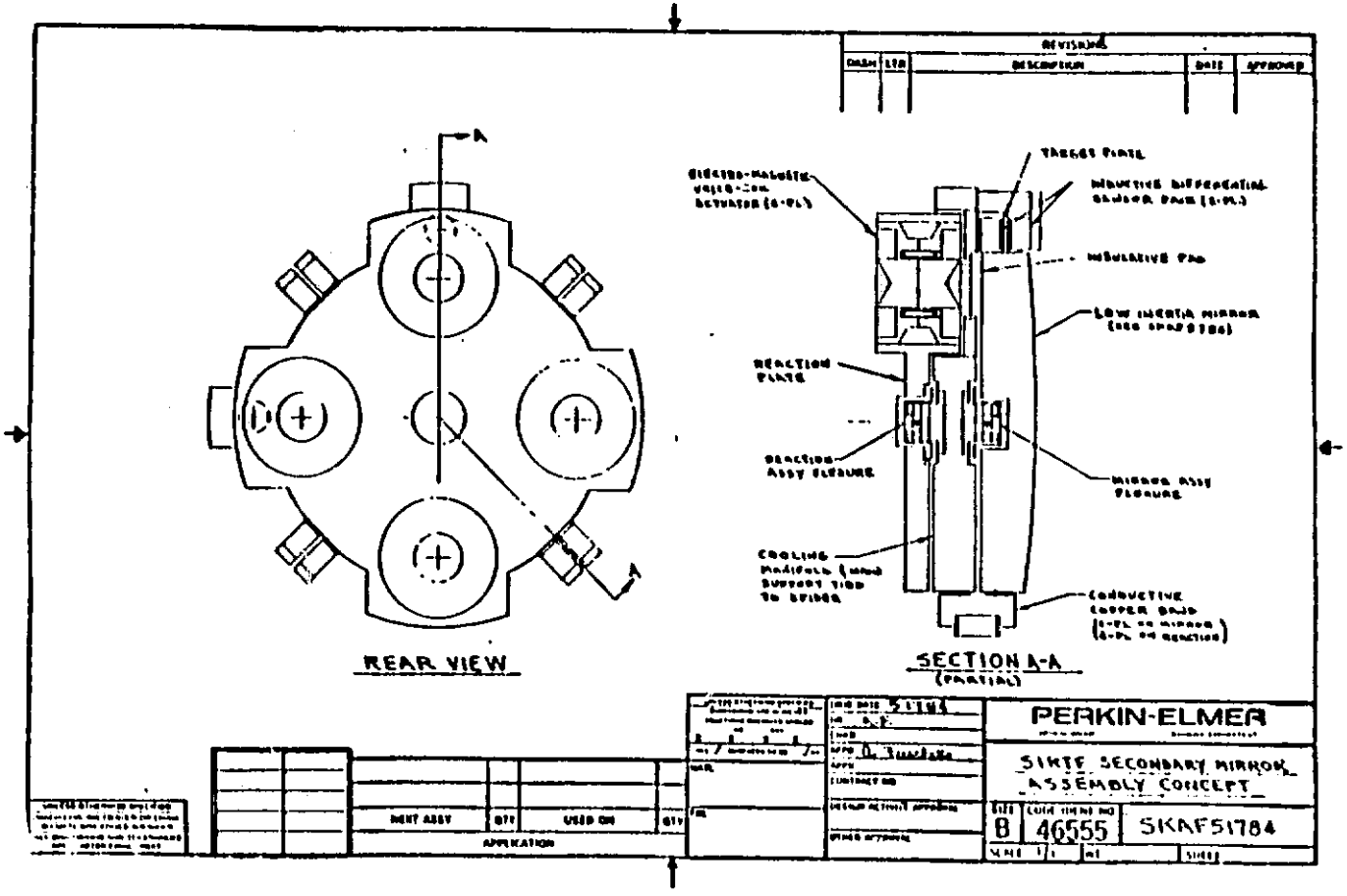

Estimate of Secondary Mirror Assembly Weights and Inertias
Natural Frequency and Edge Deflection

The parameter most critical in determining the power that must be handled by the secondary mirror actuator is the total moving inertia executing the chopping motion. The chart shown opposite gives the summation of the weight and moment of inertia about the pivot point (the cg). Note that the total inertia is less than the goal of 1×10^{-4} kg-m*2. The chart also gives the frequency of the first mode of the mirror in torsion, and the peak deflection caused by maximum acceleration. Both values indicate that the design will provide ample performance margin in the SIRTF 1×10^{-4} kg-m^2 application.

ESTIMATE OF SECONDARY MIRROR ASSEMBLY WEIGHTS AND INERTIAS NATURAL FREQUENCY AND EDGE DEFLECTION

ITEM	WEIGHT (LB)	INERTIA ($KG-M^2$)
SECONDARY MIRROR	0.151	5.917×10^{-5}
ACTUATOR COILS	0.048	2.966×10^{-5}
ACTUATOR PAD	0.018	0.816×10^{-5}
TOTAL	0.217	9.7×10^{-5}

- FIRST TORSIONAL RESONANT FREQUENCY 15 KHZ
- PEAK DEFLECTION AT EDGE OF MIRROR DUE TO MAXIMUM ACCELERATION 0.15 μ IN (λ/533 PEAK AT 2 μM)

Power Dissipation on Secondary Mirror

The chart shows our current estimates of the power that would be dissipated in the design shown on the previous pages. The parasitic power losses cannot now be reasonably estimated, but future experiments will provide these data. Note that the largest item (60 milliwatts) of power dissipation is the result of eddy currents in the magnetic circuit structure and that the magnet is mounted on the reaction plate. The reaction plate is separated from the mirror by the cooling manifold and faces away from the telescope focal plane. The voice coil is shown with zero heat dissipation because the superconducting coil will contribute negligible heat, a significant advantage over the copper coils considered in previous concepts.

ESTIMATE OF POWER DISSIPATION ON SECONDARY MIRROR

Heat Source	On Mirror (mW)	On Reaction Plate (mW)
Voice Coil	0	0
Eddy currents in magnetic circuit structure	0	60
Position sensors (due to Eddy currents)	0.01	0
Hysteresis (Flexures)	0.003	0.003
Parasitic	TBD	TBD

Electromagnetic Actuator Characteristics

Based on technology previously proven at Perkin-Elmer, an electromagetic actuator design has been studied having the characteristics shown in the chart. A double-ended magnet design with a central air gap provides a very efficient magnetic circuit structure with minimum size.

ELECTROMAGNETIC ACTUATOR CHARACTERISTICS

- CENTRAL AIR GAP DESIGN
- SUPER PERFORMANCE, HIGH-ENERGY (35×10^6 GAUSS-OERSTED) MAGNETIC MATERIAL
- FLUX DENSITY ACROSS AIR GAP, 9000 GAUSS
- SUPERCONDUCTING COIL
- FORCE/CURRENT RATIO ESTIMATE, 3.56 LB/AMP
- PEAK CURRENT PER ACTUATOR, 0.126 AMP

Position Sensor Characteristics

A modified inductive differential type position sensor was selected for the mirror position sensors because Perkin-Elmer has considerable favorable experience with the device and we know of use at temperatures as low as 20K. These sensors will meet the requirements of the SIRTF secondary mirror actuator.

POSITION SENSOR CHARACTERISTICS

- INDUCTIVE DIFFERENTIAL TYPE (KAMAN INSTRUMENTATION)
- EQUIVALENT RMS INPUT NOISE, MM = $0.64 \times 10^{-7} / \sqrt{Hz}$ (DC TO 5 KHZ)
- FOR A 1-KHZ BANDWIDTH, NOISE = 2.0 NM (SYSTEM SPEC IS 20 NM)
- HAVE BEEN USED AT CRYOGENIC TEMPERATURES TO 20K

Thermal Straps Characteristics

The properties of copper at cryogenic temperatures are quite favorable for the transport of heat from the secondary mirror which is itself a very good conductor because it is beryllium. Note that for the copper strap dimensions of the design, the heat removed will be 2.5W for a 1K temperature difference. The straps are designed to act purely as springs (adding only to the restoring torque of the flexures that mount the mirror). Thus, ample design margin in the thermal performance of the mirror assembly is available. The thermal straps and the position sensors are both located behind the cold aperture stop and baffle located at the secondary mirror postion. They do not have direct line-of-sight access to the focal plane.

THERMAL STRAPS CHARACTERISTICS

- COPPER CONDUCTIVE BANDS, K = 138 W/CM-K AT 5 K
- THERMAL CONDUCTANCE, 2.5 W/K
- DESIGN FOR MAXIMUM STRESS NOT TO EXCEED MICROYIELD STRESS

SECTION 4

FINE GUIDANCE SENSOR ANALYSIS

4.1 INTRODUCTION-FGS SYSTEM ANALYSIS

The flowchart describes the steps and data used for the SIRTF fine guidance sensor (FGS) analysis. The FGS noise-equivalent angle is combined with the CCD pixel size and centroiding precision (fraction of a pixel). These parameters then fix the FGS minimum effective focal length, or equivalently, the FGS plate scale. The plate scale can be combined with the size of the CCD imaging register to determine the solid angle viewed by each CCD. If multiple CCD's are used to increase the net solid angle (to increase the probability of detecting stars) then the focal plane layout must be considered. With the FGS plate scale fixed and finite SIRTF telescope field of view (limited to a 28-arcmin diameter) the physical dimension of the FGS focal plane is limited. Since the imaging register of a packaged CCD chip may only be a fraction of the total chip area, it may be difficult to package enough CCDs into a limited size FGS focal plane. One possible alternate approach would be to package bare CCD dice into a single integrated FGS focal plane.

The solid angle viewed on the sky by the CCDs can be combined with the FGS requirement for probability of detection and an equation relating probability to solid angle and star number density to yield the minimum required areal number density of stars. Using a model of the distribution of stars in our galaxy the number density can be converted to a stellar magnitude limit that must be reached by the FGS. Finally, given the FGS aperture, optical efficiency, etc. The integration time needed to reach a given signal-to-noise ratio (S/N required to obtain the image centroiding precision assumed above) can be calculated.

FGS SYSTEM DESIGN FLOWCHART

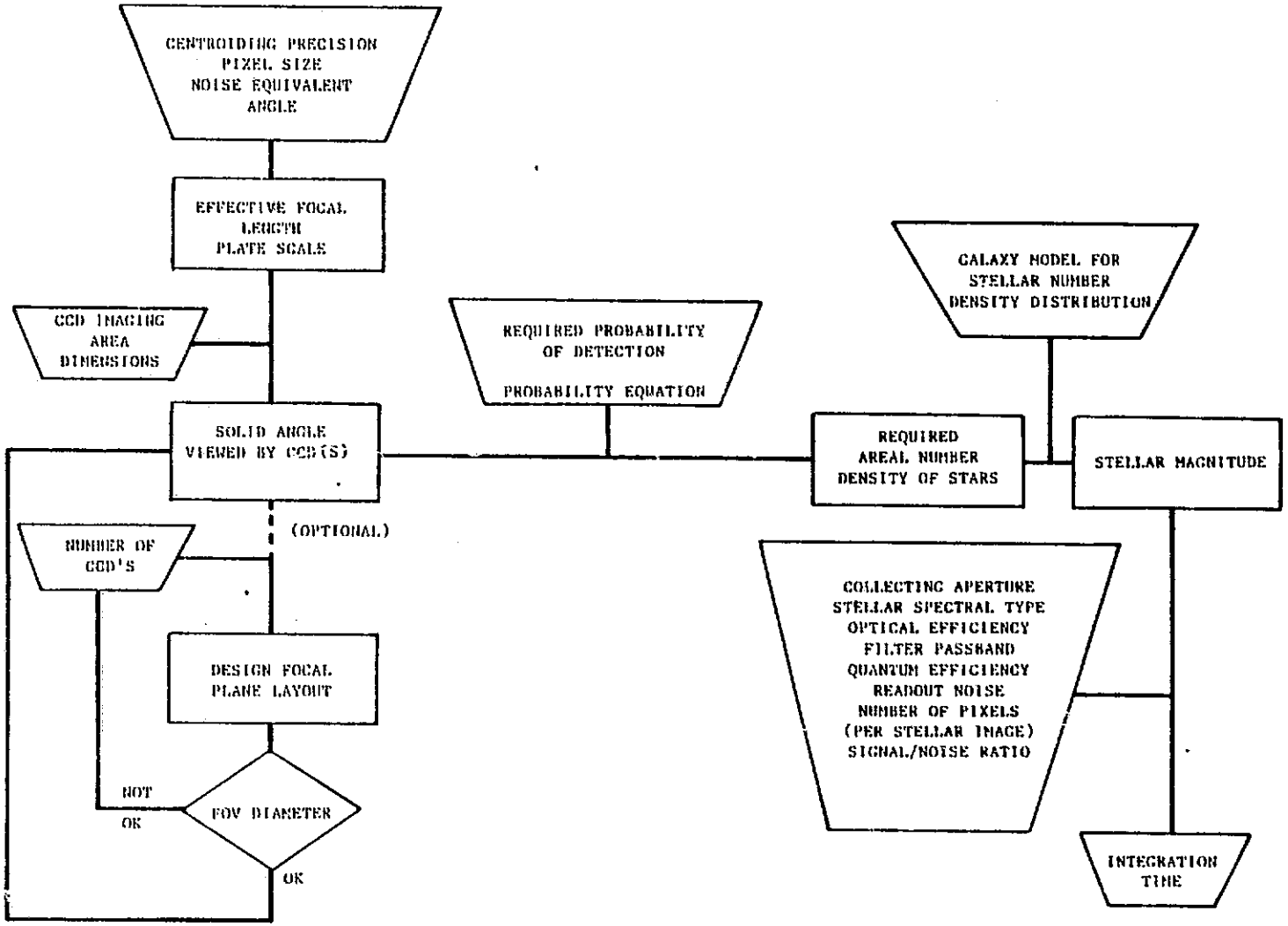

Centroiding Precision Determines FGS Plate Scale

The following figure shows the relationship between centroiding precision and plate scale, and gives an equation to compute the number of CCDs needed if the FOV required and the imaging area of the CCD is known. All equations are derived from the same assumption: the FGS's NEA error budget should correspond to the radial uncertainty in image centroiding. Thus θ arcsec corresponds to d/n micrometers. The effective focal length is simply the inverse of the plate scale (with appropriate scale factors for units.) Once the plate scale is fixed, addition of the FOV requirement and selection of a particular CCD allow a computation of the number of CCD imaging areas needed to cover the appropriate amount of sky.

NUMBER OF CCDs NEEDED FOR FGS FOV

$$\text{Plate scale (arcsec/mm)} = \frac{n\,\theta\ (\text{arcsec})}{d\ (\mu m)} \times 10^3$$

$$\text{Effective focal length (mm)} = \frac{d\ (\mu m)}{n\,\theta\ (\text{arcsec})} \times 206.3$$

$$\text{Number of CCDs} = \frac{A_{FOV}\ (\text{arcmin}^2)}{\left[\frac{n\,\theta\ (\text{arcsec})}{d\ (\mu m)}\right]^2 \quad A_{CCD}\ (\text{mm}^2)} \times 0.0036$$

d = pixel diameter

1/n = fraction of pixel diameter that stellar image centroid is known to

θ = angle corresponding to 1/nth of a pixel diameter

A_{FOV} - solid angle on sky corresponding to CCD(s) total imaging area

A_{CCD} - Imaging area per CCD

Number of CCDs

The number of RCA SID 504 CCDs required is plotted as a function of the product of n (2-D centroiding error is 1/nth of a pixel) and θ (FGS NEA error budget) for three different solid angles on the sky. The SID 504 pixels are actually 16 x 20 μm; the 18 μm average has been used for the calculations. Also shown for several points is one possible pair of $n\theta$ values and the corresponding effective focal length.

The pair of vertical lines corresponds to two different FGS error budgets. Given the value of 1/40 (2-D) pixel centroiding demonstrated by Perkin-Elmer, the 0.05 arcsec budget is consistent with the current SIRTF requirement[1] of 0.25 arcsec pointing stability. The 0.02 arcsec budget corresponds to the 0.1 arcsec goal[1] as described in CR166489, pg. 161.

Note that if RCA SID 501 CCDs (30 μm pixels with an imaging area of 73.7 mm^2) were used, the number of SID 501s needed can be calculated by multiplying the number of SID 504s obtained from the figure by 1.24. The number of 15 μm pixel SID 501s can be derived from the number of SID 504s by multiplying by 0.31.

[1]SIRTF Free Flyer Phase A concept description, PD-1006, May 1984.

NUMBER OF CCDs VS. PRODUCT OF CENTROIDING PRECISION AND NOISE EQUIVALENT ANGLE

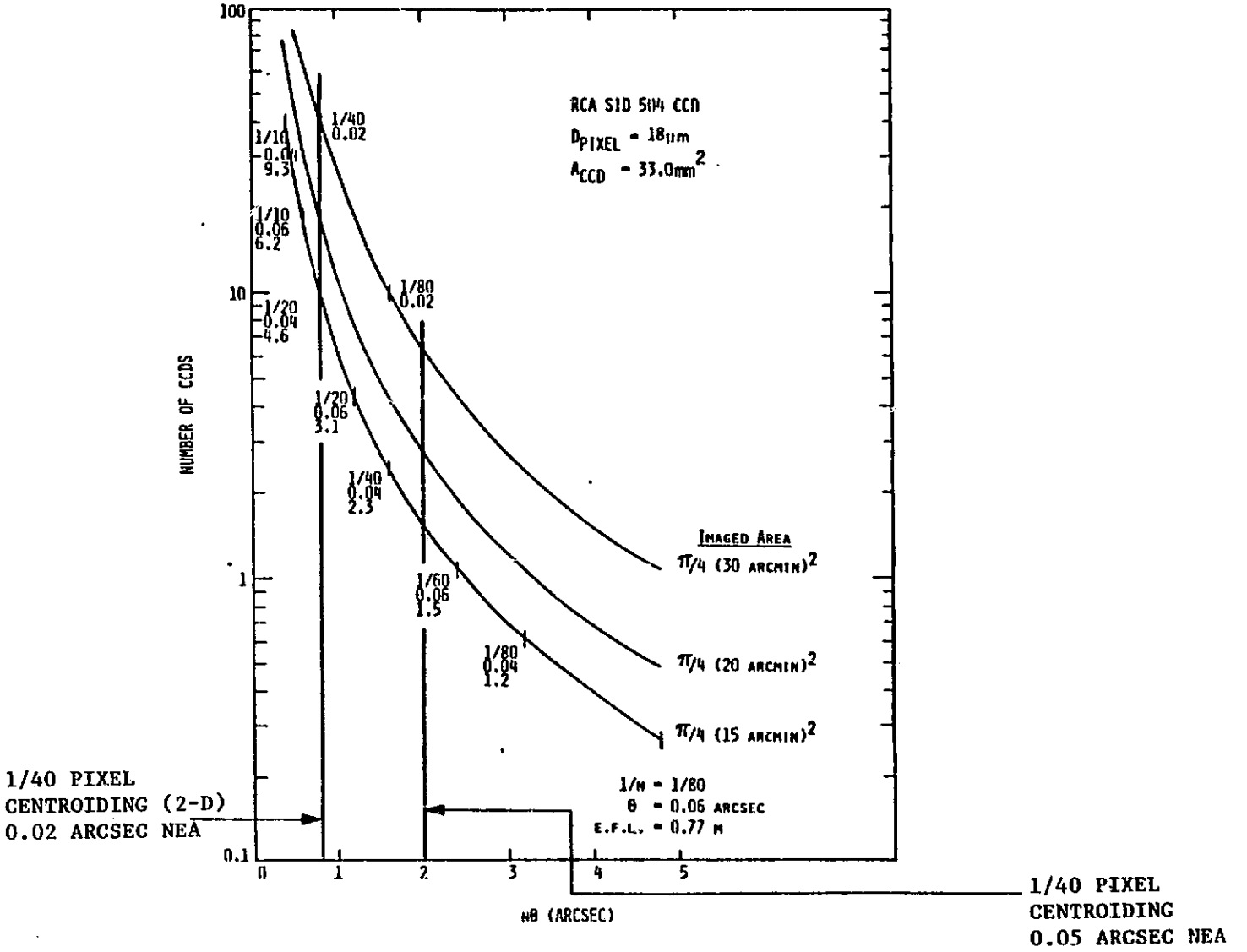

4.2 FGS FIELD OF VIEW SIZING

The integrated star densities used in this study of the FGS were based on the results of a galaxy model by Bahcall and Soneira. The number of stars brighter than or equal to visual magnitude m_v per square degree of sky is plotted and tabulated. While the Bahcall and Soneira model yields values for various galactic latitudes, in this study we have used only the values for the galactic pole ($b = 90^o$) where the stars are least dense.

While the galaxy model is useful for statistical calculations, we note that for a given SIRTF FGS stellar magnitude limit, dynamic range, and field of view, the data exist in the form of photographic plates, (for example the Palomar Sky Survey) for the galactic pole regions such that the statistical approach to the FGS requirement of detecting a pair of stars would be unnecessary.

STELLAR DENSITY AS A FUNCTION OF VISUAL MAGNITUDE AND GALACTIC LATITUDE

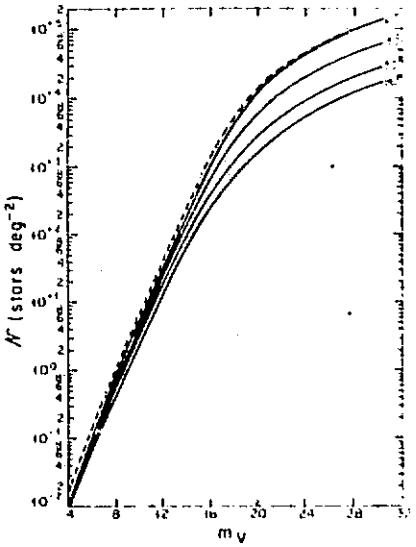

GALAXY MODELS

INTEGRATED STAR DENSITIES, $N(\leq m)$ PER SQUARE DEGREE IN THE V AND B BANDS[1,2]

	m	b=90°	b=50°			b=30°			b=20°		
			ℓ=0°	90°	180°	ℓ=0°	90°	180°	ℓ=0°	90°	180°
V	10	2.38(0)	3.19(0)	3.01(0)	2.90(0)	4.21(0)	3.84(0)	3.62(0)	6.23(0)	5.54(0)	5.13(0)
B		1.42(0)	2.01(0)	1.88(0)	1.80(0)	2.56(0)	2.26(0)	2.13(0)	3.76(0)	3.23(0)	2.99(0)
V	11	5.46(0)	7.77(0)	7.13(0)	6.78(0)	1.04(1)	9.09(0)	8.48(0)	1.55(1)	1.31(1)	1.20(1)
B		3.29(0)	4.85(0)	4.34(0)	4.11(0)	6.29(0)	5.27(0)	4.90(0)	9.43(0)	7.53(0)	6.89(0)
V	12	1.31(1)	1.96(1)	1.72(1)	1.16(1)	2.65(1)	2.16(1)	1.98(1)	3.94(1)	3.04(1)	2.74(1)
B		7.68(0)	1.19(1)	1.02(1)	9.50(0)	1.58(1)	1.22(1)	1.12(1)	2.37(1)	1.72(1)	1.55(1)
V	13	3.05(1)	4.91(1)	4.08(1)	3.73(1)	6.97(1)	5.13(1)	4.60(1)	1.05(2)	7.11(1)	6.27(1)
B		1.76(1)	2.94(1)	2.37(1)	2.16(1)	4.04(1)	2.85(1)	2.56(1)	6.14(1)	3.92(1)	3.47(1)
V	14	6.64(1)	1.19(2)	9.20(1)	8.17(1)	1.85(2)	1.20(2)	1.04(2)	2.92(2)	1.67(2)	1.43(2)
B		3.84(1)	7.05(1)	5.29(1)	4.69(1)	1.04(2)	6.52(1)	5.69(1)	1.64(2)	8.93(1)	7.71(1)
V	15	1.35(2)	2.74(2)	1.93(2)	1.65(2)	4.83(2)	2.69(2)	2.25(2)	8.12(2)	3.85(2)	3.16(2)
B		7.92(1)	1.62(2)	1.11(2)	9.56(1)	2.66(2)	1.44(2)	1.22(2)	4.39(2)	2.01(2)	1.67(2)
V	16	2.53(2)	5.86(2)	3.72(2)	3.07(2)	1.19(3)	5.64(2)	4.51(2)	2.15(3)	8.48(2)	6.62(2)
B		1.53(2)	3.52(2)	2.19(2)	1.81(2)	6.49(2)	3.02(2)	2.45(2)	1.14(3)	4.38(2)	3.49(2)
V	17	4.17(2)	1.15(3)	6.54(2)	5.18(2)	2.44(3)	1.08(3)	8.36(2)	5.25(3)	1.74(3)	1.29(3)
B		2.74(2)	7.13(2)	4.00(2)	3.17(2)	1.52(3)	5.93(2)	4.50(2)	2.79(3)	9.06(2)	6.86(2)
V	18	7.04(2)	2.09(3)	1.06(3)	8.02(2)	5.43(3)	1.88(3)	1.37(3)	1.15(4)	3.26(3)	2.28(3)
B		4.58(2)	1.33(3)	6.71(2)	5.09(2)	3.17(3)	1.07(3)	7.97(2)	6.25(3)	1.74(3)	1.25(3)
V	19	1.10(3)	3.52(3)	1.61(3)	1.17(3)	9.89(3)	2.97(3)	2.07(3)	2.24(4)	5.50(3)	3.65(3)
B		7.24(2)	2.30(3)	1.05(3)	7.62(2)	5.91(3)	1.78(3)	1.26(3)	1.26(4)	3.08(3)	2.11(3)
V	20	1.64(3)	5.56(3)	2.31(3)	1.63(3)	1.64(4)	4.14(3)	2.93(3)	3.89(4)	8.42(3)	5.38(3)
B		1.09(3)	3.69(3)	1.55(3)	1.08(3)	1.01(4)	2.71(3)	1.85(3)	2.29(4)	4.98(3)	3.25(3)
V	22	3.26(3)	1.18(4)	4.39(3)	2.88(3)	3.62(4)	8.02(3)	5.15(3)	8.97(4)	1.61(4)	9.81(3)
B		2.22(3)	7.99(3)	3.00(3)	1.97(3)	2.35(4)	5.26(3)	3.40(3)	5.65(4)	1.03(4)	6.31(3)
V	24	5.66(3)	2.10(4)	7.35(3)	4.62(3)	6.53(4)	1.31(4)	8.08(3)	1.64(5)	2.64(4)	1.56(4)
B		3.94(3)	1.45(4)	5.12(3)	3.24(3)	4.35(4)	8.84(3)	5.51(3)	1.07(5)	1.75(4)	1.04(4)
V	26	8.85(3)	3.31(4)	1.12(4)	6.83(3)	1.04(5)	1.95(4)	1.17(4)	2.60(5)	3.92(4)	2.27(4)
B		6.27(3)	2.32(4)	7.98(3)	4.92(3)	7.07(4)	1.36(4)	8.26(3)	1.75(5)	2.69(4)	1.57(4)
V	28	1.27(4)	4.79(4)	1.57(4)	9.35(3)	1.51(5)	2.70(4)	1.58(4)	3.79(5)	5.44(4)	3.09(4)
B		9.21(3)	3.44(4)	1.15(4)	6.96(3)	1.06(5)	1.95(4)	1.17(4)	2.62(5)	3.89(4)	2.23(4)
V	30	1.70(4)	6.51(4)	2.06(4)	1.19(4)	2.06(5)	3.47(4)	1.98(4)	5.19(5)	7.02(4)	3.91(4)
B		1.26(4)	4.80(4)	1.55(4)	9.03(3)	1.49(5)	2.62(4)	1.52(4)	3.72(5)	5.28(4)	2.98(4)

[1]These numbers were computed using the standard model of Table 1 (main text) with $A_V = 0.15$ and $A_B = 0.28$ (equation 6) for latitudes b of 20° and 30°, and $A_V = A_B = 0$ for latitudes b of 50° and 90°.

[2]For each apparent magnitude, the numbers on the first line are the star densities in the V-band; the numbers on the second line are the B-band star densities.

from J. N. Bahcall and R. M. Soneira, Astrophysical Journal Supplement, 44, 73 (1980).

For CCD imaging areas equivalent to areas covered by FOVs of 15, 20, and 30 arcmin, the probability of detecting one or more $m_v \leq 14$ stars near the galactic pole is 0.962, 0.997, and 0.9999998 respectively. The rapid increase in required FOV with decreasing m_v makes it infeasible for an internal FGS to use brighter stars when pointed near the galactic pole. However, Perkin-Elmer has made an f/1.525 CCD-based star mapper system with a field of view diameter of 5.8 degrees. This design precisely maintains the image size over the entire field with 75 percent of the encircled energy within a 15 μm diameter circle.[1, 2] (The 5.8° FOV would have a 95 percent probability of detecting two $m_v \leq 7$ stars at the galactic pole.) The star mapper optical design could be adapted for an external (boresighted) FGS.

[1] Technology for Space Astrophysics Conference: The Next 30 Years," AIAA/SPIE/OSA," Vol. CP-827, p. 164, 1982.

[2] K. M. Bystricky and P. R. Yoder, Jr., "Optical Design of a Catadioptric Lens with Aberrations Balanced by Aspherizing One Surface," submitted to Applied Optics and presented at OSA Annual Meeting, San Diego, CA, Oct. 1984.

FIELD OF VIEW NEEDED AS A FUNCTION OF VISUAL MAGNITUDE
FOR SEVERAL STELLAR DETECTION PROBABILITIES

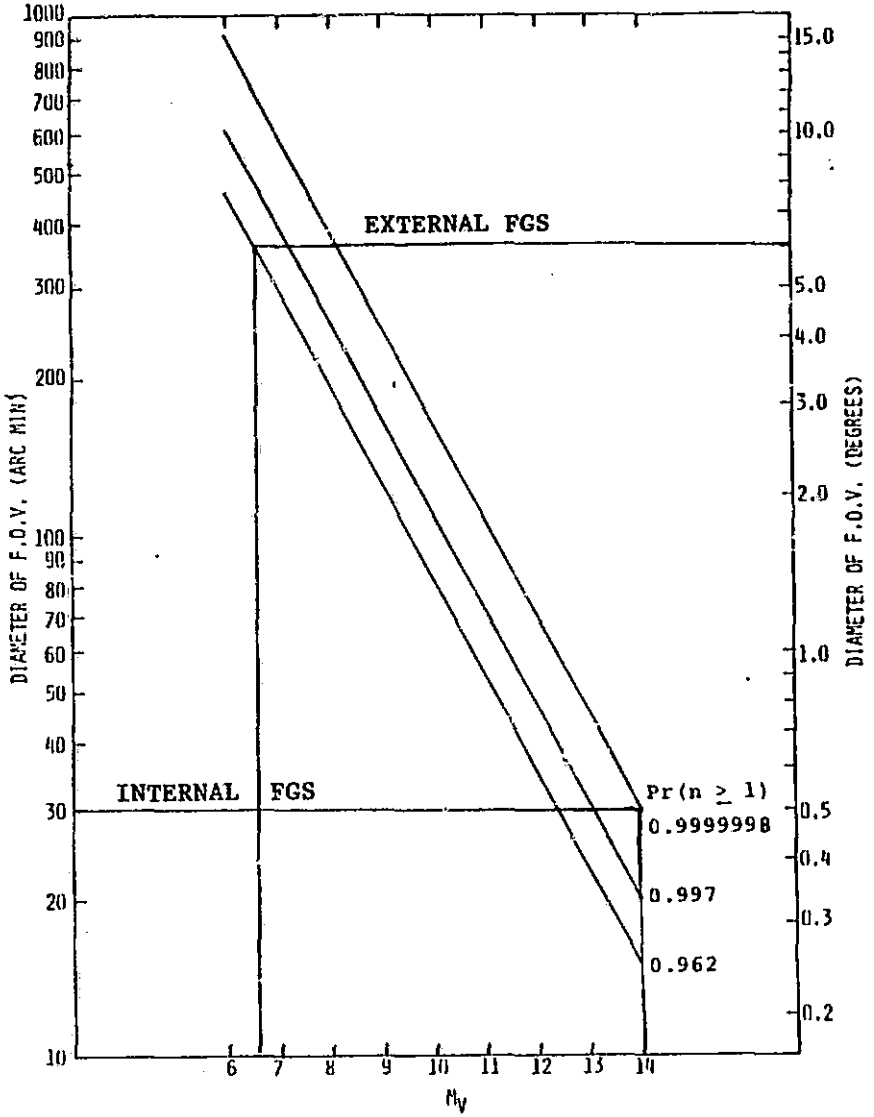

Field of View vs. Centroiding Precision

SIRTF's FGS must have a greater than 0.95 probability of tracking two stars and the internal FGS FOV must be smaller than the 28 arcmin diameter limit of the SIRTF telescope.

The simplest FGS focal plane will have the CCD imaging area inscribed within the FGS FOV. Given an FGS capable of detecting $m_V < 14$ stars, even for the case of having a 95 percent probability of detecting one or more stars, for an FGS noise equivalent angle error budget of 0.02 arcsec each of the stellar image's coordinates would have to be determined to about 1/170* of a pixel. This accuracy is well beyond current capabilities of 1/60 pixel (one-dimension or 1/40 pixel 2-D). If the size of the FGS's FOV were increased in order to obtain a 0.95 probability of detecting two or more stars, then the centroiding precision requirements become even more severe.

A modified approach that decreases the FOV that must be imaged is to allow the FGS to integrate long enough to detect stars as faint as $m_V = 15$; however, even in this case the required centroiding precision is still beyond current capabilities.

An alternate approach would be to use multiple CCDs in the FGS focal plane. If two CCDs are used and each has a $\sqrt{0.95}$ probability of detecting one or more stars then the pair will have a 0.95 probability of detecting two or more stars. Unfortunately, for both $m_V = 14$ and $m_V = 15$ limits, the necessary centroiding precision is excessive. In addition, since each CCD would need such a large FOV (as will be shown), the total FOV needed will exceed what is available from the SIRTF telescope.

In the above comparison we have ignored the (as yet unspecified) requirement that the pair of stars that are tracked must have a minimum separation to allow adequate roll stability. Clearly, such an additional requirement also increases the FOV needed by the FGS, thereby compounding the difficulty.

Relaxation of the 95 percent probability requirement to 85 percent would allow the FOV to be reduced to 0.6 of the former. The net result is that centroiding precision would be easier by about a factor of only 1.25, not enough to bring the necessary precision within the current state of the art. But using the SIRTF requirement of 0.25 arcsec line of sight stability instead of 0.1 arcsec goal dramatically reduces difficulty. Scaling the 0.02 arcsec FGS error budget allocation used in the table by a factor of 2.5 brings the required centroiding precision close or within the state of the art.

*$(= 1/\sqrt{2} \cdot 1/120)$

FIELD OF VIEW VS. CENTROIDING PRECISION

$Pr(n_* \geq 1) = 1 - e^{-NA}$ $P_r(n_* \geq 2) = 1 - e^{-NA} - NAe^{-NA}$ FGS NEA = 0.02 ARCSEC

N = number of stars per unit area, A = FOV of CCD imaging area. At galactic pole $N(m \leq 14) = 66.4$ stars/deg^2, $N(m \leq 15) = 135$ stars/deg^2

	$m_v \leq 14$			$m_v \leq 15$		
	A(arcmin^2)	D_{FOV}(arcmin)	Pixel* Fraction	A(arcmin^2)	D_{FOV}(arcmin)	Pixel* Fraction
One RCA SID 504 CCD						
Pr (n $\geq$ 1) = 0.95 (does not meet SIRTF requirements)	162	19	1/120	79.9	13	1/85
Pr (n $\geq$ 2) = 0.95	257	23	1/150	126	16	1/110
Two RCA SID 504 CCDs						
Pr (n $\geq$ 1) = $\sqrt{0.95}$	199	21 (each CCD)	1/140	98.0	14 (each CCD)	1/95

*Radial (2-Dimensional) fraction of an 18 μm pixel corresponding to 0.02 arcsec.
Note that the precision in each orthogonal direction must be smaller by factor of $1/\sqrt{2}$

NOTE: 1/60 PIXEL (1/40 IN 2-D) HAS BEEN DEMONSTRATED AT PERKIN-ELMER

4.3 CCD-BAND VS. V-BAND PHOTOMETRY

This figure compares the spectra of various stars to both the visual ("V") band filter (taken from Allen's Astrophysical Quantities) and the typical spectral response of a bare RCA CCD. This comparison is important since the basis for stellar population counts is visual magnitude, M_V, but the SIRTF FGS can be designed to take advantage of a CCD's extended wavelength response. A CCD's red sensitivity allows for some design margin when using M_V-based star counts. This derives from the fact that very red stars that have large (faint) V magnitudes would seem preferentially bright to a CCD-based FGS. If the entire CCD wavelength response were assumed for the FGS then for a G0-type star the effective wavelength is 0.64 μm and the effective bandwidth is 0.42 μm.

STELLAR SPECTRAL TYPES COMPARED WITH CCD- AND V-BANDS

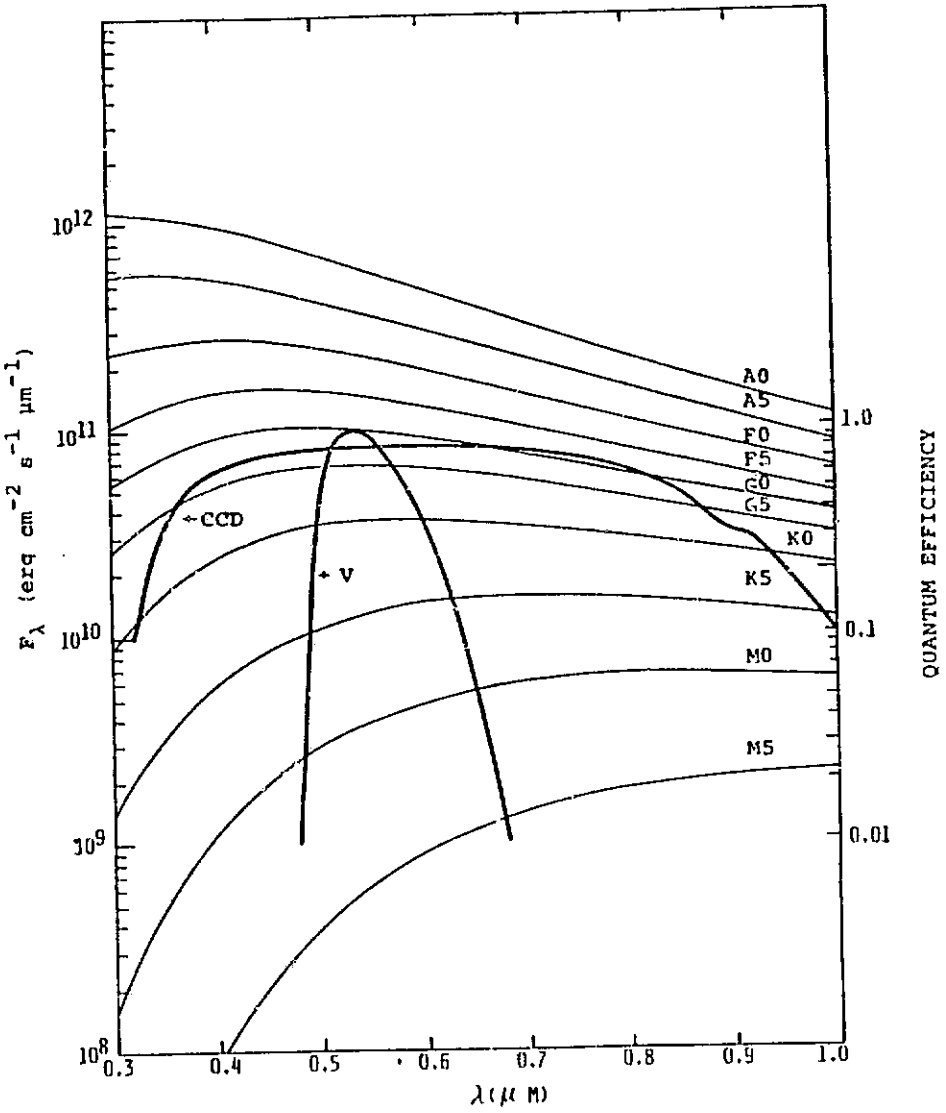

When SIRTF points to a new target, an astronomer (or computer algorithm) checking the new stars being tracked by a CCD-based FGS will need to know the star's spectral types (particularly if one of the stars is unusually red) to allow comparison with V-band-based stellar catalogs. Note that such information is not generally available for faint stars.

COMPARISON OF CCD-BAND AND V-BAND FLUXES

SPECTRAL TYPE	EFFECTIVE TEMPERATURE	$\frac{\int CCD_\lambda F_\lambda d\lambda}{\int V_\lambda F_\lambda d\lambda}$	RELATIVE FLUX
A0	9900	5.04	1.06
A5	8500	4.89	1.03
F0	7400	4.79	1.01
F5	6580	4.76	1.00
G0	6030	4.76	1.00
G5	5520	4.81	1.01
K0	4900	4.96	1.04
K5	4130	5.43	1.14
M0	3480	6.37	1.34
M5	2800	8.88	1.87

This figure compares the photon flux from a G0-type star detected by a CCD-based FGS to the definition of visual magnitude given in Allen's Astrophysical Quantities. The CCD is assumed to have unit peak quantum efficiency and response from 0.32 μm to 1.06 μm; the fluxes are tabulated per square centimeter of telescope collecting aperture.

Since SIRTF's FGS is likely to have transmitting elements the optical properties of the glass must be taken into consideration. It is desirable to have stellar images that are essentially independent of stellar spectral type; as a result it may be necessary to exclude a small portion of the blue wavelengths where CCD's still have some response but the various glasses are difficult to use. For a G0-type star, allowing transmission only longward of 0.4, 0.45, and 0.5 μm would decrease the tabulated N_{CCD} values by 6, 14, and 24 percent respectively. This correction is approximately independent of stellar spectral type; and the 0.45 μm cutoff was used in several of the following analyses but not in the facing-page table.

FLUX IN CCD-BAND VS. VISUAL MAGNITUDE

$$m_v = -2.5 \log_{10}(F_v) - 13.74$$

$$F_v = \int V_\lambda f_\lambda d\lambda \text{ erg cm}^{-2} \text{ s}^{-1}$$

$$N_{CCD} = F_v \frac{\int CCD_\lambda N_\lambda d\lambda}{\int V_\lambda F_\lambda d\lambda} \qquad 0.32 \text{ μm} \leq \lambda \leq 1.06 \text{ μm}$$

m_v	F_v (erg cm^{-2} s^{-1})	N_{CCD} (photons cm^{-2} s^{-1})
0	3.192 E-6	4.58 E6
1	1.271 E-6	1.82 E6
2	5.058 E-7	7.25 E5
3	2.014 E-7	2.89 E5
4	8.017 E-8	1.15 E5
5	3.192 E-8	4.58 E4
6	1.271 E-8	1.82 E4
7	5.058 E-9	7.25 E3
8	2.014 E-9	2.89 E3
9	8.017 E-10	1.15 E3
10	3.192 E-10	4.58 E2
11	1.271 E-10	1.82 E2
12	5.058 E-11	7.25 E1
13	2.014 E-11	2.89 E1
14	8.017 E-12	1.15 E1
15	3.192 E-12	4.58 E0
16	1.271 E-12	1.82 E0

4.4 APERTURE SIZING

The standard equation gives the signal-to-noise (S/N) ratio in terms of the defining parameters listed. We have set the product of dark current and integration time, $i_D(\Delta t)$, to zero in all calculations since the CCD will be cooled and integration times will be short. Thus, the two noise sources that are included are photon shot noise and readout noise. Ignoring dark current fluctuations and (small) noise sources, such as scattered zodiacal light, means that the given equation is an upper limit to the achievable S/N ratio.

SIGNAL-TO-NOISE RATIO

$$S/N = \frac{N_{CCD}\,\eta\,t_{opt}\,\pi\frac{D^2}{4}\,\Delta t}{\left[\,N_{CCD}\,\eta\,t_{opt}\,\pi\frac{D^2}{4}\,\Delta t + n\,i_D\Delta t + n\,N_R^2\,\right]^{1/2}}$$

or, given $i_D = 0$ and solving for Δt

$$\Delta t = \frac{S/\sqrt{N}}{2N_{CCD}\,\eta\,t_{opt}\,\frac{\pi D^2}{4}}\left[S/N + \sqrt{(S/N)^2 + 4nN_R^2}\,\right]$$

N_{CCD} is flux from star in CCD band (photons $cm^{-2}\,s^{-1}$)

t_{opt} is the net optical efficiency

η is CCD peak quantum efficiency

$\pi D^2/4$ is net collecting area (cm^2) after allowing for central obscuration

Δt is net integration time (sec)

i_D is dark current (electrons s^{-1})

N_R is readout noise (electrons)

n is number of pixels per stellar image

Aperture Size vs. Visual Magnitude

The FGS's aperture is plotted as a function of m_v, for a range of values of S/N, N_R, and n. Peak quantum efficiency is taken to be 0.83; all curves are for a t_{opt} (Δt) product of 0.4. Perkin-Elmer's star mapper features a catadioptic optical system with an optical efficiency of 0.8.[1]

An external FGS with a lens corresponding to an unobscured aperture of 30 cm diameter could obtain S/N = 50 to 100 on stars between about m_v = 13 and m_v = 12 in an 0.5 sec integration time.

[1]"Optical Design of a Catadioptric Lens with Aberrations Balanced by Aspherizing One Surface", K.M. Bystrickey and P.R. Yoder, Jr., submitted to Applied Optics.

APERTURE SIZE VS. VISUAL MAGNITUDE (0.8 OPTICAL EFFICIENCY)

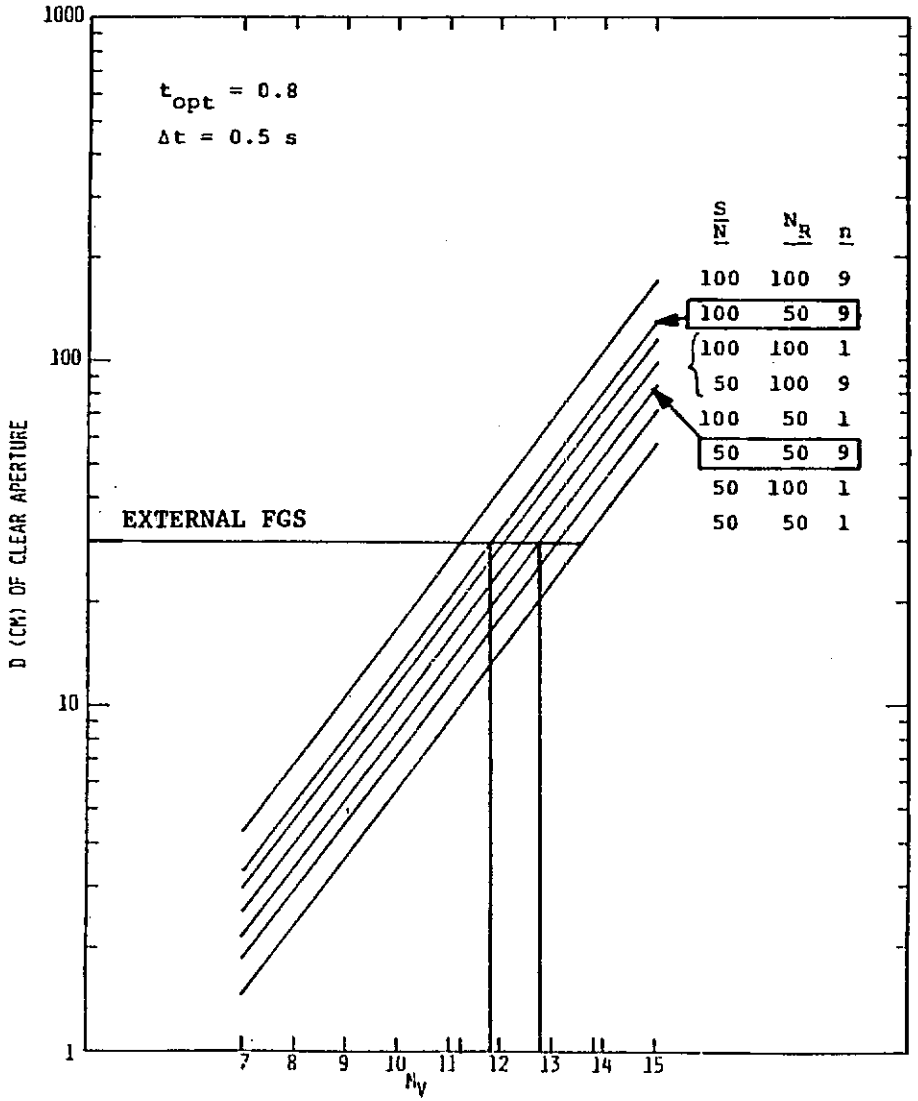

The $t_{opt}(\Delta t) = 0.2$ is consistent with a SIRTF internal FGS and an integration time of 0.5 sec. The optical efficiency for the SIRTF internal FGS can be estimated by

$$t_{opt} = (0.9)^2\,(0.65)\,(0.9975)^2\,(0.9975)^2\,(0.9)^2\,(0.9975)^2 = 0.42$$

where the first term accounts for the SIRTF primary and secondary, the second term for the beamsplitter transmission, the third for the beamsplitter compensator plate, the fourth for a field lens, the fifth for an inverted Cassegrain telescope, and the sixth for a Schmidt plate.

The SIRTF aperture of 85 cm corresponds to 79 cm of "clear aperture" when the linear obscuration of 0.37 is accounted for. If the readout noise is 50 e^- and the stellar image is spread over a 3 x 3 pixel array, then S/N = 100 is achievable with a 0.5 sec integration only for stars brighter than about $m_V = 14$. S/N = 50 could be achieved for stars as faint as about $m_V = 15$.

SIRTF

TIS STUDY

APERTURE SIZE VS. VISUAL MAGNITUDE (0.4 OPTICAL EFFICIENCY)

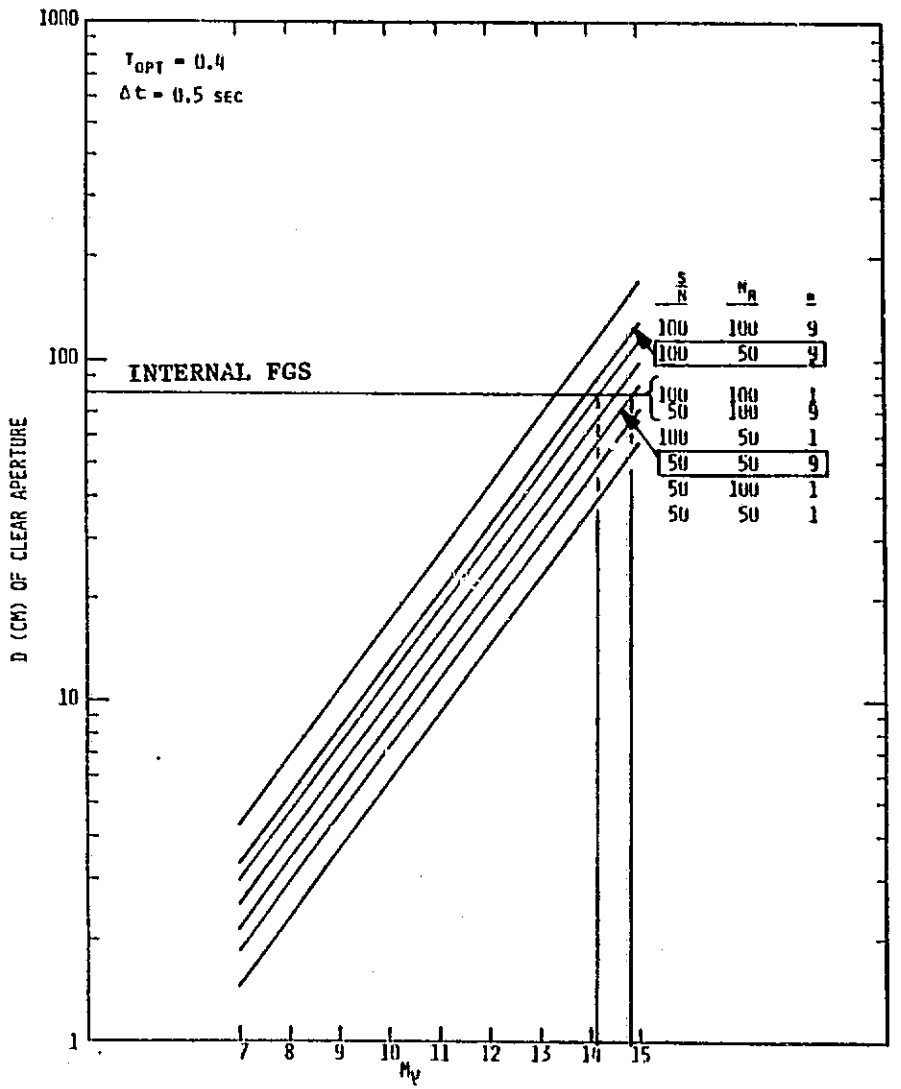

4.5 CCD TRACKER CENTROIDING PRECISION

The figure shows the effect of propagation of error on the uncertainty in the position of a stellar image if the center of mass algorithm is used for centroiding data from a 3 x 3 array of pixels. The number of electrons collected in a pixel is denoted by c_i. The uncertainty in c_i is taken to be the RSS of photon shot noise and CCD readout noise. The uncertainty in pixel location is denoted by σ_{x_i}. Because other possible sources of error (for example time-varying uncertainty in the FGS point spread function) are ignored, this analysis yields only a lower limit to the uncertainty in the centroided position. The equation is derived for only one dimension; if the CCD pixels are approximately square, the radial uncertainty will be about $\sqrt{2}$ larger than given by the one-dimensional case.

PROPAGATION OF ERROR IN CENTER OF MASS ALGORITHM (3 x 3 ARRAY)

$$\bar{x} = \frac{\sum_{1}^{9} c_i x_i}{\sum_{1}^{9} c_i} \qquad \bar{y} = \frac{\sum_{1}^{9} c_i y_i}{\sum_{1}^{9} c_i}$$

Two noise sources contribute to σ_{c_i}

Photon shot noise = $\sqrt{c_i}$

CCD readout noise = N_R

The uncertainty in c_i is $\sigma_{c_i} = \sqrt{c_i + N_R^2}$.

The uncertainty in x_i is υ_{x_i}

For an arbitrary function $z = f(a,b)$

$$\sigma_z^2 = \left(\frac{\partial f}{\partial a} \Big| \bar{a},\bar{b}\right)^2 \sigma_a^2 + \left(\frac{\partial f}{\partial b} \Big| \bar{a},\bar{b}\right)^2 \sigma_b^2 + \left(\frac{\partial^2 f}{\partial a \partial b} \Big| \bar{a},\bar{b}\right)^2 \sigma_a^2 \sigma_b^2$$

Evaluating the CM algorithm (x-direction only)

$$\sigma_{\bar{x}}^2 = \beta \left[1 + \frac{\sum_{1}^{9} (c_i + N_R^2)}{\left(\sum_{1}^{9} c_i\right)^2}\right], \quad \beta = \frac{\sum_{1}^{9} \left[x_i^2 (c_i + N_R^2) + c_i^2 \sigma_{x_i}^2 + (c_i + N_R^2) \sigma_{x_i}^2\right]}{\left(\sum_{1}^{9} c_i\right)^2}$$

If σ_{x_i} = constant σ_x then

$$\sigma_{\bar{x}}^2 = \beta \left[1 + \frac{9N_R^2 + \sum_{1}^{9} c_i}{\left(\sum_{1}^{9} c_i\right)^2}\right], \quad \beta = \frac{\sum_{1}^{9} (x_i^2 c_i) + N_R^2 \left(\sum_{1}^{9} x_i^2\right) + \sigma_x^2 \left[\sum_{1}^{9} c_i^2 + \sum_{1}^{9} c_i + 9N_R^2\right]}{\left(\sum_{1}^{9} c_i\right)^2}$$

Centroiding Error Evaluation

We used the propagation of error equations to compute two examples. In both cases 75 percent of the energy in the stellar image is assumed to fall within the central pixel. The remaining 25 percent is distributed among the surrounding 8 pixels. An $m_v = 14$ star is assumed along with typical parameters of a SIRTF internal FGS. A pixel size of 15 μm is assumed, somewhat smaller than is widely available. The uncertainty in pixel position is taken as 0.2 μm, approximately at the limit of optical microscope capabilities. The 2-dimensional uncertainty in the position of the image centroid because of photon shot noise, readout noise, and pixel position uncertainty is approximately 1/40 and 1/60 of a pixel for 0.5 s and 1.3 s integrations respectively. Since other potential noise sources have been ignored, this is a lower limit to the uncertainty in the image centroid position.

CENTROIDING ERROR DEPENDENCE ON S/N

1	2	3
4	5	6
7	8	9

75 percent of photons in pixel 5

4 percent of photons in each of pixels 2, 4, 6, 8

2.25 percent of photons in each of pixels 1, 3, 7, 9

M_V = 14 G0-type star (9.89 photons cm^{-2} s^{-1}, 0.45 μm 1.06 μm in CCD band)

0.4 optical efficiency; 0.83 CCD peak quantum efficiency

85 cm telescope with 0.37 linear obscuration

50 e^- CCD readout noise on each of the 9 pixels

15 μm pixels; 0.2 μm pixel position uncertainty

	t_{integ} = 0.5 s	t_{integ} = 1.3 s
Total signal (e^-)	8050	20900
S/N	46	100
$\sigma_{\bar{x}}$ (μm)	0.28 (1/53 pixel)	0.18 (1/83 pixel)
2-D CENTROIDING UNCERTAINTY	1/38 pixel	1/59 pixel

Integration Time and Centroid Position Error

The upper table gives lower limits for the integration time needed to achieve S/N = 50 and 100 for two different values of CCD readout noise (10 and 50 electrons) and two different stellar magnitudes (m_V = 14 and 15). Only photon shot noise and CCD readout noise are included. The range of values was calculated for an internal FGS using the SIRTF telescope.

The lower table gives lower limits to the uncertainty in the position of an image centroid determined with the center of mass algorithm. As the position uncertainty depends on S/N ratio and not on the stellar magnitude, the effect of two different CCD pixel sizes is shown. Keeping S/N constant and reducing the noise yields a relatively small improvement in centroiding precision compared to its effect on reducing the integration time.

INTEGRATION TIME AND CENTROID POSITION ERROR
INTEGRATION TIME (SEC.)
INTERNAL FGS

M_v	$N_R = 10e^-$		$N_R = 50e^-$	
	S/N = 50	S/N = 100	S/N = 50	S/N = 100
14	0.20	0.67	0.55	1.3
15	0.50	1.7	1.4	3.2

CENTER OF MASS CENTROID ERROR (3 X 3 ARRAY)
PIXEL POSITION UNCERTAINTY $\sigma_{x_1} = 0.2$ μm

PIXEL (μm)	$N_R = 10e^-$		$N_R = 50e^-$	
	S/N = 50	S/N = 100	S/N = 50	S/N = 100
15	0.22 μm (1/69 pix 1-D) (1/49 pix 2-D)	0.17 μm (1/90 pix 1-D) (1/64 pix 2-D)	0.27 μm (1/57 pix 1-D) (1/40 pix 2-D)	0.18 μm (1/83 pix 1-D) (1/59 pix 2-D)
30	0.35 μm (1/86 pix 1-D) (1/61 pix 2-D)	0.20 μm (1/150 pix 1-D) (1/110 pix 2-D)	0.46 μm (1/65 pix 1-D) (1/46 pix 2-D)	0.25 μm (1/120 pix 1-D) (1/86 pix 2-D)

4.6 CCD-BASED FOCAL PLANE LAYOUTS

To minimize the difficulties (which are nonetheless severe), we minimized the FOV (18.3 arcmin) by requiring only that one or more stars be detected with probability of 0.95 at the galactic pole. Using the RCA SID 504 CCD's imaging area of 33 mm^2 implies a plate scale of 133 arcsec/mm. The error budget of $\sim$0.02 arcsec then corresponds to about 1/120 of a pixel. In each of the two orthogonal directions, stellar images would have to be determined to about 1/170 of a pixel. Note than an FGS error budget of 0.05 arcsec would correspond to 1/48 an 18 μm pixel.

Using the RCA SID 501 CCD with 73.7 mm^2 imaging area would require a plate scale of 89 arcsec/mm. In this case 0.02 arcsec would correspond to 0.22 μm or 1/130 of a 30 μm pixel. Thus, in terms of fraction of a pixel, the centroiding requirement is comparable to the SID 504. We emphasize that increasing the FOV to have a 0.95 probability of detecting two or more stars would make the centroiding requirements yet more severe.

SINGLE-CCD FGS FOCAL PLANE

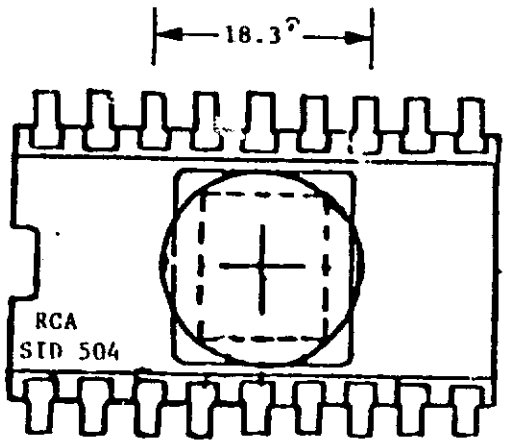

IMAGING AREA

$6.45 \times 5.12 = 33.0\ mm^2$

403 x 16 μm x 256 x 20 μm PIXELS

$N\ (m_v \leq 14) = 66.4\ stars/deg^2$ at Galactic Pole

Note: Binary pairs not rejected

$Pr\ (n \geq 1) = 0.95$

i.e. FGS does not measure roll

$0.95 = 1 - e^{-NA}$ or $A = 0.045\ deg^2 = 162\ arcmin^2$

plate scale $= \sqrt{\frac{162}{33}} = 2.22$ arcmin/mm $= 0.133$ arcsec/μm

For $\theta = 0.02$ arcsec $\equiv 0.150$ μm $= \boxed{\frac{1}{120}}$ (18 μm)

$\frac{\text{CCD IMAGING AREA}}{\text{FOV AREA}} = 0.62$

e.f.l. = 1.55 m (f/1.8)

CONCLUSION: 1/120 OF PIXEL CENTROIDING ACCURACY REQUIREMENT EXCEEDS STATE OF THE ART.

CCD-Pair Focal Plane

Doubling the number of CCDs has two important effects. First, the centroiding requirement is relaxed by $\sqrt{2}$. Second, the diameter of the FGS FOV more than doubles because of the inefficiency of the packing of the packaged CCDs; the CCD imaging areas cover only 15 percent of the total FOV. The 37 arcmin FOV substantially exceeds that available from the SIRTF telescope. Given the 0.02 arcsec FGS error budget, the centroiding requirements are still severe since the FOV is sized for only one or more stars detected with 0.95 probability, the actual centroiding requirements would be yet more stringent. (A pair of RCA 501 CCDs would require a 35 arcmin diameter FOV.) However, the multiple-CCD-based FGS has the clear advantage of at least partial redundancy.

CCD-PAIR FOCAL PLANE

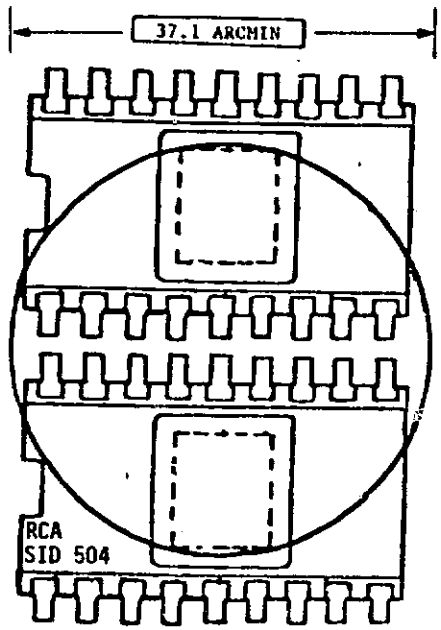

$P_r\ (n \geq 1) = 0.95 \quad m_v \leq 14$

plate scale = $\sqrt{\frac{162}{33*2}} = 1.57$ arcmin/mm

$\theta = 0.02$ arcsec $\equiv 0.21\ \mu m = \boxed{\frac{1}{85}}\ (18\ \mu m)$

$\frac{\text{CCD IMAGING AREA}}{\text{FOV AREA}} = 0.15$

CONCLUSION: FOV EXCEEDS SIRTF TELESCOPE AND CENTROIDING REQUIREMENT EXCEEDS STATE OF THE ART.

Rotating CCD-Pair Focal Plane

If we allow the pair of CCDs to rotate about the optical axis, the CCD imaging area is effectively increased by allowing the imaging area to cover 83 percent of the total FOV area. A diameter of about 16 arcmin would result in a 95 percent probability that one or more $m_v \leq 14$ stars would fall within the annular area when SIRTF was pointed toward the galactic pole. This configuraiton implies that 1/37 (radial) of a pixel centroiding would correspond to the 0.02 arcsec FGS error budget; this value is at the current state of the art.

While this approach is feasible in terms of centroiding, especially if the FGS error budget were 0.05 arcsec, the FOV cannot be easily scaled to provide a high probability of detecting two or more stars. The difficulty results from the fact that although a modest increase in FOV (to 20 arcmin diameter) would result in a 0.95 probability of two galactic polar region stars in the annular area, since the pair of CCDs rotate together, in general one of the CCDs will not be located at the second stellar image. With the plate scale shown, the second CCD has only a 25 percent probability of detecting a second galactic polar region star.

While there are significant advantages to rotating the CCD pair, this approach will not meet the requirement to detect two stars except near the galactic plane. In addition, the mechanical positioning requirements are severe: while the mechanism could step in 12-degree increments, the pixels must repeatedly be placed (or their position measured) with a precision of a few tenths of a micrometer.

ROTATING CCD-PAIR FOCAL PLANE

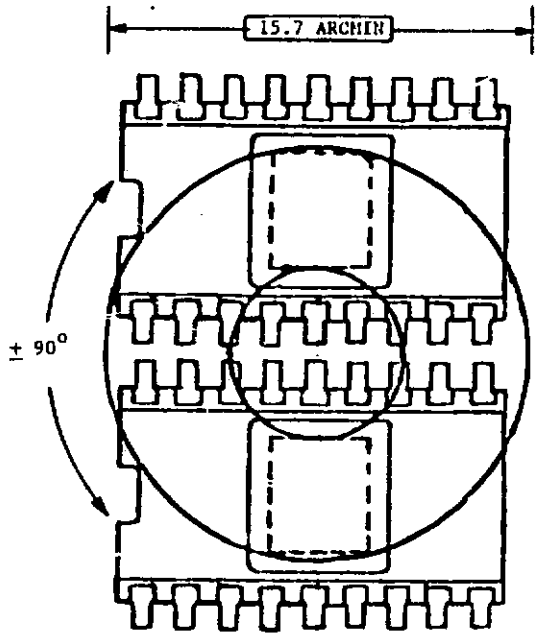

Rotate pair of CCD's ± 90° to cover entire annular area.

Pr (n ≥ 1) = 0.95 at Galactic Pole
(Binary stars not rejected)

plate scale = 0.692 arcmin/mm

θ = 0.02 arcsec ≡ 0.48 μm = $\boxed{\frac{1}{37}}$ (18 μm)

$\frac{\text{CCD ACCESSED AREA}}{\text{FOV AREA}} = 0.83$

Probability that 2nd CCD also sees 1 or more stars is $\boxed{0.25}$ at Galactic Pole.

CONCLUSION: IMAGE CENTROIDING REQUIREMENT WITHIN THE STATE OF THE ART, BUT PROBABILITY OF ACQUIRING A SECOND STAR (FOR ROLL STABILIZATION) IS TOO LOW

Quad-CCD Focal Plane for $m_V \leq 15$

This design for SIRTF's internal FGS focal plane would meet the requirement to detect two stars near the galactic pole with 95 percent probability while keeping the centroiding requirements within the current state of the art. The design is based on the following approach.

At the galactic pole there are 135 $m_V \leq 15$ stars/deg^2. We have allocated a pair of CCD imaging areas for each of the two required stars; then a pair of CCDs must have a $\sqrt{0.95}$ probability of detecting one or more stars. This corresponds to 98 arcmin^2 per CCD pair. With RCA SID 501 CCDs, each with an imaging area of 73.7 mm^2, the plate scale necessary to get the FOV needed is 48.9 arcsec/mm.

The standard RCA SID 501 CCD has 30 μm pixels. Assuming that 1/40 pixel radial centroiding uncertainty corresponds to 0.02 arcsec implies a plate scale of 27 arcsec/mm. This plate scale would not be sufficient to have a 95 percent probability of detecting two $m_V \leq 15$ stars at the galactic pole. But RCA has recently produced a version of the SID 501 with 15 μm pixels. In this case, setting 0.02 arcsec to correspond to 1/40 of a 15 μm pixel results in a 53 arcsec/mm plate scale. As this value slightly exceeds the plate scale needed to get a sufficiently large FOV, the new 15 μm SID 501 version would meet the requirements.

An additional design constraint, however, is the limited, 28 arcmin FOV diameter of the SIRTF telescope. If the CCD dice are left in their standard package, the four imaging areas would require a 34 arcmin diameter FOV. The figure shows bare SID 501 dice mounted on a single cooled substrate. In this case the imaging areas fit within a 25.3 arcmin diameter FOV. The set of leads between the dice must be run out underneath the dice.

It is not RCA's policy to sell unpackaged CCD dice. They may be willing to do so; if not, if should be possible to remove the dice from their package, but this will probably be a low-yield process.

In a sense, this design has a larger FOV than may be needed to detect two $m_V \leq 15$ galactic pole stars with 0.95 probability. Given Poisson statistics, a 127 arcmin^2 area has a 0.95 probability of having two stars within it. The four CCDs cover a total of 196 arcmin^2 because of the more stringent approach, that is one or more stars on each pair of CCDs. Thus three CCDs (147 arcmin^2) provide adequate FOV if the probability that the pair of stars might be too close together for adequate telescope roll stabilization is ignored. In this sense, the four-CCD focal plane contains one redundant CCD. For any given star field only two CCDs need to be read out simultaneously.

Note that $m_V \leq 15$ stars are necessary to limit the FOV required to detect two stars. Given a CCD readout noise of 50 electrons (each of 9 pixels), optical efficiency of 0.4 and RCA CCD response between $0.45 < \lambda < 1.06$ m, a signal-to-noise ratio of 50 could be achieved with a 1.4 sec integration. An S/N = 100 would require a 3.2 sec integration.

QUAD-CCD DICE FOCAL PLANE

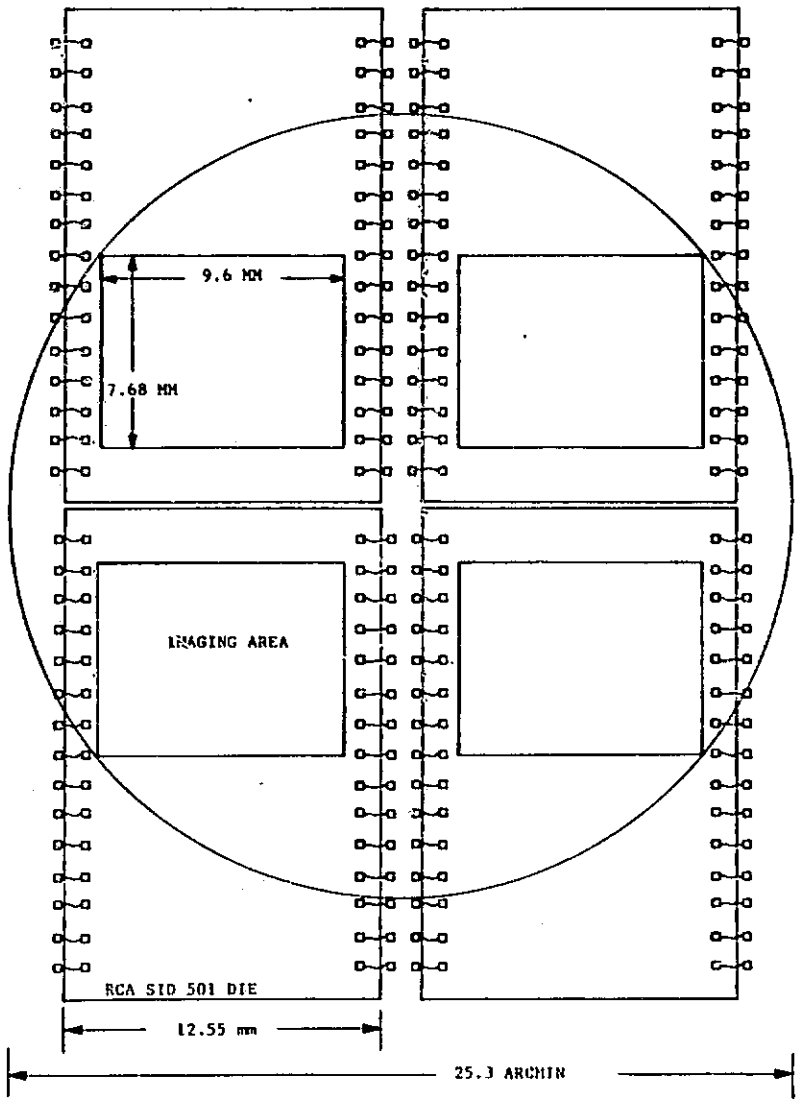

CONCLUSION: MEETS REQUIREMENTS IF INTEGRATION TIME > .5 SEC. IS TOLERABLE.

Quad-CCD Focal Plane for $m_v \leq 14$

The table shows the effect of limiting the FGS integration time in such a way that only stars brighter than $m_v = 14$ (rather than $m_v \leq 15$ as described previously) can be centroided with adequate precision. The FOV must be double the $m_v \leq 15$ FOV to maintain the 0.95 probability of detecting two or more $m_v \leq 14$ stars. The plate scale for the quad RCA SID 501 CCD concept is then 69.8 arcsec/mm, implying an FGS FOV diameter of 49 arcmin. Hence, this concept would exceed the FOV available for an internal FGS but would be suitable for an external FGS. (Limiting the FOV to the 28 arcmin diameter maximum of the SIRTF telescope would lead to the quad-CCD design having only a 49 percent probability of detecting two or more $m_v \leq 14$ stars at the galactic pole.)

Given the 0.02 arcsec error budget, centroiding would have to be done to 1/105 (2-D) of a 30 μm pixel. While 1/105 substantially exceeds the current centroiding state of the art (1/40 pixel in 2-D, 1/60 in 1-D), the 0.052 arcsec value corresponds to 1/40 of a 30 μm pixel. Thus the external FGS quad-CCD concept for $m_v \leq 14$ would be adequate for the current SIRTF pointing requirement of 0.25 arcsec line of sight stability, and the $m_v \leq 15$ concept (with the 15 μm pixel version of the SID 501) would be necessary only for an 0.02 arcsec FGS error budget corresponding to the 0.1 arcsec stability goal.

QUAD CCD FOR $m_v \leq 14$

- NEED 199 ARCMIN^2 PER CCD PAIR
  (2.0 TIMES SOLID ANGLE FOR $m_v \leq 15$)

- NEED 69.8 ARCSEC/MM PLATE SCALE
  ($\sqrt{2}$ TIMES PLATE SCALE FOR $m_v \leq 15$)

- NEED 49 ARCMIN DIAMETER FOV

- SUITABLE FOR EXTERNAL FGS

PIXEL (μm)	FRACTION OF PIXEL FOR 0.02 ARCSEC (2-D)	ARCSEC FOR 1/40 PIXEL
15	1/52 (1/74, 1-D)	0.026
30	1/105 (1/150, 1-D)	0.052

We show here a figure from a 3 November 1979 Technical memo recently brought to our attention by W. F. Hoffmann and J. R. P. Angel of the University of Arizona. The part of the design that we find most interesting is the concept of projecting the optical beam out to a warm area behind the MIC. In the collimated space it may be possible to incorporate a star selector mechanism similar to the Hubble Space Telescope's Fine Guidance Sensor that would allow the SIRTF FGS to function with $m_V < 14$ stars without requiring large number of CCDs or image centroiding beyond the current state of the art. The fiducial lights allow the relative motion between the warm part of the FGS and the SIs to be measured and hence compensated for. The images of the fiducial lights would be located in the corner(s) of the CCD(s) and would have a very minor effect on the FOV usable for stellar images. Several areas require further study:

- Effect on FGS optical efficiency of both the series of windows in the MIC and other optics that the beam must pass through
- The extent to which the fiducial lights reduce the need for great structural rigidity between the FGS and the SIs
- Thermal effect of the window on the MIC head load
- An intensified CCD may be necessary to keep the FGS integration time short.

OPTICS FOR PROJECTING OPTICAL GUIDING BEAM OUT OF MIC

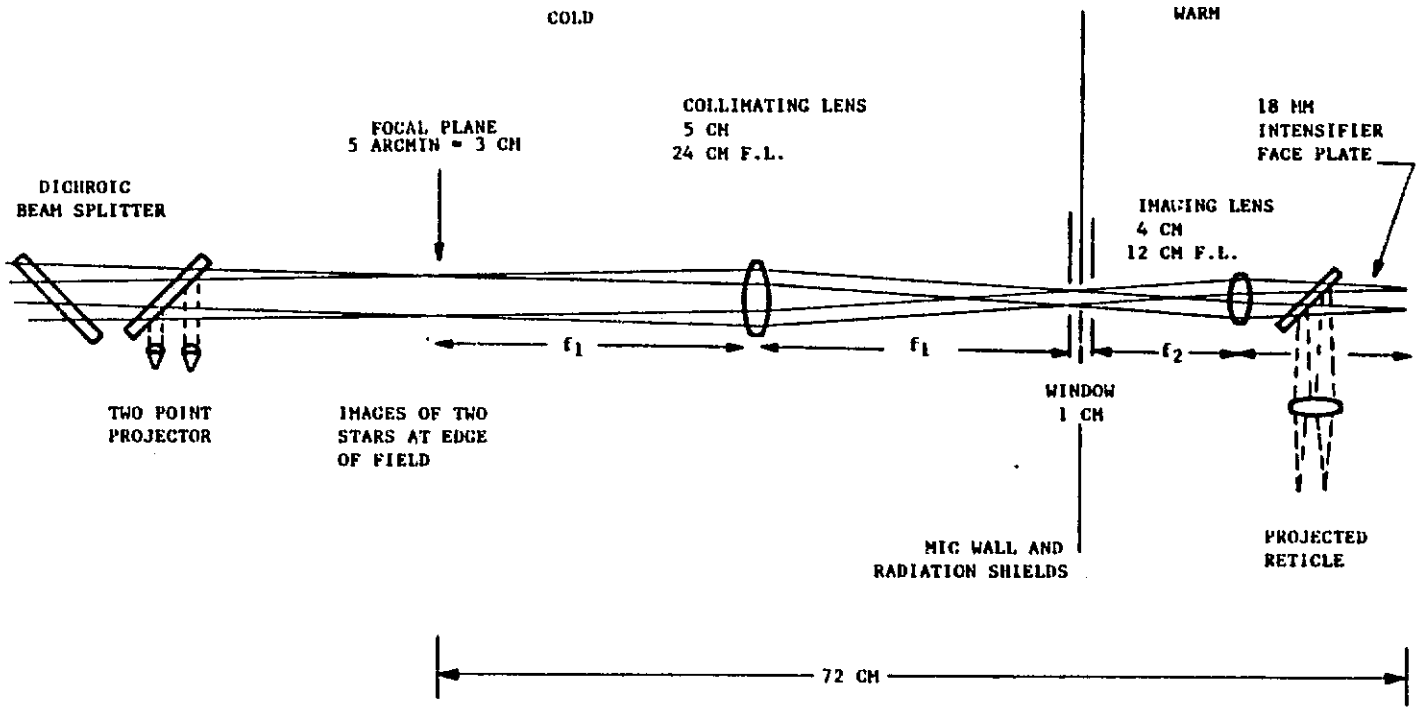

4.7 NEP CONTRIBUTION OF A SMALL MIRROR ON SIRTF TELESCOPE APERTURE

An external (boresighted) FGS must have some means of relating its line of sight to that of the SIRTF telescope. One possible approach would be to place, at the edge of the SIRTF focal plane, a light source that would shine out the aperture after reflection on the secondary and primary mirrors. (For serviceability the source could be mounted outside the MIC with light coupled in through a fiber optic cable.) A small "pick-off" mirror in the aperture would then reflect some of the light through windows in the telescope's forebaffle and vacuum vessel to an external FGS. Rotation of the external FGS in relation to the telescope's line of sight would then be sensed as a displacement of the image of the light source. This section explores the contribution of such a mirror to the noise equivalent power (NEP).

The small mirror located on the spider would be oriented at 45° in relation to the optical axis to reflect a light beam (originating at the focal plane) through a window in the forebaffle and into an externally-mounted detector. Changes in the orientation of the external FGS in relation to the telescope line of sight would then result in a displacement of the image of the light source. SIRTF's performance considerations may require that the mirror be hinged in such a way that it does not continuously protrude beyond the spider; this would, of course, require that the external FGSs motion be negligibly small (or known) during non-reference periods.

LOCATION OF MIRROR

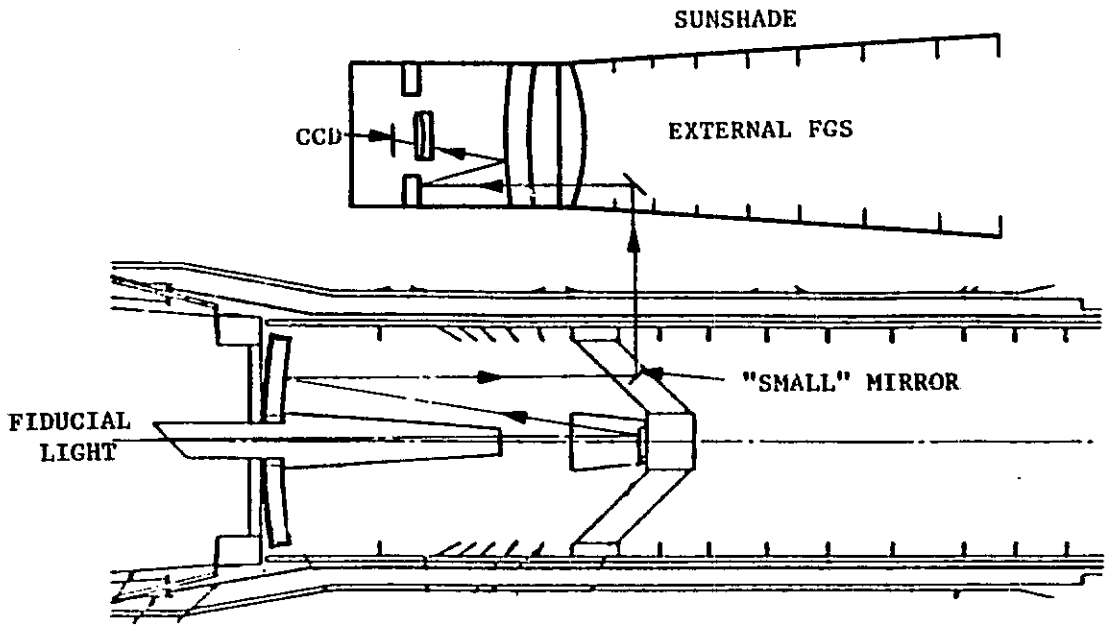

d = DIAMETER OF "SMALL" MIRROR = 2.5 CM

D_p = DIAMETER OF PRIMARY MIRROR = 85 CM

D_s = DIAMETER OF SECONDARY MIRROR = 10.7 CM

l_{ps} = l_m = PRIMARY-SECONDARY SPACE = 170.94 CM

l_{bfl} = BACK FOCAL LENGTH = 85.34 CM

NOTE: The annular SfHe tank (not shown) would cause the external FGS to be located away from the SIRTF telescope.

NEP Equations

We used these equations to calculate the contribution to SIRTF's NEP for a small mirror emitting into the aperture. The solid angle includes a small correction to account for the variation with wavelength in IR detector FOV due to diffraction.

NEP EQUATIONS

$$NEP = \left[\varepsilon N_\lambda \, (\Delta\lambda) \, \frac{\pi}{4} \, d^2 \, \Omega\right]^{1/2} \frac{hc}{\lambda}$$

$$\text{Planck function } N_1 = \frac{2c}{\lambda^4}\left(\frac{1}{e^{hc/\lambda kT}-1}\right)$$

Solid angle of small mirror as seen by detector is

$$\Omega = \pi \left[\frac{D_s\left(\frac{d}{2} + 1.22\, l_m \frac{\lambda}{D_p}\right)}{D_p\left(l_{ps} + l_{bfl}\right)}\right]^2$$

ε = mirror emissivity

d = diameter of small mirror

D_p = diameter of primary

D_s = diameter of secondary

l_m = small mirror - primary mirror spacing

l_{ps} = primary-secondary spacing

l_{bfl} = back focal length

NEP From a Small Mirror

The following table gives the NEP resulting from placing a 2.5 cm mirror in SIRTF's aperture as a function of mirror temperature and wavelength. The mirror's emissivity is taken to be one percent; the detector bandwidth is 50 percent of the tabulated wavelength. The tabulated values are slight overestimates since the peak value of N_λ in the detected band was multiplied by the bandwidth rather than evaluating the actual integral.

NEP FOR A 2.5-CM DIAMETER MIRROR

T(K) \ λ (μm)	2	5	10	20	50	100	200	500
10		7.8E-64	1.4E-39	7.6E-28	2.4E-21	1.4E-19	4.4E-19	5.6E-19
20		7.7E-39	4.3E-27	1.3E-21	7.7E-19	2.5E-18	2.8E-18	1.6E-18
50	7.6E-38	7.6E-24	1.3E-19	7.6E-18	2.4E-17	3.0E-17	1.5E-17	3.8E-18
100	2.4E-25	7.6E-19	4.3E-17	1.3E-16	1.7E-16	8.3E-17	2.8E-17	5.5E-18
200	4.2E-19	2.4E-16	7.6E-16	8.6E-16	4.6E-16	1.6E-16	4.6E-17	8.2E-18
300	5.1E-17	1.6E-15	2.0E-15	2.3E-15	7.0E-16	2.1E-16	5.8E-17	1.0E-17

Required NEP

This figure plots the NEP's resulting from the 2.5-cm mirror and compares them with a "required NEP" derived from the equation

$$NEP = 10^{-17} K_\lambda \left(\frac{D}{80\ cm}\right) \left(\frac{\theta}{1\ arcmin}\right)$$

given in CR166489, Volume 2 (TIS Study Final Report), page E-17. Page E-19 tabulates the values of K_λ. D was taken to be 85 cm; θ was taken to be 2.44 λ/D. A one percent emissivity mirror whose temperature is below 20K would meet the NEP requirements. As a mirror mounted on the secondary mirror spider is expected to be at about 6K this approach to referring an external FGS to SIRTF's LOS is feasible. Note that the window needed in the forebaffle would also have to be cold and low emissivity.

We have identified an approach that allows an external FGS to be referred to the telescope's line of sight. Such an approach, however, would result in a telescope asymmetry and would complicate forebaffle and vacuum vessel design. A straylight analysis would be required to assess the effect of the small mirror on SIRTF straylight rejection.

NEP DUE TO SMALL MIRROR VS. WAVELENGTH

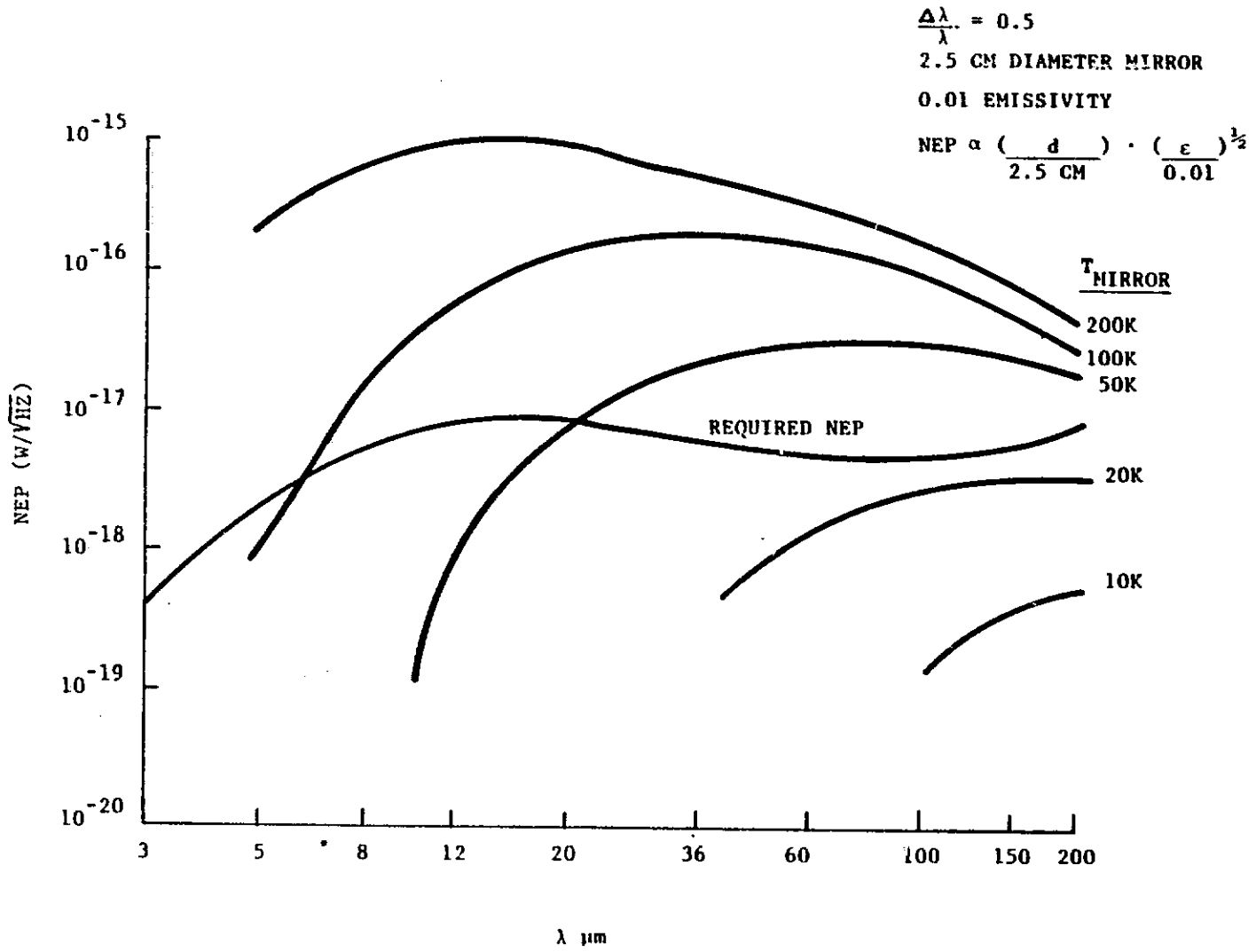

4.8 FIBER OPTIC IMAGE DIVIDER

One alternative to locating the FGS's CCD detector in the MIC would be to couple the optical light out to a warm area via four fiber optic strands. While the FIRAS instrument on the COBE satellite will use fiber optics at cryogenic temperatures, this approach is not applicable to the SIRTF FGS since optical fiber diameters are much too large. However, SIRTF may be able to use an optical fiber that has a divider polished onto its end. The "selfoc" optical divider shown terminates in a tetrahedron; a precision mechanism moves the apex of the divider to the image of a guide star. Light falling on each quadrant travels down one of four separate optical fibers to a detector outside the MIC. The relative intensity in the four quadrants would be used to determine the centroid of the image. Four photomultipliers (low quantum efficiency) or four separate areas of a CCD would be the detectors.

This photograph shows the tetrahedral surface of NSG America's optical divider OPDV-5G4. The diamater of the tetrahedral surface is approximately 1.5 mm. The optical fiber is optimized for wavelengths of 0.8-0.9 μm. We attempted to clean the foreign matter from the tetrahedral surface without success; the material may be excess glue used by NSG to mount the divider in its connector. The quality of the edges and apex may be suitable for use of this type of device as part of SIRTF's FGS.

NSG AMERICA OPDV-5G4 TETRAHEDRAL OPTICAL DIVIDER

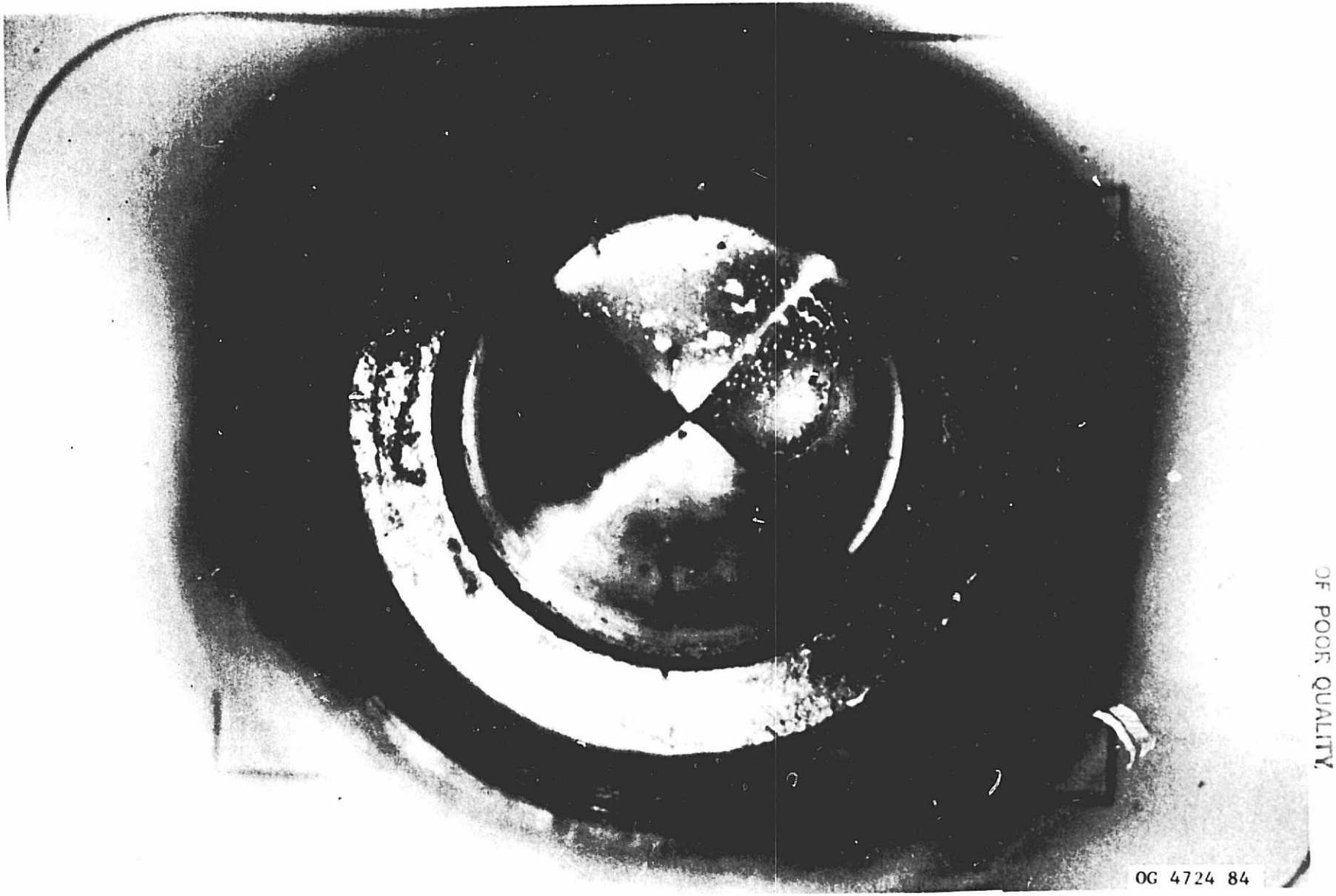

Optical Divider

The sample optical divider we received from NSG is clearly unsatisfactory for SIRTF. However, the rapidly developing fiber optic and merits close attention. Additional analysis would be required to determine whether a more carefully fabricated image divider would have the necessary optical efficiency. The major drawback of the fiber optic image divider is that a precision mechanism would be required to operate at cryogenic temperatures.

NSG AMERICA OPDV-5G4 TETRAHEDRAL OPTICAL DIVIDER (ALTERNATE VIEW)

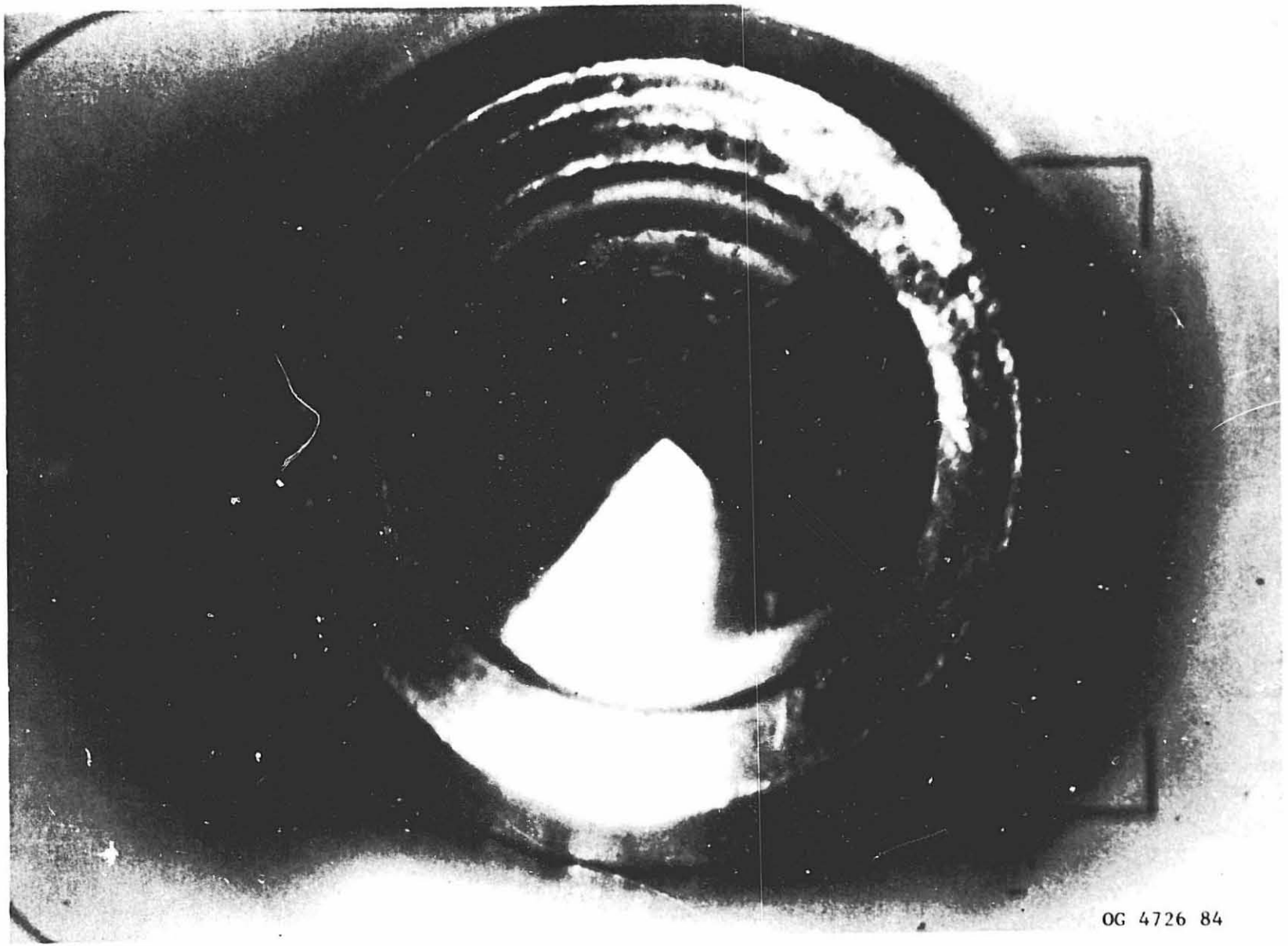

OG 4726 84

4.9 POTENTIAL APPLICATIONS OF SPACE TELESCOPE TECHNOLOGY

The Optical Telescope Assembly (OTA) of the Hubble Space Telescope contains three fine guidance sensors (FGSs). Each FGS is capable of providing pointing error signals at a 40-Hz sampling rate on a single 15th magnitude star. Pitch, yaw and roll pointing control signals are derived from the output of two FGSs operating simultaneously.

The FGSs are very closely coupled to the science instruments (SIs) through a common invar mounting ring located on the focal plane structure some distance ahead of the telescope focal plane. Both the SIs and the FGSs are held to this ring by astronaut-operable latches that permit on-orbit replacement and re-registration of the SIs and FGS.

Although much of the telescopes optical path is common to both the FGSs and the SIs, approximately 0.5 meter just in front of the focal plane is not. The alignment stability of the image is provided by the mechanical rigidity of the SIs, FGSs, and focal plane structure and latches.

EXPLODED VIEW OF THE OTA

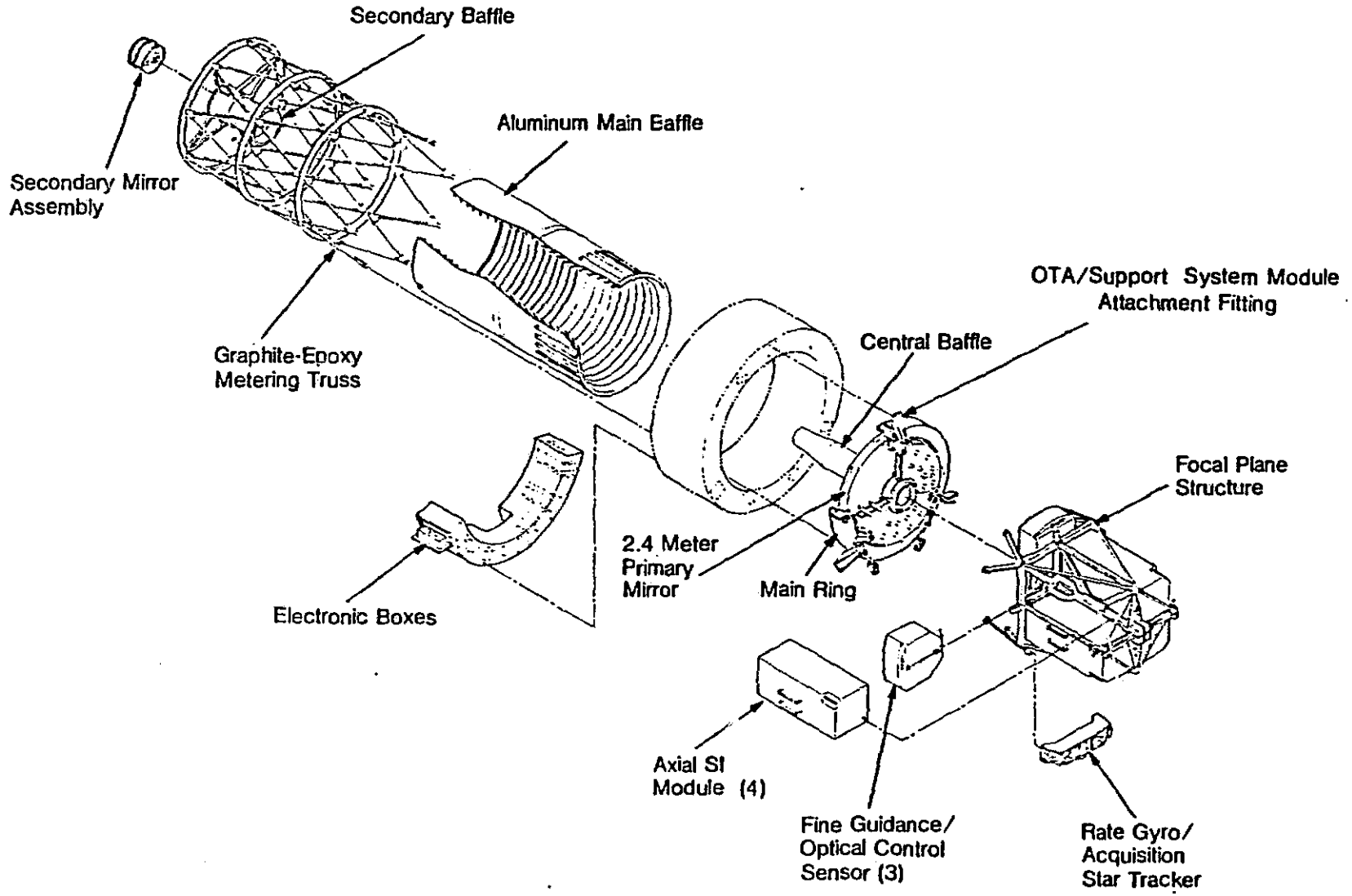

The Hubble Space Telescope's Field of View

The Hubble Space Telescope's field of view is divided into several parts by fold mirrors that extend into the beam in front of the focal plane. The shaded bands around each portion represent the vignetting that occurs because the fold mirrors are not at the focal plane.

The three fine guidance sensors are allocated an annular part of the field extending from 10.2 arcmin to 14.0 arcmin. Two of the FGSs are operated for pointing control while the third FGS is used for astrometric measurements.

FIELD OF VIEW

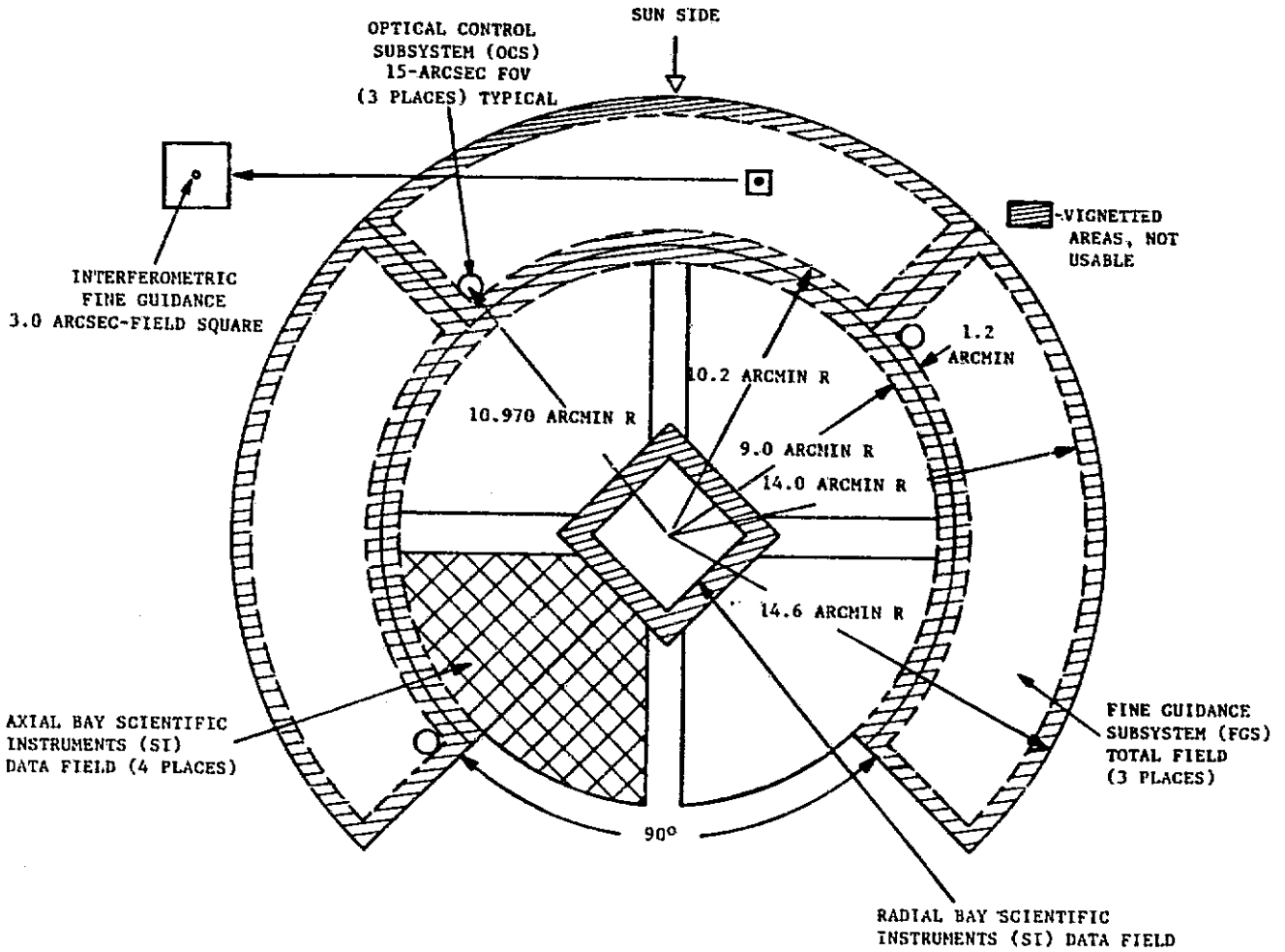

Fine Guidance Subsystem

The fine guidance sensor, shown schematically for one sensing axis, consists of a collimator; refractive astigmatism corrector lens group; the two star selectors (to be described in detail below); Koesters prism, wavefront, tilt-sensing interferometer, condensing lenses; and photomultiplier photodetectors.

The effect of telescope mispointing is to produce a tilt of the optical wavefront in the collimated space in the FGS, and the Koesters prism is adapted to sensing this tilt. The optical system is designed to place an image of the pupil of the telescope at the base of the prism. A field stop between the condensor lens and the phototube limits the field of view of the FGS to 3 arcsec in order to reduce the amount of stray background light sensed.

FINE GUIDANCE SUBSYSTEM, SIMPLIFIED OPTICAL SCHEMATIC DIAGRAM

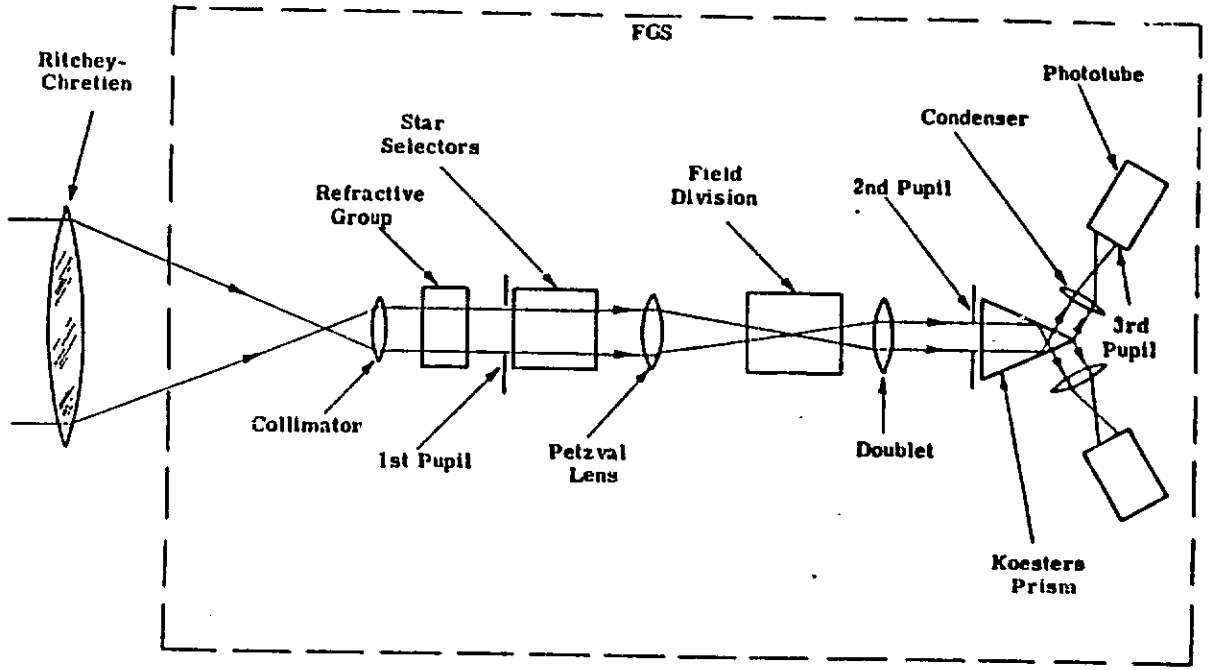

Risley Prisms Used to Deviate Line of Sight

The FGS's small instantaneous field of view must coincide with the position of the guide star preselected for each observation. The star selector assemblies are the operational devices for matching the null point of the sensor to the known location of the guide star. The principle of operation of the star selectors is based on the so-called "Risley Prisms". Each prism deviates the light rays an amount δ. When the prisms are both in the beam as shown, the deviations add vectorially. Rotation of the prisms in relation to each other varies the amount of deviation, while rotation of the prisms as a set varies the direction of the deviation.

RISLEY PRISMS

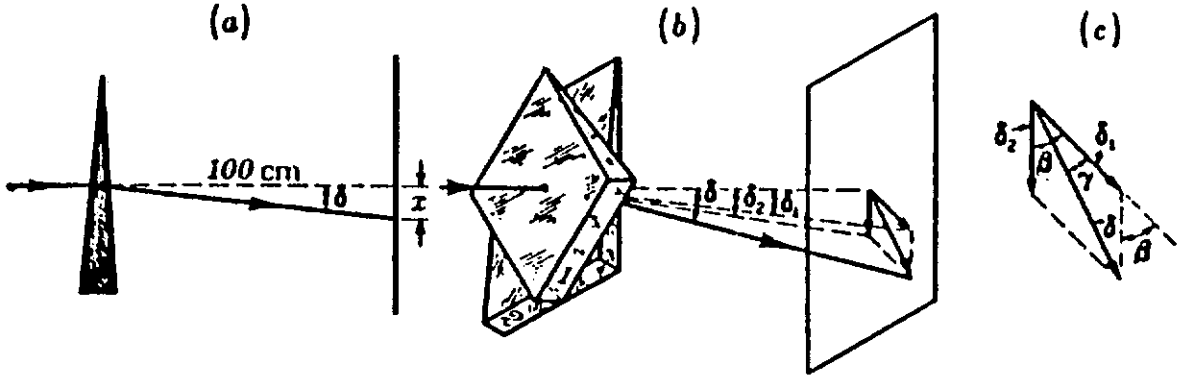

Thin prisms: (*a*) the displacement x in centimeters at a distance of 1 m gives the power of the prism in diopters; (*b*) Risley prism of variable power; (*c*) vector addition of prism deviations.

The Star Selector's Function

If one Risley prism is labeled "A" and the second "B", and the direction of the undeviated beam (that is, the beam direction when the bases of the prisms are 180 degrees from each other) is made to coincide with the optical axis of the telescope, then the effect of rotating the prisms is as shown. The vectorial addition of the deviation vectors (now labeled "A" and "B") permits the positioning of the instantaneous field of view anywhere in the FGS focal plane.

POSITIONING OF THE INSTANTANEOUS FIELD OF VIEW OF THE TOTAL FIELD OF VIEW BY THE TWO STAR SELECTOR ASSEMBLIES

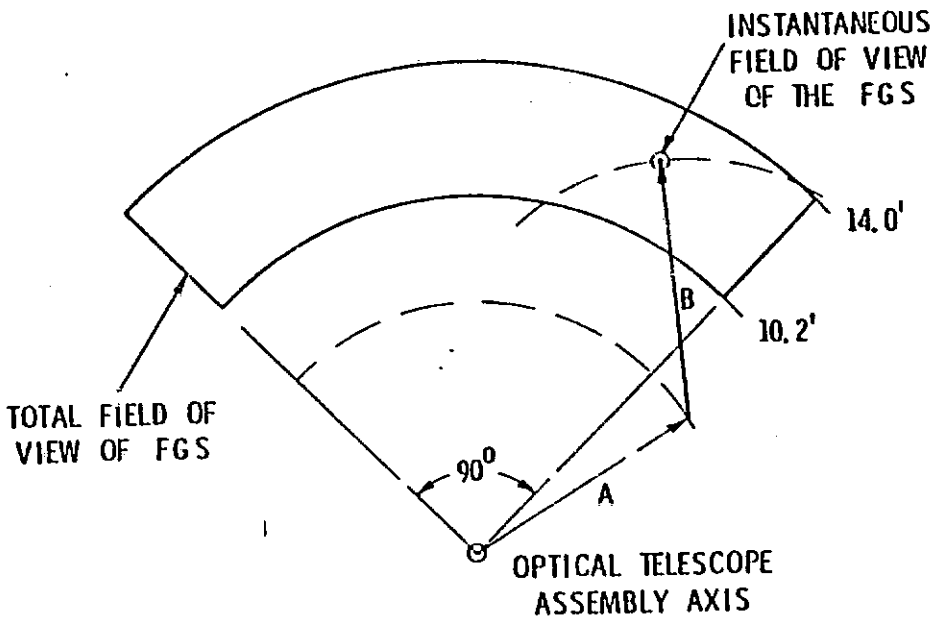

	A	B
OBJECT SPACE	7.1'	7.1'
PUPIL SPACE	6.77°	6.77°

The Star Selectors

The four mirrors in each assembly are the reflective counterparts of the Risley prisms. The mirror assemblies are mounted inside the bore of an optical encoder-motor assembly.

The concept has several advantages over competing concepts.

- It is mechanically simple, involving only two moving parts.
- The encoder's accuracy and resolution are enhanced by about an order of magnitude, since one revolution of the encoder corresponds to a line-of-sight deviation of 7.1 arcmin.
- The accuracy requirements of the encoder bearings are relieved by the properties of the optical rhomb formed by each mirror pair in the star selectors.

STAR SELECTOR SCHEMATIC DIAGRAM

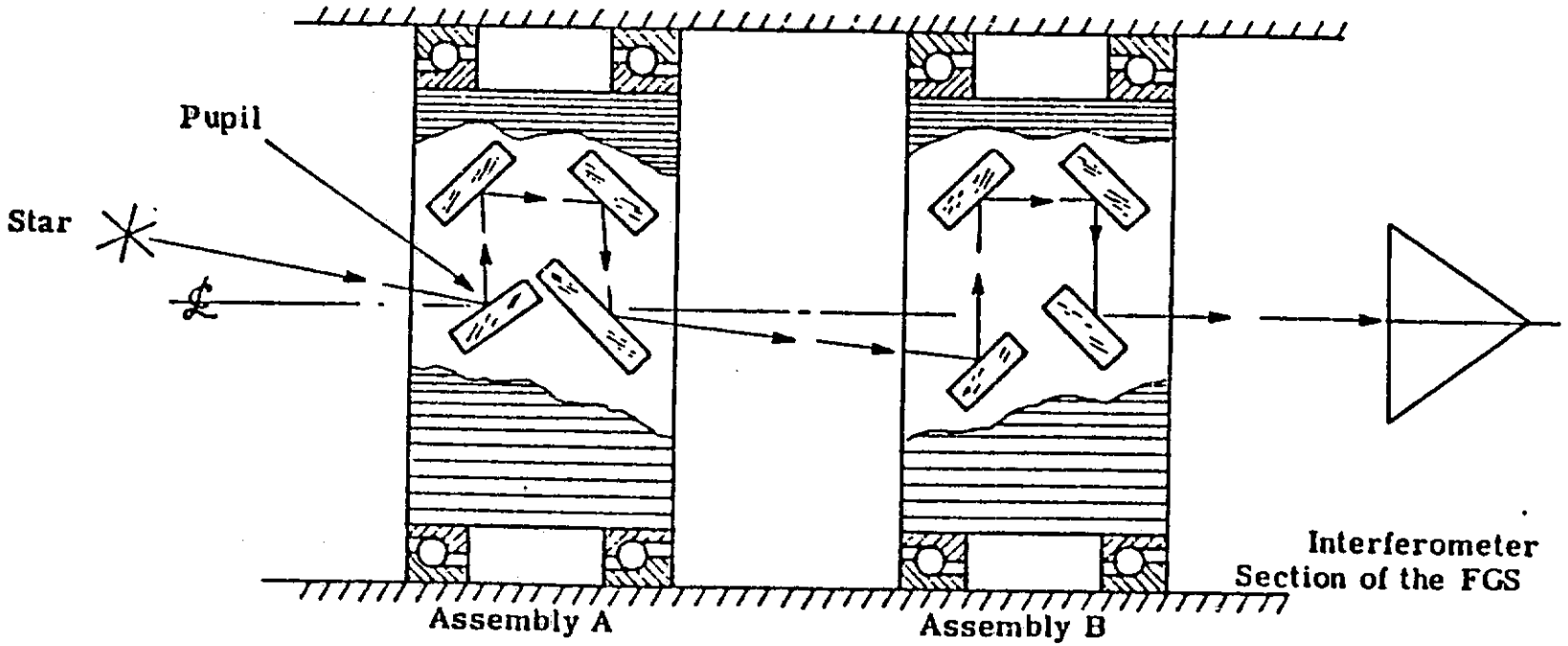

The next two illustrations show the packaging of the FGS optical system. The first shows the arrangement of the optical path for the FGS. The light from the telescope enters at the bottom of the figure and is reflected upward by the pickoff mirror. It next is reflected from the aspheric collimating mirror and then through the first star selector and the corrector group. After passing through the second star selector, the light path is folded across the bottom of the FGS box to the filters, used only for the astrometry mission. Another fold directs the light upward again to the beamsplitter cube. The cube divides the light so that wavefront tilt about both axes can be sensed. Two Koesters prisms, one oriented at 90 degrees to the other, provide the sensing of the wavefront tilt. The doublet lenses and pinhole lens assemblies complete the optical train to the photomultipliers.

FGS OPTICAL PATHS

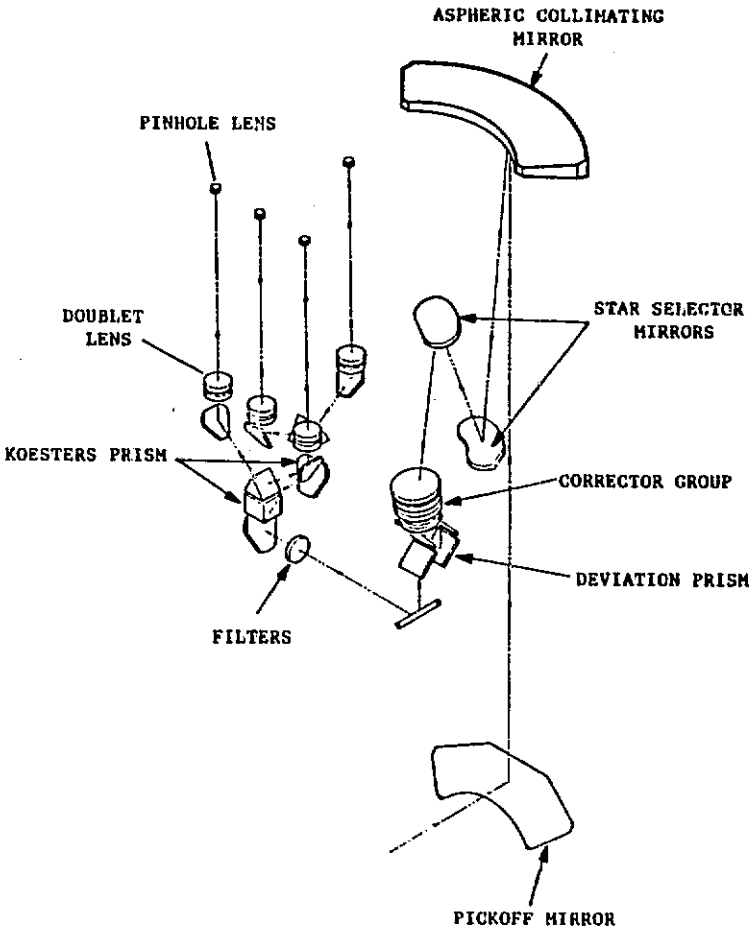

This figure illustrates the packaging of the ST's FGS optical design. The entire unit is replaceable on-orbit by a space-suited astronaut.

FGS PACKAGE

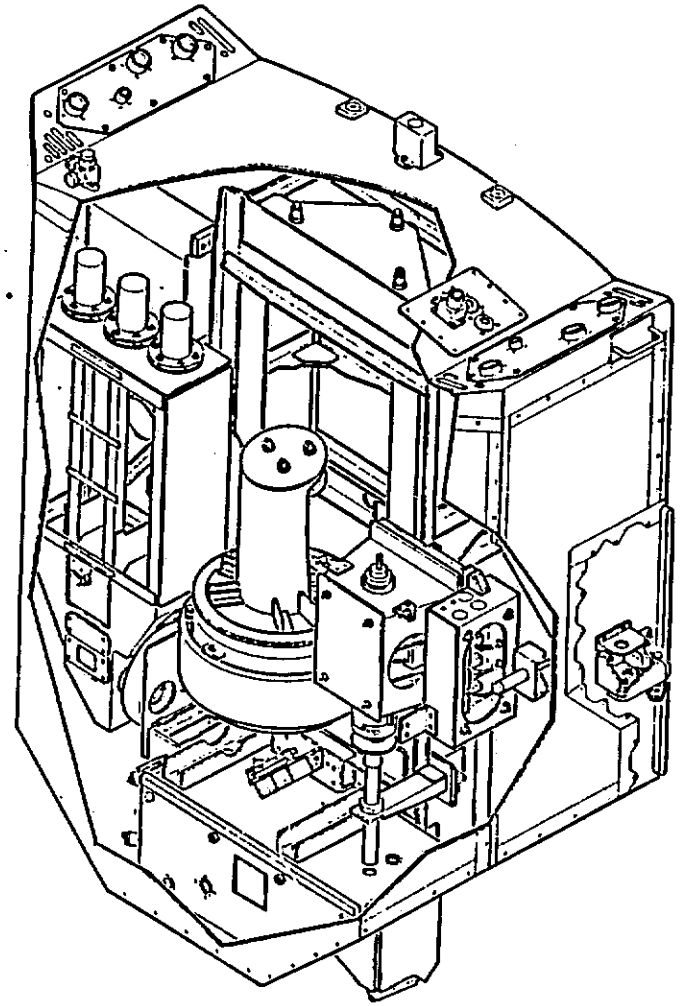

4.10 FGS ANALYSIS CONCLUSIONS

Using a conservative error budget allocation for the FGS of 0.02 arsec leads to a quad-CCD design using the new 15 μm pixel version of the RCA SID 501 and $m_V < 15$ stars. This device has not yet been fully characterized and the integration time required to obtain a high signal-to-noise ratio would exceed the 0.5 sec baseline. At most, two of the four CCDs would have to operate simultaneously. The need for the 15μ m pixel version rather than the standard 30 μ m pixels results from limiting the image centroiding to the 1/40 pixel (2-D) that has been achieved at Perkin-Elmer. While it is theoretically possible to centroid with higher precision, 1/40 pixel (1/60 pixel in each orthogonal direction) is currently state-of-the-art and can only be achieved with considerable difficulty.

A re-allocation of the error budget, however, can dramatically affect the number of CCDs needed by the FGS. Because SIRTF is limited to a 28 arcmin diameter FOV, requiring a high probability of detecting two stars near the galactic pole approximately corresponds to a sensitivity limit of $m_V = 14$ or fainter. For example, if the probability of detecting of two stars were reduced from the 0.95 requirement to 0.85 and the FGS NEA allocation were about 0.09 arcsec then $m_V \leq 14$ stars would be sufficient given image centroiding of 1/40 pixel. We emphasize, however, that such a large error budget allocated to the FGS would probably preclude SIRTF's having an overall line-of-sight stability of 0.1 arcsec.

The Hoffmann/Angel concept of placing the heat-dissipating portion of the FGS behind the MIC shows promise, but a number of areas must be studied in more detail. First, the heat load resulting from a MIC window must be compared with the heat load resulting from internal-MIC CCD(s). Second, although the use of fiducial lights inside the MIC allows for measuring the relative motion of the warm and cold areas, its effect on the pointing error budgets should be carefully analyzed. Third, the concept may allow the use of a room-temperature star selector mechanism similar to that developed by Perkin-Elmer for the Hubble Space Telescope (HST). While such a mechanism clearly adds mechanical complexity to the baseline FGS, it would allow the plate scale at the CCD to be greatly expanded so that very high precision image centroiding would no longer be needed because the CCD or other detector need only image a small portion of the FGS's field of view. Fourth, locating the CCD(s) (and, if needed, a star selector mechanism) outside the MIC would greatly enhance the possibility of on-orbit servicing as will be done with the HST's FGSs.

A major concern for any SIRTF FGS that uses the IR telescope optical images is the quality of those images. Precise centroiding requires both accurate knowledge and control of the image point spread function. Both are easily attained with an optical telescope, but the effect of SIRTF's being diffraction-limited at 5 μm (or even 2 μm) has yet to be analyzed.

The optical fiber image divider, while greatly reducing the FGS heat load on the SIRTF cryogen, would require a high-precision cryogenic mechanism to place the divider at the image of a star and cannot be recommended.

FGS ANALYSIS CONCLUSIONS SUMMARY

- FGS may require multiple CCDs
  - Number of CCDs needed depends quadratically on the FGS Noise Equivalent Angle (NEA) error budget.
  - Interal FGS Quad-CCD concept is suitable for $m_V \leq 15$ stars but requires 15 μm pixel versions of RCA SID 501 if FGS NEA is about 0.02 arcsec.
  - External FGS Quad-CCD concept is suitable for $m_V \leq 14$ stars and needs standard 30 μm pixel versions of RCA SID 501 if FGS NEA is about 0.05 arcsec.
  - An alternative to internal FGS with multiple CCDs would be to use precision cryogenic mechanisms to translate star images optically onto one CCD.
  - Single-CCD approach would be subject to single-point failure, but one RCA SID 501 (30 μm pixels) with sufficient FOV so that there is an 85 percent probability of detecting 2 or more $m_V \leq 14$ stars at the galactic pole would need a noise-equivalent-angle error budget of about 0.09 arcsec to maintain centroiding precision at 1/40 pixel.
- Hoffmann/Angel concept of internal FGS with CCD(s) behind MIC shows promise but should be studied further for
  - Effect of MIC window or yogen heat load compared to heat load from CCD(s) within MIC
  - Necessary mechanical stability of warm components in relation to cold components
  - Integration time needed due to reduced optical efficiency
  - Need for star selector mechanism (like HST FGS)
  - On-orbit serviceability of FGS
  - Quality of optical image produced by an infrared-diffraction-limited telescope.
- Optical fiber image divider could greatly reduce MIC heat load, but cannot be recommended now because
  - Precision cryogenic mechanism needed to translate image divider
  - Unknown cryogenic performance

FGS ANALYSIS CONCLUSIONS (Continued)

An external, or boresighted, FGS could be aligned to the SIRTF line of sight by using a small optical element in the SIRTF aperture to view fiducial lights in the MIC. With stellar images formed through an optical telescope like that of Perkin-Elmer's Star Mapper, rather than through the IR telescope, such an approach also requires a window into the cryogenic volume and, consequently, a heat leak that must be compared to the thermal load of an internal FGS. A major drawback of the external FGS concept is that it would induce an asymmetry into a chopped IR telescope. Still, the emission from the pick-off element would only be significant at SIRTF's longest wavelengths, where the boresight reference mechanism may not be needed due to the large IR image size. If the mechanism could be retracted during long wavelength observations, the asymmetry would not be a major factor. The effect on straylight rejection and glints, however, should be analyzed. The additional complexity of the external FGS has led us to conclude that the boresighted FGS is not the preferred approach.

FGS ANALYSIS CONCLUSIONS (Continued)

- An external (boresighted) FGS could be aligned to the SIRTF LOS. However,
  - Use of stars brighter than $m_v = 14$ would probably require a star selector mechanism (possibly as in HST FGS) to keep the number of CCDs at four or fewer
  - Reference path would introduce asymmetries into IR telescope
  - External FGS would be considerably more complex than internal FGS because of its higher mass, increased number of components, and long optical path.